

Physical properties and environments of nearby galaxies

Michael R. Blanton and John Moustakas

*Center for Cosmology and Particle Physics, Department of Physics,
New York University, 4 Washington Place, New York, NY 10003*

michael.blanton@gmail.com

ABSTRACT

We review the physical properties of nearby, relatively luminous galaxies, using results from newly available massive data sets together with more detailed observations. First, we present the global distribution of properties, including the optical and ultraviolet luminosity, stellar mass, and atomic gas mass functions. Second, we describe the shift of the galaxy population from “late” galaxy types in underdense regions to “early” galaxy types in overdense regions. We emphasize that the scaling relations followed by each galaxy type change very little with environment, with the exception of some minor but detectable effects. The shift in the population is apparent even at the densities of small groups and therefore cannot be exclusively due to physical processes operating in rich clusters. Third, we divide galaxies into four crude types — spiral, lenticular, elliptical, and merging systems — and describe some of their more detailed properties. We attempt to put these detailed properties into the global context provided by large surveys.

Contents

1	New windows on the nearby Universe	2
2	A global view of galaxy properties	3
2.1	Optical broad-band measurements	4
2.2	Optical spectroscopic measurements	5
2.3	Luminosity and stellar mass functions	7
2.4	Systematic effects in luminosity functions	8
2.5	Environmental dependence	8
2.6	Exceptions to environmental trends	10
3	Spiral galaxies	11
3.1	General description and identification	11
3.2	Quantitative morphological measures	12
3.3	Bulges, pseudobulges, and bars	13
3.4	Atomic and molecular gas content	15

3.5	Star formation	16
3.6	Dust content	17
3.7	Chemical history	18
3.8	Disk edges and extended galactic disks	18
3.9	Tully-Fisher relation	19
4	Lenticulars	20
5	Ellipticals	22
5.1	General description and identification	22
5.2	Structural trends	23
5.3	Nuclear properties	23
5.4	Fundamental plane and dynamics	24
5.5	Brightest cluster galaxies and cD galaxies	25
5.6	Deviations from smooth profiles	27
5.7	Stellar populations	28
5.8	Cold gas content	29
6	Interactions, mergers, starbursts, and post-starbursts	30
7	Discussion	31

1. New windows on the nearby Universe

As early as the work of Hubble (1936), astronomers recognized the existence of distinct galaxy types — smooth “early-types” preferentially found in groups and clusters and complex-looking “late-types” preferentially found in less dense regions of the sky. Despite this long history, we have not yet determined with certainty the physical mechanisms that differentiate galaxies into classes. The past decade of astronomers’ effort has yielded both massive new surveys of the nearby Universe and more detailed observations of individual objects. Although many of these observations have yet to be digested and fully understood, already we have a clearer view of the detailed physical properties than we did only a decade ago. Focusing on nearby galaxies comparable in mass to the Milky Way, we review some of the latest results on the census of the galaxy population.

Recently developed observational tools for understanding galaxy formation fall into two general types: wide-field surveys and targeted (but more detailed) observations. The wide field surveys we focus on are the Galaxy Evolution Explorer in the ultraviolet (*GALEX*; Martin et al. 2005), the Sloan Digital Sky Survey in the optical (SDSS; York et al. 2000), the Two-Micron All Sky Survey in the near infrared (2MASS;

Skrutskie et al. 2006), as well as 21-cm radio surveys such as the HI Parkes All Sky Survey (HIPASS; Meyer et al. 2004) and ALFALFA on Arecibo (Giovanelli et al. 2007). Each of these surveys covers a substantial fraction of the sky with imaging; redshifts from the SDSS and the 21-cm surveys then provide a third dimension. Along with the Two-degree Field Galaxy Redshift Survey (2dFGRS; Colless et al. 2001), the Six-degree Field Galaxy Redshift Survey (6dFGRS; Jones et al. 2004) and the 2MASS Redshift Survey (Crook et al. 2007), these massive surveys supply a detailed map of the galaxy density field and the framework of large-scale structure within which galaxies evolve. In addition, they supply a host of spectroscopic and photometric measurements for each galaxy: luminosities, sizes, colors, star-formation histories, stellar masses, velocity dispersions and emission line properties.

The second type of tool consists of targeted but more detailed programs that are too expensive to conduct on massive scales right now, but for which even small numbers of galaxies can be revealing. Such programs include the Spectroscopic Areal Unit for Research on Optical Nebulae (SAURON; Bacon et al. 2001), the *Spitzer* Infrared Nearby Galaxy Survey (SINGS; Kennicutt et al. 2003), The HI Nearby Galaxy Survey (THINGS; Walter et al. 2008), new large Hubble Space Telescope (*HST*) programs, and large compilations of individual efforts such as detailed radio observations, long-slit spectroscopy, and deep optical and near-infrared imaging.

Using the results of these recent efforts, we begin by exploring the global demographics of galaxies and their dependence on environment. Then, dividing galaxies into classes (spirals, lenticulars, ellipticals, and mergers), we review recent results concerning the scaling relations, star-formation histories, and other properties of each class.

We cannot hope to be exhaustive, and instead focus on recent results rather than historical ones. We omit discussion of dwarf systems, which are rather different than their more massive counterparts, being generally more gas-rich, disk-dominated, and usually lacking in spiral structure (a topic ripe for review; meanwhile, see Geha et al. 2006). Because of our focus on global properties, we also deemphasize central black holes (Kormendy 2004) and active galactic nuclei (AGN; Ho 2008), which might have an important influence on galaxy evolution as a whole (Kauffmann et al. 2003a; Best et al. 2006; Khalatyan et al. 2008). For elliptical galaxies, we refer the reader to multiple other reviews examining their more detailed properties, including their stellar populations (Renzini 2006), their structure and classification (Kormendy et al. 2009), and their hot gas content (Mathews & Brighenti 2003). A final warning is that we adopt some of the language of morphology (elliptical or “E”, lenticular or “S0”, and spiral galaxies) without fully addressing the problem of classification (Sandage 2005).

Throughout, we assume a standard cosmology of $\Omega_m = 0.3$ and $\Omega_\Lambda = 0.7$, with $H_0 = 100h$ km s⁻¹ Mpc⁻¹. All magnitudes are on the AB system unless otherwise specified.

2. A global view of galaxy properties

A breakthrough of recent surveys has been the ability to explore many dimensions of galaxy properties simultaneously and homogeneously, in order to put galaxy scaling relationships in context with respect to one another. In this section, we describe these general properties, their distribution, and their dependence on environment. We concentrate in this section primarily but not exclusively on SDSS results, which currently yield the most homogeneous and consistent measurements for the broadest range of galaxy varieties. In particular, in the subsections below we will make use of 77,153 galaxies with $z < 0.05$ in the SDSS Data Release 6 (DR6; Adelman-McCarthy et al. 2008), an update of the low-redshift sample of Blanton et al.

(2005c).

2.1. Optical broad-band measurements

Figure 1 shows the simplest measurable properties of galaxies from the SDSS sample: the absolute magnitude M_r , the $g - r$ color, the Sérsic (1968) index n in the r -band, and the physical half-light radius r_{50} (sometimes called the “effective radius”). These properties reveal a variety of correlations, most known for many years, but now quantified much more precisely.

The absolute magnitude M_r is a critical quantity, correlating well with stellar mass as well as with dynamical mass (see the discussion of the Tully-Fisher relation in §3.9 and the fundamental plane in §5.4). Clearly, the other properties are a strong function of overall mass. Although Figure 1 shows the raw distribution for the flux-limited SDSS sample, in §2.3 we correct for selection effects and calculate the luminosity and stellar mass functions.

In many of these plots, particularly those involving $g - r$ color, there is a bimodal distribution — galaxies can be divided very roughly into red and blue sequences (Strateva et al. 2001; Blanton et al. 2003; Baldry et al. 2004). The red and blue classification is not always related in a simple way to classical morphology — though of course there is some relationship (Roberts & Haynes 1994). In particular, galaxies in the blue sequence are very reliably classifiable as spiral galaxies with ongoing star-formation (§3). However, the red sequence contains a mix of types. The lower luminosity end consists of compact ellipticals (cEs) and dwarf ellipticals (dEs; sometimes known as spheroidals, Sph). Around $M_r - 5 \log_{10} h \sim -20$, the red sequence is a mix of early-type spirals, dust-reddened spirals (§3.6), lenticulars (S0s; §4), and giant ellipticals (Es; §5). At the highest luminosities, it consists of cD galaxies (§5.5).

For a rough quantification of how these types populate the red sequence, we use the classifications of our sample galaxies stored in the NASA Extragalactic Database (NED). In practice, most of these classifications come from The Third Reference Catalog of Bright Galaxies (RC3; de Vaucouleurs et al. 1991). For our purposes we select galaxies within $\Delta(g - r) \sim 0.03$ of the red sequence, with no detected lines associated with star-formation (see §2.2 and Figure 2). For any luminosity $M_r - 5 \log_{10} h < -17$, only about 40% of these galaxies are Es. About 25%–50% of them are S0s, with the lowest fractions at around $M_r - 5 \log_{10} h \sim -20$, increasing to both higher and lower luminosities. We suspect these fractions are in practice overestimates, since spiral systems are far more commonly misclassified as E/S0s than vice-versa. It remains clear, however, that restricting to red sequence galaxies does not suffice to guarantee an E/S0 sample — at $M_r - 5 \log_{10} h \sim -20$ at least one-third of the red sequence population is Sa or later.

Both the red and blue sequences have mean colors that are a function of absolute magnitude. Blue galaxies have recent star-formation, and their color is strongly related to the recent star-formation history (§3.5) and the dust reddening in the galaxy (§3.6). As galaxy mass increases, the change in color reflects both the increased reddening due to dust and the decreased fraction of recent star-formation (related to an increased importance of red central bulges; §3.3). The strong dependence on recent star formation history translates into the large range of colors on the blue sequence. As one might expect given this trend, at high masses the atomic and molecular gas fractions are low (§3.4), whereas the metallicities are high (§3.7).

Red galaxies have (generally) little recent star-formation, and their color is weakly related to both mean stellar age and to metallicity, both of which rise with mass (§5.7). Because the dependence of color on these properties is weak relative to their intrinsic variation, there is a small range of red galaxy colors in Figure

1. Although their old stellar age is related to their relatively gas-poor nature, they are not entirely devoid of cold gas (§5.8) or perhaps of relatively recent star-formation (§5.7).

The Sérsic index n is a measurement of the overall profile “shape,” and is defined by the profile:

$$I(r) \propto \exp \left[- \left(\frac{r}{r_0} \right)^{1/n} \right], \quad (1)$$

where r_0 is a scale factor that one can relate to the half-light radius r_{50} given n (Sérsic 1968; see Graham & Driver 2005 for the mathematical relationship). In general, this model is usually generalized to non-axisymmetric cases by allowing for an axis-ratio $b/a < 1$ (that is, elliptical rather than circular isophotes). While r_{50} reflects the physical size of the galaxy, n reflects what we define as the “concentration.” As $n \rightarrow 0$, the Sérsic profile approaches a uniform disk of light with radius r_0 . As n increases, the Sérsic function simultaneously concentrates the surface brightness profile towards the center and pushes flux further out, passing through a Gaussian ($n = 0.5$), an exponential ($n = 1$), a de Vaucouleurs profile ($n = 4$; de Vaucouleurs 1948), and even higher for some galaxies. This index often is used as a proxy for morphology (e.g., Bell et al. 2003; Shen et al. 2003; Mandelbaum et al. 2006), though it is only partially related to classical morphological determinations (§3.2).

For many galaxies a single Sérsic index model does not explain the profile completely. For elliptical galaxies, the central regions are often not well fit by such a model (§5.3). For spiral and lenticular galaxies a better model is an exponential disk plus a Sérsic bulge (§3.3). However, as Graham (2001) shows, measures of the overall concentration are well-correlated with bulge-to-disk ratios for real galaxies.

Consequently, in Figure 1 the single component Sérsic n does reveal some interesting trends. Blue galaxies generally have low Sérsic indices, while red galaxies span a range of Sérsic indices. Overall, both blue galaxies and red galaxies tend to be more concentrated at higher luminosity. For blue galaxies this reflects an increased importance of the bulge, and a simultaneous increase in concentration of the bulge itself (§3.3). For red galaxies the trend appears to reflect an overall structural difference between low luminosity and high luminosity early-type galaxies (§5.2).

Finally, the plots also demonstrate that the optically emitting regions of galaxies are larger for more massive galaxies. Luminous galaxies achieve $r_{50} > 10 h^{-1}$ kpc, while the low luminosity population typically has $r_{50} < 1 h^{-1}$ kpc. The full extent of the galaxies in the optical tends to be at least $2\text{--}4 \times r_{50}$ for most systems depending on the concentration. For disk galaxies, even this optical radius does not trace the outer gas disk often visible in HI and in very sensitive ultraviolet (UV) measurements (§3.8).

2.2. Optical spectroscopic measurements

More detailed information on stellar populations and the interstellar medium can be obtained from integrated spectrophotometry (Kennicutt 1992; Jansen et al. 2000; Moustakas, Kennicutt & Tremonti 2006). In Figure 2, we show a small sampling of the major trends in galaxy spectroscopic properties in the optical, using the same sample as in Figure 1, with parameters determined by Brinchmann et al. (2004) and Tremonti et al. (2004) for our SDSS sample. The SDSS spectra are taken through 3 arcsec diameter fibers, a generally small radius within nearby galaxies, and so aperture effects are not ignorable; however, the general conclusions we draw here are not affected much by this consideration.

For the purposes of these plots, we replace luminosity by the stellar mass. There are numerous methods

for calculating stellar mass; see the compilation of major techniques in Baldry, Glazebrook & Driver (2008). Here we use the simple technique of Bell et al. (2003), which assigns a mass-to-light ratio according to the galaxy broad-band colors. This technique is robust at least for most galaxies, because in practice increasing dust, age, and metallicity all both increase the mass-to-light ratio and redden the colors, in roughly similar proportions. Of course, galaxies with large, recent bursts of star-formation or extreme amounts of dust attenuation will not be well-described by this simple technique (Bell & de Jong 2001). But the greater unknown in determining stellar masses is the initial mass function (IMF) of stars assumed, because the lowest mass stars contribute considerable mass but very little light. In fact, as Baldry, Glazebrook & Driver (2008) show, a number of disparate techniques for calculating stellar masses agree well at fixed IMF. The Bell et al. (2003) estimate we use employs the non-physical “diet” Salpeter IMF, which yields stellar masses slightly higher (~ 0.05 dex) than the popular Kroupa (2001) and Chabrier (2003) IMFs.

The upper left panel of Figure 2 shows the distribution of stellar mass and the quantity $D_n(4000)$, a measure of the 4000-Å break, according to the “narrow” definition of Balogh et al. (1999) and using the determination of Brinchmann et al. (2004). As Kauffmann et al. (2003b) point out, the 4000-Å break traces stellar population age better than broad-band colors, and it is less sensitive to dust reddening. Star-forming galaxies tend to have weak breaks, with $D_n(4000) \sim 1.1$ – 1.4 , whereas passive stellar populations tend to have strong breaks, with $D_n(4000) \sim 1.8$ – 2.1 . Indeed, similar to galaxy color, $D_n(4000)$ clearly separates these two populations; older populations dominate at high stellar mass and the star-forming systems dominate at low stellar mass. Based on this diagram, Kauffmann et al. (2003) define a critical stellar mass of $1.5 \times 10^{10} h^{-2} M_\odot$ separating these two galaxy populations.

From SDSS spectra, we can also determine galaxy velocity dispersions; for a sample of galaxies without emission lines, we show the results in the upper right panel of Figure 2. Here we see a clear correlation between velocity dispersion and stellar mass, related of course to the classic relation of Faber & Jackson (1976). This relationship is merely a projection of the fundamental plane (§5.4). Both the fundamental plane and the Tully-Fisher relation (§3.9) show that the dynamical masses of galaxies are correlated with their stellar masses.

The bottom right panel of Figure 2 shows the “BPT” diagram (Baldwin, Phillips & Terlevich 1981), based on the $H\alpha$ and $H\beta$ recombination lines and the $[N\ II] \lambda 6584$ and $[O\ III] \lambda 5007$ collisionally excited forbidden lines. The position of an object in the BPT diagram is a function of metallicity and the ionization state of the emitting gas (e.g. Kennicutt et al. 2000) and can be roughly divided into three regions (following Kauffmann et al. 2003a). The lower left region contains emission line galaxies dominated by star-formation. The upper triangle contains Seyfert galaxies, which have higher ionizing fluxes and are likely associated with AGN. The lower right contains Low Ionization Nuclear Emission-line Regions (LINERs; Heckman 1980; Kewley et al. 2006), also most likely associated with AGN. Ho (2008) discuss the classification and physical properties of nearby AGN in much greater detail than possible here.

Finally, we isolate the star-forming galaxies (those with emission lines falling in the star-formation region of the BPT diagram). The lower left panel of Figure 2 shows their gas-phase metallicity (from Tremonti et al. 2004). We use the standard quantification of oxygen abundance, $12 + \log_{10} (O/H)$. Clearly more massive galaxies are more metal-rich, saturating around 9.2 dex (about 0.5 dex more oxygen-rich than the newly revised solar abundance; Meléndez & Asplund 2008). Closed-box chemical evolution models do predict an increase in metallicity as the fraction of gas turned into stars rises, since more generations of star-formation have occurred. However, in fact, the observed increase in metallicity is likely also driven by metal-rich outflows in low-mass galaxies, or another violation of the closed-box model (§3.7).

2.3. Luminosity and stellar mass functions

A fundamental measurement of the galaxy distribution is the luminosity function (LF): the number density as a function of luminosity. With flux-limited samples, such as those shown in Figures 1 and 2, one needs to apply corrections for the fact that faint galaxies cannot be observed throughout the survey volume. A number of statistical techniques have been developed over the years to correct for this effect, the simplest of which is the $1/V_{\text{max}}$ method (Schmidt 1968). Using this method, one counts each galaxy with a weight equal to the inverse of the volume over which it could have been observed. In the integral over volume, one must include any weighting for survey completeness as well as flux or other selection effects, based on the galaxy’s particular properties. Then, in any bin of any set of properties one can calculate the number density of galaxies in that bin as $\sum_i 1/V_{\text{max},i}$. For modern samples, the results from this method agree with others designed to be insensitive to accidental correlations between large-scale structure and redshift (e.g. Efstathiou, Ellis & Peterson 1988; Takeuchi, Yoshikawa & Ishii 2000).

The upper left panel of Figure 3 shows the optical r -band LF from the SDSS DR6 sample, using V_{max} calculations described in Blanton et al. (2005b). We show both the overall LF and the LF split among galaxy types, using some very basic criteria. The “late” population consists of any blue galaxies plus any star-forming red galaxies. The “early” population consists of other galaxies, split into concentrated early-types, which have $n > 2$, and diffuse early-types, with $n < 2$. These classifications are crude, of course — this method describes many legitimate Sa galaxies and basically all S0 galaxies as “early-type,” for example.

Nevertheless, this panel begs comparison with Figure 1 of Binggeli, Sandage & Tammann (1988), who show very similar trends in the LF using visual morphological classifications. As they found, early type galaxies dominate the bright-end, while late-types dominate the faint end. Diffuse early-types become increasingly important at low luminosity.

As Binggeli, Sandage & Tammann (1988) also showed, a Schechter (1976) function fit to the LF is insufficient. We overplot the double-Schechter function fit of Blanton et al. (2005b), which uses a broken power-law for the faint end:

$$\Phi(L)dL = \frac{dL}{L_*} \exp(-L/L_*) \left[\phi_{*,1} \left(\frac{L}{L_*} \right)^{\alpha_1} + \phi_{*,2} \left(\frac{L}{L_*} \right)^{\alpha_2} \right] \quad (2)$$

The parameter L_* is a fundamental one, indicating the approximate onset of the exponential cut-off. At the faint-end the luminosity function is approximately a power law with slope α_2 ranging between -1.35 and -1.52 in the r -band depending upon assumptions about the low surface brightness population (§2.4).

The upper right panel of Figure 3 shows the stellar mass function, using the same stellar mass determinations as used in Figure 2. Because the stellar mass-to-light ratios of red galaxies are higher than blue galaxies, the stellar mass function accentuates the distinction between the blue and red populations: the early-types become even more dominant. Overlaid is the double Schechter fit of Baldry, Glazebrook & Driver (2008), who present a comprehensive treatment of recent estimates of the stellar mass function (the results shown here use the Chabrier 2003 IMF). After accounting for differences in the adopted IMF, these results are in rough agreement with determinations of Cole et al. (2001), Kochanek et al. (2001), and Bell et al. (2003) based on 2MASS K -band data.

The lower left panel of Figure 3 shows the near-UV luminosity function, which traces recent star-formation, obtained by matching the SDSS sample to the *GALEX* Release 3 (GR3; Martin et al. 2005). We separate the galaxies according to the same classifications as used above. We K -correct here to the near-UV band shifted blueward by a factor $1 + z = 1.1$ (Blanton & Roweis 2007) for consistency with

Schiminovich et al. (2007). Overlaid as the smooth black line is their full luminosity function. Clearly the early-types are very subdominant — the UV luminosity of the Universe is completely dominated by blue, star-forming galaxies.

Finally, in the lower right panel of Figure 3 we show the HI mass functions determined by the compilation of Springob, Haynes & Giovanelli (2005), which is comparable to the HIPASS result of Zwaan et al. (2005). Since they did not publish their full functions, we only show the Schechter function fits (which are accurate descriptions). They limited their sample to spiral galaxies; most ellipticals have very low atomic gas content and would not contribute significantly to this plot (§5.8), though they often have significant hot ionized gas (Mathews & Brighenti 2003). They split the sample according to morphological type (though virtually all of the types would fall into the “late-type” histograms in the other plots). The most notable effect is that the mass cut-off scale for the HI mass function is far lower than for the stellar mass function: the most massive galaxies are dominated by stars, not neutral hydrogen. That situation changes dramatically at lower masses (§3.4).

2.4. Systematic effects in luminosity functions

For the luminosity and stellar masses in this section, we relied upon SDSS Petrosian magnitudes (Petrosian 1976; Blanton et al. 2001; Strauss et al. 2002), which have the virtue that they are roughly redshift-independent quantities. Some researchers advocate the use of “total” flux, using extrapolated radial profiles. The difference is largest for de Vaucouleurs profiles (with SDSS Petrosian fluxes less by 10%–20%, depending on the ratio of the half-light radius to the seeing). For very detailed work, such as the build-up of stellar mass on the red sequence, it is therefore necessary to know the flux estimator used (e.g., Brown et al. 2007). In the context of SDSS, another problem exists: the biggest galaxies on the sky have their fluxes significantly underestimated owing to oversubtraction of the background (Blanton et al. 2005a; Bernardi et al. 2007), yielding a 20% bias at $r_{50} \sim 20''$ and rising at larger sizes (Lauer et al. 2007b). For that reason, the effect on the luminosity function is minimal, since virtually all of the brightest galaxies in the sample are far away and thus small in angular size.

All luminosity and stellar mass function estimates are affected at some level by surface brightness selection effects. Blanton et al. (2005c) estimate that for the SDSS these effects become important at the 10% level at $M_r - 5 \log_{10} h \sim -17$ or so. At lower luminosities, the SDSS spectroscopic survey starts to become incomplete; for 2MASS-based surveys like Cole et al. (2001) or Kochanek et al. (2001), the incompleteness probably sets in at higher luminosities, though no quantitative estimate exists. A less traditional view is that of O’Neil et al. (2004), who suggest that a substantial reservoir of baryons could be in massive low surface brightness galaxies, with large H I masses ($> 10^{10} \mathcal{M}_{\odot}$) but barely detectable in optical surveys. Such galaxies exist, but no quantitative estimate of their number density has been made.

2.5. Environmental dependence

As has long been established, all of these properties are a strong function of the local environment — whether a galaxy is in a cluster or in a void. With the latest data sets, we now have a much more detailed understanding of this dependence. To illustrate these effects, we estimate environment using the number N_n of neighboring galaxies with $M_r - 5 \log_{10} h < -18.5$, within a projected distance of $500 h^{-1}$ kpc and a velocity of 600 km s^{-1} . The luminosity threshold is roughly that of the Large Magellanic Cloud. Other

measures of galaxy environment have been explored recently: group environment (Yang et al. 2007), nearest neighbor distance (Park et al. 2007), and kernel density smoothing (Balogh et al. 2004). The results we describe here seem to hold no matter which estimate of density one uses.

First, let us consider the variation of the stellar mass function with environment, as shown in Figure 4. The panels are broken up, as labeled, into bins of N_n — the upper right panel is roughly the environment of galaxies in the Local Group. The first notable fact is that most galaxies with $0.01L_* \lesssim L \lesssim L_*$ are in relatively underdense environments, at the scale of the Local Group or less. Generally speaking, the massive galaxies are relatively more likely to exist in dense regions, reflecting the variation of the shape of the optical luminosity function from void regions (Hoyle et al. 2005), through average regions (Blanton et al. 2005c), to clusters (Popesso et al. 2005).

Even in the least dense environments, the “early-type” galaxies are a substantial population — and indeed dominant at high masses. At lower masses the population is completely dominated by blue disk galaxies. As density increases, the characteristic mass of the red population increases. Clearly most of the brightest objects are red and in dense regions. In addition, the blue population declines in importance as density increases, becoming almost outnumbered even at the faint end.

Second, let us consider the more detailed properties of galaxies as a function of environment. For example, Figure 5 shows the relationship between $D_n(4000)$ and stellar mass as a function of environment. For reference, we show the rough location of each galaxy sequence as the red and blue lines, identically in each panel of Figure 5. Though the position of each sequence changes only a little with environment, how each sequence is populated changes considerably, with old galaxies preferentially located in dense regions, as found for these parameters by Kauffmann et al. (2004).

Other measurements of the change of galaxy properties with environment track this same segregation of galaxy types: broad-band color and Sérsic index (e.g., Hashimoto & Oemler 1999; Blanton et al. 2005a; Yang et al. 2007); $H\alpha$ emission, star-formation rate, and other spectral properties (e.g., Lewis et al. 2002; Norberg et al. 2002; Gomez et al. 2003; Boselli & Gavazzi 2006); and of course classical morphology (e.g., Dressler 1980; Postman & Geller 1984; Guzzo et al. 1997; Giuricin et al. 2001). It appears that among all these properties, the controlling variables are those related to mass and star-formation history — not those having to do with structure (Kauffmann et al. 2004; Blanton et al. 2005a; Christlein & Zabludoff 2005; Quintero et al. 2006).

Figure 6 demonstrates this conclusion. The top two rows compare the relationship between Sérsic index and stellar mass for a “young” population and an “old” population, where the division is taken to be at $D_n(4000) = 1.6$. Each relationship remains remarkably fixed as a function of density. This means that once the stellar population age and stellar mass are fixed, the environment of a galaxy does not relate to its overall structure. In contrast, if we classify galaxies according to Sérsic index, their stellar population ages are a strong function of environment.

This theme persists for almost all properties of galaxies as a function of environment. Once galaxies are appropriately classified — that is, by some parameter related to the star-formation history — then galaxy scaling laws are usually weak functions of environment. For example, Park et al. (2007) classified galaxies by color and color gradient, and explored the scaling relationships of each type thoroughly, finding only weak dependencies on environment. Similarly, Ball, Loveday & Brunner (2008) found that once color was fixed, there was no relationship between environment and their artificial neural network determination of morphology. Eyeball classifications of tens of thousands of galaxies into general early and late types have been compiled from the general public by the Galaxy Zoo project (Bamford et al. 2009). They too conclude

that morphology does not depend strongly on environment once color is fixed. Furthermore, more refined eyeball measures of spiral and ring structure and bar strength (van den Bergh 2002a,b) also appear to be weak functions of environment.

The other striking fact in this plot is that the effect of environment sets in at low density — even the upper right panels of Figures 4 and 5, which correspond to Local Group type environments, show more old galaxies than found in isolated regions. A skeptic might worry that the environmental indicator used here does not distinguish between being in a small group or at the edge of a big cluster. However, the group-based environmental indicators of Blanton & Berlind (2007) show explicitly that even belonging to a small group leads to a larger fraction of red galaxies. These results were hinted at long ago by Postman & Geller (1984), who found environmental dependence all the way down to density enhancements similar to $N_n \sim 1$ in our units.

A final point that the major new surveys have demonstrated about environment is that its effects are relatively local. Much of the environmental dependence can be understood in terms of the group environment: what mass halo hosts the galaxy, and its position within that halo (Blanton & Berlind 2007). The larger scale density field appears to be much less important (Kauffmann et al. 2004; Blanton 2006; Park et al. 2007). The results of Gomez et al. (2003), which show a dependence of star-formation on distance from the nearest cluster out to several virial radii, are sometimes said to illustrate large scale effects at work. However, Lewis et al. (2002) showed that this trend is indeed due to group-scale effects and simply reflects the decreasing incidence of groups as a function of distance from the cluster.

In this section, we have argued that environmental effects are comparatively local (within the host halo), are important even at low density, and keep galaxy scaling relationships constant with environment. These results suggest that the processes that transform galaxies from one type to another are similar in all environments — but that they more commonly occur in dense regions. Certainly no effect that only acts in rich clusters can explain the observed segregation of galaxy colors, concentrations, sizes and luminosities.

Although it is difficult to make quantitative comparisons with theory, the observations favor an important role for so-called pre-processing of galaxies in groups, possibly by mergers (Mihos 2004), by gas-dynamical interactions with warm or hot gas (Fujita 2004), or by tidal harassment (Moore, Lake & Katz 1998). Such a picture could explain why the segregation begins even at low densities. In addition, if most galaxy transformations occur on the small group scale, then clusters may be regions that have subsumed many older groups and thus have more than their share of “transformed” galaxies. This scenario would create the shift in galaxy populations as a function of environment, without necessarily altering the scaling relations of galaxies dramatically.

2.6. Exceptions to environmental trends

There are always important exceptions to the rules! First, as we discuss in §3 and §5, there have been recent detections of small shifts in scaling relations as a function of environment.

Second, Blanton & Berlind (2007) and Park et al. (2007) both found a tendency for galaxies with very close neighbors to be red or early-type at fixed group environment. The more detailed analysis of Park, Gott & Choi (2008) revealed that galaxies within each others’ virial radii tend to have preferentially the same morphology (at fixed environment on larger scales). Weinmann et al. (2006) similarly found a tendency towards “conformity” between central galaxies and their satellites. On small scales, galaxies ap-

pear to “share” information about their type in a manner that is not explained by the larger-scale trends. Whether these effects are related to the star-formation enhancements that interacting galaxies and close pairs experience (§6) is currently unknown.

Third, central galaxies in clusters seem to be a special case. Though such galaxies are early-type and similar to ellipticals, their positions in the centers of clusters appear to affect them substantially (§5.5). Blanton et al. (2005a) found a tendency for the most luminous galaxies (mostly central galaxies in clusters) to be larger and more diffuse in dense regions. Such a tendency could result from cD galaxies undergoing multiple “dry” mergers with other red galaxies.

Fourth, a more subtle effect exists for central galaxies: their properties appear to be related to the large scale density field (not just to the host halo). For low mass host halos ($\mathcal{M} < 10^{14} \mathcal{M}_{\odot}$), all results agree that the central galaxy tends to be “earlier” type in denser regions on large scales (e.g., Yang, Mo & van den Bosch 2006; Berlind et al. 2006). For massive host halos, there is disagreement — Berlind et al. (2006) find that the trend reverses, whereas Yang, Mo & van den Bosch (2006) do not. It may be that the spectroscopic classification used by Yang, Mo & van den Bosch (2006), based on a principal component analysis (PCA) of the 2dFGRS spectra, yields different trends than the color classification of Berlind et al. (2006).

3. Spiral galaxies

3.1. General description and identification

We begin exploring the population of galaxies in more detail with the spirals, which for our purposes we define as disk galaxies with ongoing star-formation. In Figure 7, we show a sampling of optical images of nearby spirals from the SDSS, according to the NED classifications mentioned in §2.1. We have sorted these galaxies by absolute magnitude on the horizontal axis and $g - r$ color on the vertical axis. An overall trend can be seen that the reddest spirals tend preferentially to have visible dust, and are often edge-on (§3.6). The more luminous spirals tend (with exceptions) to have more evident and more regular spiral structure. A prominent feature in many spirals is a reddish, smooth, central component, the “bulge” (§3.3).

Figure 8 shows the distribution of spirals in the space of absolute magnitude, color, size and Sérsic index. Here we have colored the points according to the spiral subtype: blue for Sc and Sd galaxies, cyan for Sb galaxies, and green for Sa galaxies. Figure 8 (and Figure 12, described later) represent an updated look at the physical properties along the Hubble sequence that we first learned from Roberts & Haynes (1994). There is a strong trend for the later type spirals to be lower in luminosity, closer to exponential, and bluer. The early type spirals define a (broad) red sequence, and are concentrated and luminous. They occupy a different place in the size-luminosity relation, one that overlaps considerably with the ellipticals (§5; see also Courteau et al. 2007). Indeed, in these gross properties Sa galaxies are remarkably similar to ellipticals.

The overall morphological separation according to Sérsic index is driven by the relative importance of the bulge to morphological classification. Of course, the meaning of the Sérsic index for spiral galaxies is different than for elliptical galaxies. For spiral galaxies n reflects the balance between the disk and the bulge, two clearly distinct components. By contrast, for elliptical galaxies n usually reflects the overall structure of what is apparently a single component (§5.2).

3.2. Quantitative morphological measures

Astronomers have traditionally classified spiral galaxies from early to late type based on three criteria: the spiral arm pitch angle, the organization of the spiral arms, and the prominence of the bulge (Hubble 1936; Sandage 1961; de Vaucouleurs 1959). Traditional classifications are performed by eye from experience, but that technique is subjective and cannot be applied to massive samples. The influence of the bulge criterion as reflected in the Sérsic index n is evident in Figure 8. In contrast, the relative importance of the spiral structure considerations vary among classifiers. As an example, classifiers differ on at least two cases: low bulge-to-disk ratio galaxies with little spiral structure (Koopmann & Kenney 1998), and high bulge-to-disk ratio galaxies with late-type spiral structure (Hameed & Devereux 2005). One particular consequence of the latter ambiguity is that RC3 types (which emphasize the bulge-to-disk ratio) tend to be earlier than those from the Revised Shapley-Ames Catalog (Sandage & Tammann 1981). These concerns have prompted a good deal of work on the “quantitative morphology” of galaxies. This work has two general goals, often conflated: (1) to reduce the complex information in galaxy images to a few simple measurements; and (2) to classify galaxies.

Quantitative morphology often focuses on the separation of the disk from the bulge component, often using standardized packages such as GIM2D (Simard 1998), GALFIT (Peng et al. 2002) or BUDDA (de Souza, Gadotti & dos Anjos 2004). We discuss the detailed nature of bulges and bars in §3.3; here we discuss their demographics and relationship with galaxy morphology. Image decomposition methods usually treat the disk as exponential, but use more complex models for the central component. At minimum they must include a general Sérsic profile bulge (they are only rarely exactly de Vaucouleurs profiles; Graham 2001; de Jong et al. 2004; Laurikainen et al. 2007). More generally, as §3.3 discusses, there are at least three classes of central galaxy components — classical bulges (usually $n > 2$), pseudobulges (usually $n < 2$; Fisher & Drory 2008), and bars (usually $n \sim 0.5$ –1; Gadotti 2009). These components can and often do co-exist within the same galaxy. As a further caveat, ground-based observations of even relatively nearby galaxies may have Sérsic indices artificially raised by the presence of nuclear components (Balcells et al. 2003).

For these reasons, three-component galaxy fits (disk, general Sérsic profile bulge, and bar) are now the state-of-the-art. In particular, investigators have recognized that the bar component has a strong influence on the fits (e.g. de Jong 1996; Wadadekar, Robbason & Kembhavi 1999; Laurikainen, Salo & Buta 2005; Reese et al. 2007; Gadotti 2008b; Weinzirl et al. 2009). Relative to two-component analyses, the remaining bulges after bar subtraction are smaller (often by a factor of two or more), have lower n , and are more likely to be pseudobulges.

These complications make the demographics of bulges, pseudobulges and bars difficult to measure in large surveys. Among the larger analyses are those of Allen et al. (2006) and Driver et al. (2007), who fit two-component models in the Millenium Galaxy Catalogue redshift survey, and Gadotti (2009), who fit three-component models in the SDSS. Although the stellar mass fractions of each analysis are not easily comparable, they both conclude that classical bulges account for at least ten times the stellar mass that pseudobulges do. As a cautionary note, other (typically smaller but more carefully analyzed) samples do find pseudobulges more commonly at least for low B/T galaxies (Graham 2001; de Jong et al. 2004; Laurikainen et al. 2007). All things considered, probably the best current accounting of the stellar mass fractions in various components is that of Gadotti (2009), who report that for $\mathcal{M} > 10^{10} \mathcal{M}_{\odot}$, 32% of the stellar mass is in ellipticals, 36% is in disks, 25% is in classical bulges, 3% is in pseudobulges, and 4% is in bars.

Beyond disk/bulge decompositions, a number of sophisticated techniques have been developed to measure more complex “morphological” information. Some methods depend on high-order decompositions of the galaxy images, for example using Fourier modes (Odehahn et al. 2002) or shapelets (Kelly & McKay 2004). Other approaches have used a combination of measured parameters, for example, concentration (Abraham et al. 1994), asymmetry (Schade et al. 1995) and smoothness (Conselice 2003; Yamauchi et al. 2005). More recently explored parameters are the Gini coefficient — a measure of the evenness of the light distribution — and a concentration-like parameter called M_{20} (Lotz, Primack & Madau 2004; Zamojski et al. 2007). Most investigators eschew color information, for reasons we do not fully understand, with the notable exception of Choi, Park & Vogeley (2007), who utilize galaxy color and color gradient.

Once galaxies properties are measured, classification can be performed using these parameters with simple cuts in parameter space (e.g., Choi, Park & Vogeley 2007), with the aid of dimensionality reduction techniques like principal component analysis (e.g., Ellis et al. 2005; Scarlata et al. 2007), or using artificial neural networks (e.g., Storrie-Lombardi et al. 1992; Ball et al. 2004). Doing so can effectively classify galaxies into groups such as mergers, elliptical galaxies, early-type spirals, late-type spirals and irregulars. In some cases these classifications are reproducible and do a reasonable job of reproducing classical morphological classes (e.g., Scarlata et al. 2007).

None of these methods, however, distinguish well between face-on S0s, Sa galaxies and Es — the essential ambiguity also present in Figures 8 and 12. In addition, the agreement of quantitative morphological classification with eyeball determinations obscures the differences in approach. The quantitative schemes do not measure in detail the differences in spiral structure in the later types that are essential to classical morphology and apparent to the eyes of experts (e.g. Elmegreen & Elmegreen 1987; van den Bergh et al. 2002). Generally speaking, although quantitative measures of spiral structure exist (e.g., Elmegreen & Elmegreen 1984; Rix & Zaritsky 1995; Seigar & James 2002; Buta et al. 2005; Kendall et al. 2008), they are rarely used for morphological classification.

Therefore, the agreement among galaxy classification systems reflects the importance of the relatively easily measureable B/T and not the nature of the spiral structure. The latter awaits a quantitative, objective, and large-scale analysis.

3.3. Bulges, pseudobulges, and bars

Spirals often have reddish, smooth central components (see Figure 7). As we alluded to in §3.2, these components can be divided into at least three classes: classical bulges, pseudobulges and bars, each of which has different detailed properties and probably different formation mechanisms (Wyse, Gilmore & Franx 1997; Kormendy & Kennicutt 2004). The common interpretation holds that while classical bulges are built by mergers, pseudobulges are built by secular processes within disks, perhaps abetted by the presence of the bar in the bulge component. The formation of the bars themselves and the role of their interaction with the surrounding density field is a matter of debate (Sellwood 2000; Athanassoula 2003; Gadotti & de Souza 2005). We discuss all three components together here because observationally they are difficult to distinguish.

The classical bulges usually but not always contain older stellar populations than the stellar disks that surround them (Moorthy & Holtzman 2006). They are often enhanced in α -elements, but less so than comparably luminous elliptical galaxies and with more scatter (Ganda et al. 2007; Peletier et al. 2007). Dynamically, many are likely “oblate rotators:” consistent with having an isotropic velocity dispersion and being flattened by rotation (Kormendy & Kennicutt 2004, and references therein). Finally, many but not all

have concentrated Sérsic-like profiles with high n . Typically, the larger the bulge-to-disk ratio of the galaxy as a whole, the more concentrated the bulge itself is as well (Graham 2001; Gadotti 2009).

In contrast, as the review of Kormendy & Kennicutt (2004) emphasizes, pseudobulges have significant rotation support, are flatter than classical bulges, have exponential profiles, and have circumnuclear star-formation. Spectroscopically, they tend to have $D_n(4000)$ similar to galaxies on the blue sequence (Gadotti 2009). Although classical bulges lie on the relationship between luminosity and size defined by elliptical galaxies (the Kormendy relation), pseudobulges have lower surface brightness and thus lower luminosity for a given size (Gadotti 2009). Pseudobulges are more common and more dominant in later type (or alternatively, lower B/T ratio) spiral galaxies (Ganda et al. 2006; Barazza, Jogee & Marinova 2008). In this manner they form a continuous sequence of increasing bulge Sérsic index n with bulge-to-disk ratio (Gadotti 2009).

Although photometrically pseudobulges and classical bulges are difficult to disentangle within the same galaxy, integral field spectroscopy allows it more easily. For example, the recent analysis of about 40 galaxies using SAURON suggests that many bulges (of order half of them) may actually consist of both a classical bulge and a pseudobulge, with the pseudobulge occasionally dominating (Ganda et al. 2006; Peletier et al. 2007).

Bars are elongated stellar structures located in the central regions of disk galaxies (Kormendy & Kennicutt 2004; Gadotti 2008a). They are not simply extrema in the distribution of bulge axis ratios, but rather are a separate population (Whyte et al. 2002). Historically, bars have been identified by eye using a variety of (presumably subjective) criteria (de Vaucouleurs 1963; Eskridge et al. 2000). The most widely adopted *quantitative* technique for identifying bars is the ellipse-fitting method, in which a bar must exhibit a characteristic signature in both the ellipticity and position angle profiles (Marinova & Jogee 2007; Barazza, Jogee & Marinova 2008; Sheth et al. 2008). A simplified version of this technique measures the difference in the axial ratio and position angles of a best-fit ellipse to one interior and exterior isophote (Whyte et al. 2002). In general, the visual and ellipse-fitting methods agree about 85% of the time, with egregious disagreement only $\sim 5\%$ of the time (Menéndez-Delmestre et al. 2007; Sheth et al. 2008). In edge-on galaxies, as Combes & Sanders (1981) first pointed out, bars result in “boxy” or “peanut” shaped bulges (Athanasoula 2005; Bureau et al. 2006).

About 50%-70% of luminous spiral galaxies have bars (de Vaucouleurs 1963; Eskridge et al. 2000; Whyte et al. 2002; Marinova & Jogee 2007; Menéndez-Delmestre et al. 2007; Barazza, Jogee & Marinova 2008). The fractional luminosity of the bar relative to the total light varies by more than an order-of-magnitude, ranging from below 2% up to 20% (Elmegreen & Elmegreen 1985; Gadotti 2009). Eskridge et al. (2000) found that the bar fraction in the near-infrared was independent of morphology, while a more recent study by Barazza, Jogee & Marinova (2008) with a considerably larger sample found that the bar fraction is higher in blue, lower-luminosity, late-type disks compared to more massive, red, early-type galaxies. However, bars in early-type galaxies tend to be stronger (i.e., more elongated) and longer, both in an absolute sense and relative to the size of the disk (Kormendy 1979; Elmegreen & Elmegreen 1985; Erwin, Beckman & Pohlen 2005; Menéndez-Delmestre et al. 2007).

Bars are typically dominated by evolved stellar populations (Gadotti & de Souza 2006), although they are also associated with enhanced nuclear and circumnuclear star formation (Ho, Filippenko & Sargent 1997), and frequently exhibit dust lanes, which is a signature of radially inflowing gas (Kormendy 1982; Athanasoula 1992; Sellwood & Wilkinson 1993; Friedli & Benz 1993). Barred galaxies are also observed to have larger reservoirs of molecular gas in their centers relative to unbarred galaxies (Sakamoto et al. 1999; Sheth et al.

2005) and flatter chemical abundance gradients (Zaritsky, Kennicutt & Huchra 1994; Martin & Roy 1994).

Simulations suggest that strong interactions can trigger the formation of a bar (Berentzen et al. 2004). This hypothesis is supported by observations showing that bars are two times more likely to be present in “perturbed” galaxies (i.e., galaxies with a nearby companion), relative to isolated galaxies (Varela et al. 2004). Kannappan, Jansen & Barton (2004) argue similarly that blue bulges, that may be growing due to star-formation today, are more common in close pairs. However, we found no publications describing a large-scale exploration of whether the detailed nature of the bulges or the presence of a bar is otherwise strongly related to environment.

3.4. Atomic and molecular gas content

Most of the baryons in the Universe appear to be in warm or hot gas in the space between galaxies (in groups and clusters, this gas is directly detectable in the X-rays; Mulchaey 2000; Rosati, Borgani & Norman 2002). According to the census of Read & Trentham (2005), about $\sim 80\%$ of the remaining baryons are in stars, and the rest are in atomic gas ($\sim 10\%$) and molecular clouds ($\sim 10\%$). The cold gas is overwhelmingly located in galaxies with gas disks (though not completely absent in ellipticals; §5.8). In particular, luminous spirals tend to have about 10%–20% of their baryonic content in the form of neutral hydrogen and molecular clouds.

The census of atomic hydrogen in galaxies relies on the 21-cm hyperfine transition, either in blind surveys such as HIPASS and ALFALFA, or in compilations such as those of Springob et al. (2005). THINGS has recently released a survey of 34 nearby galaxies with extremely detailed observations (Walter et al. 2008). As an illustration, the top panel of Figure 9 shows the ratio of atomic to stellar gas mass, as a function of stellar mass. The greyscale shows the results from Springob et al. (2005) (using galaxies for which we have the stellar mass from SDSS). The overlaid points are from HI observations of SINGS galaxies (Kennicutt et al. 2003; Draine et al. 2007; Walter et al. 2007; Leroy et al. 2008). Clearly low mass galaxies tend to have much higher atomic gas content than massive galaxies, as has been known for a long time (Young & Scoville 1991).

Determinations of molecular hydrogen mass in galaxies typically rely on carbon monoxide as a tracer, using the CO (1 \rightarrow 0) transition at 2.6 mm (Young et al. 1995). In the middle panel of Figure 9, we show the ratio of H₂ to atomic hydrogen content for the SINGS galaxies. Although for luminous galaxies a substantial fraction of the gas, indeed often the majority, is in molecular form, the fraction appears to decline at lower luminosities. The bottom panel of Figure 9 shows the total gas fraction for SINGS galaxies as a function of stellar mass. Owing mainly to a fractional increase in atomic hydrogen, low mass galaxies are much more gas rich — they have been less efficient at turning gas into stars than their massive counterparts.

A class of spiral galaxies exists with very little atomic gas; they are known as “anemic” or “passive” spirals (van den Bergh 1976; Elmegreen et al. 2002). For spiral galaxies of a given optical diameter and morphological type, those in clusters tend to be “HI-deficient” relative to those in the field, and to have a correspondingly smaller HI radius as well, and are thus more likely to be anemic (e.g., Giovanelli & Haynes 1983; Haynes, Giovanelli & Chincarini 1984; Warmels 1988; Cayatte et al. 1994; Vogt et al. 2004; Boselli & Gavazzi 2006; Levy et al. 2007; Chung et al. 2008). Clearly the atomic hydrogen in galaxies is being affected by the cluster environment, likely by ram pressure stripping or related processes (Gunn & Gott 1972) — often seen in the process of happening, e.g. by Chung et al. (2007) — and at least in some cases is resulting in the stripping of atomic gas from the outside in. Meanwhile, the molecular gas content is not deficient, at least when based on CO tracers (Kenney & Young 1988; van den Bergh 1991; Boselli et al. 1994; Casoli et al.

1998; Boselli & Gavazzi 2006). The high molecular clouds densities may prevent their stripping.

Despite its importance, ram pressure stripping in rich clusters cannot explain the broader segregation of galaxy types, which extends even to small groups (§2.5). In those regions, which do exhibit environmental effects according to galaxy color, most analyses nevertheless have found few H I deficient galaxies (Stevens et al. 2004; Kilborn et al. 2005). In small groups, mergers or other processes might be lowering the HI content while simultaneously altering the galaxy morphology, which would not necessarily result in deficiencies as they are currently defined.

3.5. Star formation

A variety of both direct and indirect techniques have been developed to measure the globally averaged star-formation rates (SFRs) of galaxies, as reviewed in detail by Kennicutt (1998b) (see also Hopkins et al. 2003; Moustakas, Kennicutt & Tremonti 2006; Calzetti 2008). More recently, observations with *Spitzer* and *GALEX* have led to a new class of hybrid SFR indicators that use a weighted combination of UV/optical and infrared luminosity to minimize the systematic effects of dust obscuration (Gordon et al. 2000; Kennicutt et al. 2007; Calzetti et al. 2007; Rieke et al. 2008).

Surveys like the SDSS and *GALEX* have also quantified the star-formation histories of galaxies in unprecedented detail (e.g. Gallazzi et al. 2006; Panter et al. 2007; Cid Fernandes et al. 2007). One method of parameterizing the star-formation history is to measure the birthrate parameter $b = \text{SFR}/\langle\text{SFR}\rangle$, or the ratio of the current rate to the past-averaged rate of star formation (Kennicutt 1983; Kennicutt, Tamblyn & Congdon 1994; Boselli et al. 2001; Brinchmann et al. 2004). The birthrate parameter is also proportional to the *specific* SFR, or the SFR relative to the present-day stellar mass. Analyses using H α (Brinchmann et al. 2004) and UV measurements (Salim et al. 2007; Schiminovich et al. 2007) have shown that b is a slowly declining function of stellar mass ($b \propto M^{-1/3}$). Most galaxies are in a relatively “quiescent” state, with only about 20% in star-bursting systems ($b > 2$; Kennicutt et al. 2005). On this “star-forming” sequence, the surface density of star-formation in galaxies is nearly constant. This relationship is truncated where massive ellipticals begin to dominate the mass function, as their SFRs are often unmeasurably small using these techniques.

Comparison of the local gas surface density with the SFR surface density reveals the relationship first discussed by Schmidt (1959): $\Sigma_{\text{SFR}} \propto \Sigma_{\text{gas}}^n$, with $n \sim 1-2$ (Kennicutt 1989, 1998a; Wong & Blitz 2002; Boissier et al. 2007). Recent results suggest a much more direct relationship between SFR and molecular gas content (Blitz & Rosolowsky 2006; Kennicutt et al. 2007; Bigiel et al. 2008; Leroy et al. 2008). The anemic spiral galaxies with low atomic and molecular gas content (§3.4) show correspondingly low SFRs, probably owing to their low gas surface density (Elmegreen et al. 2002). Interestingly, the efficiency of the conversion of molecular gas into stars is nearly independent of the galaxy type, its larger-scale environment, or the particular local conditions within the galaxy (Rownd & Young 1999; Leroy et al. 2008).

Resolved H α measurements imply a threshold gas density defined by local conditions, below which the SFR is much lower than predicted by the Schmidt law (Kennicutt 1989; Martin & Kennicutt 2001). Typically, the gas density falls below the threshold in the outer disk. Theoretically, such a threshold could be imposed by the Toomre (1964) stability criterion, which predicts the conditions under which disks are stable to collapse and star formation (Schaye 2004). In contrast to the H α results, UV observations from *GALEX* reveal a much smoother transition at large disk radii and few direct signs of a stability threshold (Boissier et al. 2007; Leroy et al. 2008).

As discussed in §2.5, the fraction of galaxies with young stellar populations is a strong function of environment. However, it appears that the details of the star-formation history are not closely related to environment: in fact, long time-scale stellar population indicators such as $D_n(4000)$ and $g - r$ are sufficient to describe the dependence. Shorter time-scale indicators like H δ absorption (Kauffmann et al. 2004) and H α emission (Cooper et al. 2008) are related to $D_n(4000)$ and $g - r$ in a manner that is independent of environment. This result may imply that the time scale for any shut-off of star-formation in dense regions is usually rather long for most galaxies.

Spatially resolved studies of spiral galaxies in clusters suggest that their star formation is most significantly reduced in their outer disks, similar to the results on HI deficiency (Koopmann & Kenney 1998; Vogt et al. 2004; Koopmann, Haynes & Catinella 2006). This effect is likely a further sign of the impact of ram pressure stripping in those regions.

3.6. Dust content

A small fraction, about 0.1%, of the baryonic mass in spiral galaxies is in the form of dust, but its presence is disproportionately important to the evolution of galaxies and our observations of them. Draine (2003) reviews the properties of dust in galaxies, which consists primarily of grains of graphite or silicon a micron or less in size, with between 1%–5% of its mass in polycyclic aromatic hydrocarbons (PAHs). Most of the interstellar Mg, Si, and Fe, and much of the carbon, is in the form of dust grains. Draine et al. (2007) has performed a recent census of the dust content of galaxies using the SINGS sample (see also Dale et al. 2007).

Dust tends to efficiently absorb the UV/optical light emitted by the massive stars produced by recent star-formation. Since the dust temperatures are of order 10–100 K, this light is then reradiated in the infrared (Obrić et al. 2006). Especially in the galaxies with the greatest star-formation rates, the UV/optical light therefore traces only the unobscured star-formation, and IR observations are necessary to determine the rest (§3.5).

The optical dust extinction also of course affects the optical emission and the broad-band colors in the near-infrared and bluer. For galaxy observations, this extinction can be a confusing factor, especially since its impact is highly dependent on the inclination angle of the galaxy disk relative to the line-of-sight (as well as other geometrical effects; Witt & Gordon 2000). Thus, the colors of spirals galaxies are a strong function of their axis ratios, an effect that sometimes needs to be accounted for (e.g., Maller et al. 2009 and references therein).

Like the molecular gas content, the dust-to-gas ratio of galaxies appears to be a strong function of galaxy mass. For example, inclination-dependent reddening is substantially weaker for low mass galaxies (e.g., Tully et al. 1998, Maller et al. 2009). Using a sample of edge-on galaxies, Dalcanton, Yoachim & Bernstein (2004) claim that galaxies with $V_c < 100 \text{ km s}^{-1}$ have no dust lanes. In addition, the low mass galaxies tend to show less dust emission relative to stellar emission, and fewer PAHs relative to dust as a whole (Draine et al. 2007). That low-mass galaxies tend to be less dusty is likely related to their relatively low gas-phase metallicities (§3.7).

3.7. Chemical history

The gas phase chemistry of spiral galaxies also shows some revealing trends, as Figure 2 demonstrates. As shown by Tremonti et al. (2004), mass and metallicity are strongly correlated at low masses, with the metallicities approaching an approximately constant value at masses $\mathcal{M} \gtrsim 10^{10} \mathcal{M}_{\odot}$.

A more revealing measurement than gas phase metallicity is often the *effective yield*: the metallicity relative to the gas fraction. In closed boxed chemical evolution models, the metallicity tracks the gas fraction as $Z = y_t \ln f_{\text{gas}}^{-1}$, where y_t is the nucleosynthetic yield, the fraction of metals that are returned to the interstellar medium by stars. The effective yield is defined as:

$$y_{\text{eff}} = \frac{Z}{\ln f_{\text{gas}}^{-1}}, \quad (3)$$

The ratio y_{eff}/y_t then is simply the metallicity relative to a closed box system with the same gas mass fraction. That is, although the metallicity can be low simply because there has been not much star-formation, if the effective yield is low there must have been some violation of the closed box model (Tinsley 1980; Pagel 1997).

Estimates of the effective yield by Tremonti et al. (2004) and more direct measurements by Garnett (2002) and Pilyugin, Vílchez & Contini (2004) indicate that y_{eff} increases with circular velocity and stellar mass. Assuming that y_t is not a strong function of galaxy mass (as could be the case if the IMF is variable; Köppen, Weidner & Kroupa 2007), this trend implies for low mass galaxies either an inflow of pristine gas or a metal-enriched outflow (Martin, Kobulnicky & Heckman 2002; Veilleux, Cecil & Bland-Hawthorn 2005). However, a detailed analysis by Dalcanton (2007) demonstrates that inflow of pristine gas can only reduce y_{eff} by a limited amount (30%–50% for reasonably gas-rich galaxies) and cannot explain the observed trends. Metal-enriched outflows, on the other hand, are both physically motivated (Mac Low & Ferrara 1999) and can significantly reduce y_{eff} . Although a small but metal-rich outflow may explain the trends, there is no necessity for the ejected fraction of gas to exceed that in high-mass galaxies. In fact, most evidence suggests that low mass systems have the same baryonic fraction as high mass systems and thus have experienced the same fractional outflow (Blanton, Geha & West 2008).

Interestingly, the mass-metallicity relation seems to be a strong function of r_{50} , with the smallest galaxies at a given stellar mass having the highest metallicities (Ellison et al. 2008). These researchers conclude that the most likely explanation is that galaxies with high stellar mass surface densities are those that have most efficiently converted gas to stars. If pristine gas is not remixing from the outer radii of the galaxy, then such galaxies will have lower gas fractions locally and thus higher metallicities. In this context, it is tempting to note that the smallest spirals at a given stellar mass are the early type spirals, a possibly related fact.

This mass-metallicity relationship for spiral galaxies appears to be only a weak function of galaxy environment (Mouhcine, Baldry & Bamford 2007; Cooper et al. 2008). There are 0.02 dex trends with respect to environment, though these are small relative to the overall distribution of metallicities. According to Cooper et al. (2008), the noise in their environmental indicators may be washing out a stronger existing relationship, and these trends might explain about 15% of the scatter in the mass-metallicity relationship.

3.8. Disk edges and extended galactic disks

The optical surface brightness profiles of galaxy disks often exhibit a sharp edge, around 3–5 times the exponential scale length (van der Kruit 2001). Typically, at the edge the surface brightness dips below 25–26

mag arcsec⁻² in B , motivating classical parameters such as R_{25} (the radius at which $\mu_B = 25$ mag arcsec⁻²; de Vaucouleurs et al. 1991) and the Holmberg (1958) radius (where $\mu_B = 26.5$ mag arcsec⁻²).

However, it has recently been recognized that for many disk galaxies this truncation is not complete (Pohlen et al. 2004). The census of Pohlen & Trujillo (2006) finds that while about 56% exhibit a downward break (either a classical sharp break or one described by a steeper exponential profile), about 24% exhibit a shallower exponential profile on the outside (e.g. Erwin, Beckman & Pohlen 2005), and 10% exhibit no measurable break. Apparently the latter category includes some galaxies that extend up to 10 scale radii (e.g., NGC 300; Bland-Hawthorn et al. 2005). Pohlen & Trujillo (2006) found that the remaining 10% of their sample were more complicated and consisted of a mix of breaks.

Meanwhile, the neutral gas in galaxies as seen at 21-cm tends to extend considerably further than the disk break, typically by a factor of two (see the recent compilation by the Westerbork HI survey; Swaters et al. 2002). Therefore, the break in optical light could relate to the similar breaks implied by H α measurements of spatially resolved star-formation (§3.5).

It has recently become clear that even beyond the edges of stellar disks star-formation can still occur, which may explain why some galaxies have no downward break or edge. Thilker et al. (2007) has recently reported from *GALEX* imaging that over 20% of spiral galaxies have significant UV emission in the outer disk. As one might expect, the HII regions associated with the UV emission are low metallicity, typically 10%–20% solar (Gil de Paz et al. 2007). Galaxies with such disks tend to be gas-rich relative to other spirals at the same luminosity, and overdensities in the gas distribution tend to correlate with the UV light. Similarly, Christlein & Zaritsky (2008) detect H α up to $1.5 \times R_{25}$ on average and up to $2 \times R_{25}$ in some galaxies. Such galaxies consist of rotating disks with flat rotation curves. Both of these sets of results indicate that some star-formation can occur at large radii where most of the gas is stable against collapse, probably due to local disturbances and overdensities.

3.9. Tully-Fisher relation

The gas and (thin-disk) stars in spiral disks orbit coherently in nearly circular orbits around the galactic center: they are “rotation-supported” objects. At high luminosity at least, spiral galaxies often have flat or peaked rotation curves, allowing one to define a maximum circular velocity V_c or an asymptotic circular velocity V_a , which are often but not always similar. The most commonly used tracers of the outer disk dynamics are H α and H I emission, with the latter generally detectable at larger galactic radii than the former. The full details of measuring the internal rotation curves were recently reviewed by Sofue & Rubin (2001), and the mass-modeling of these data are the subject of considerable debate (e.g., most recently Barnes, Sellwood & Kosowsky 2004; Dutton et al. 2005; Kassin, de Jong & Weiner 2006; Spano et al. 2008). We concentrate here on the global dynamics.

According to the well-established Tully & Fisher (1977) relation (TF), galaxy luminosity L is related to V_c as a power-law $V_c \propto L^\alpha$ at high luminosities, with some scatter. Figure 10 illustrates the I -band TF relation for luminous galaxies from Courteau et al. (2007). In virtually all analyses, an attempt is made to correct for internal extinction within each galaxy, which in general is a complex function of type, luminosity, and inclination (Tully et al. 1998; Maller et al. 2009). The slope of the TF relationship is usually determined using a linear regression, either of $\log_{10} V_c$ on $\log_{10} L$ (the “inverse” TF relation) or vice-versa (the “forward” TF relation).

Because of the scatter, the inverse and forward TF relations do not have slopes that are simply inverses of each other — α will be larger if the forward fit is performed, by an amount that depends on the selection effects and error distribution of the sample. Courteau et al. (2007) instead use a bisector method that accounts for uncertainties in both variables. We do not advocate any one method; in practice, the correct choice depends on the error distributions, the sample selection effects, and the desired goals. The most complete discussion of these issues remains Strauss & Willick (1995), but see Masters et al. (2006) for a more modern view. We simply point out that the TF relations derived from different groups differ due to such choices.

Recent compilations (Verheijen 2001; Kannappan, Fabricant & Franx 2002; Masters et al. 2006; Pizagno et al. 2007; Courteau et al. 2007) find $\alpha \sim 0.27\text{--}0.35$, with a scatter equivalent to about 0.15–0.4 mag in the luminosity direction. The low scatter holds for Courteau et al. (2007) and other samples that were selected for simplicity and for best distance-measure performance. The higher scatter value from Pizagno et al. (2007) occurs because they use a wider range of morphological types, in particular including “peculiar” systems and barred galaxies. The TF slope is a function of bandpass, with α decreasing towards longer wavelengths, as one might expect as spirals become redder with increasing mass (cf. Figure 8).

The residuals from the TF relation in red bands (such as SDSS i or Bessell I) usually appear to be only weakly related to any other properties, suggesting they are dominated by the dark matter to stellar mass ratio variation. For bluer bands like g there are residuals associated with color, expected since in those bands the stellar mass to light ratio varies with color (Bell & de Jong 2001; Pizagno et al. 2007). In red bands, the strongest residuals appear to be the tendency for earlier-type (Masters et al. 2006; Courteau et al. 2007) or more concentrated or redder spirals (Kannappan, Fabricant & Franx 2002; Pizagno et al. 2007) to have higher α . In particular, at $V_c \sim 250 \text{ km s}^{-1}$, Sa galaxies are less luminous than later types by roughly 0.5 mag.

Although the standard TF relation is appropriate for massive galaxies, for less massive galaxies, for example where $V_c < 100 \text{ km s}^{-1}$, it has considerably more scatter and deviates from a power law — galaxies at a given circular velocity are less luminous than the high luminosity TF would predict (e.g., McGaugh 2005). As we saw above, at these scales the disk gas mass starts to become dominated by the gas contribution. By including the neutral and molecular gas mass to define a total baryonic mass, McGaugh (2005) and Begum et al. (2008) claim that the TF power law continues even to these scales. This change probably reflects a decrease in the time-averaged efficiency of turning baryonic matter into stars in lower mass galaxies.

These dynamical relationships appear to be at best a weak function of environment for luminous galaxies. For example, in a sample of 165 galaxies, Pizagno et al. (2007) found no evidence of environmental dependence. A hint of dependence is seen in the lower luminosity sample of Blanton, Geha & West (2008) at $V_c < 70 \text{ km s}^{-1}$.

4. Lenticulars

The lenticular galaxies, or S0s, are classified in the Hubble sequence in between the spiral population and the ellipticals. They are disk galaxies, but like ellipticals are smooth, concentrated, and have low specific star-formation rates (Caldwell et al. 1993). They are distinct from the anemic spirals (§3.5), in that they have very little molecular gas or spiral structure. However, some S0 galaxies might form from anemic spirals whose spiral wave pattern has disappeared due to its short-lived nature (Elmegreen et al. 2002), possibly

aided by tidal “harassment” in dense regions (Moore, Lake & Katz 1998).

Figure 11 shows some images of typical lenticular galaxies as classified by NED. For this figure, we rejected through visual inspection about one-quarter of the NED classifications as being clearly incorrect (ambiguous cases were kept). The broad-band properties of S0s are shown as the orange points in Figure 12. Evidently, in these properties they are practically inseparable from ellipticals.

Consequently, though there is a clear physical distinction between Es and S0s, few researchers have implemented objective measurements on large data sets that neatly separate the two populations. Visual classification schemes usually rely on the axis ratio, which for inclined S0s makes their disk-like nature clear, or the strong break in surface brightness at their disk edge (similar to that of spirals; §3.8). However, S0s with a ring or multiple rings are also obvious visually, and barred S0s can exhibit the upturn in radial profile discussed in §3.8. S0s are of particular interest because they appear to be structurally similar to spirals, but to have ended their star-formation.

Given their observed properties, the most compelling question about S0s is whether they are spirals that ran out of gas and faded onto the red sequence. One simple way of testing this hypothesis is to ask whether they scatter to low luminosities in the Tully-Fisher relation, as we would expect for a faded population. Our understanding of the Tully-Fisher relation is poorer for S0s than spirals because S0s lack significant $H\alpha$ or 21-cm emission, making dynamical mass estimates challenging. Nevertheless, beginning with Dressler & Sandage (1983), a number of investigators have tried to measure S0 dynamics using stellar absorption lines, which generally yield lower signal-to-noise velocities. Bedregal, Aragón-Salamanca & Merrifield (2006) compile a set of dynamically analyzed S0 measurements and find that the S0 Tully-Fisher relation is offset in the K -band from that of spirals by about 1 mag (see also Hinz, Rieke & Caldwell 2003). In Figure 10, we show these S0 galaxies in the I band, where the offset is closer to about 1.5 mag relative to the spirals in Courteau et al. (2007); naturally, the actual offset depends on the Tully-Fisher zeropoint and is somewhat uncertain.

This offset is about what one would expect if S0s were simply “faded” versions of spiral galaxies, whose star-formation had shut-off several billion years ago, but were otherwise well represented by the early-type spiral population today. In this manner, the S0s may form a continuum with the Sa galaxies or other red spirals, which as noted in §3.9 are also offset from Tully-Fisher by about 0.5 mag (at high V_c at least). Similar conclusions result from the study of globular cluster populations, which are substantially more frequent per unit luminosity in S0s than in spirals of similar mass; this trend would result if the stellar population faded while the globular cluster population remained unchanged (Barr et al. 2007).

However, one might naïvely expect that if S0s are merely dead spirals then the luminosity and surface brightness distributions of S0s would be systematically fainter than that of spirals, at least within a common environment. A recent analysis of Burstein et al. (2005) instead showed that S0s tend to be brighter than any other spiral type even at fixed environment. Similarly, Sandage (2005) shows that the typical surface brightness of S0s is larger than that of spirals. Similar trends can be seen in Figures 8 and 12. In more detail, S0s have larger bulge-to-disk ratios than could result from fading disks in early-type spirals (Dressler 1980; Christlein & Zabludoff 2004). As a cautionary note, analyses that account for the bar and a general Sérsic profile for the bulge indicate much smaller bulges for S0s and might change this conclusion (Laurikainen, Salo & Buta 2005).

These latter facts support a hypothesis that mergers (which would increase the overall stellar mass) are responsible for the transformation of S0s. If mergers sparked globular cluster formation they might also account for the increased globular cluster frequency. However, merger scenarios have a hard time explaining

the S0 Tully-Fisher relation unless the progenitor population was quite different from any that exists in abundance today.

Interestingly, the dependence of S0 fraction and S0 properties on environment has not been studied with the new, large samples available, in large part due to the difficulty in identifying them automatically or unambiguously. Thus, while Dressler et al. (1997) show that S0s become relatively more frequent as one approaches the centers of clusters, no significant improvement or refinement of that measurement has been undertaken for the nearby Universe.

5. Ellipticals

5.1. General description and identification

Elliptical galaxies are recognizable by their smooth, symmetric, and deceptively simple-looking appearance. Figure 13 shows some typical elliptical galaxies drawn from the SDSS, using the classifications reported by NED. In this case, we had to reject about one-third of the classifications as obviously incorrect. Figure 12 shows the distribution of their broad-band properties along with the S0s. They are concentrated, uniformly red, and follow a reasonably tight size-luminosity relation.

The past two decades of research, however, have revealed the complexity of their dynamical structure, their star-formation history, and their assembly history. In general terms they are dynamically supported by velocity dispersion, but often with significant rotational support as well. Their stellar populations are old, ongoing star-formation is rare, and their cold gas content is low (around or less than 1%). However, there are numerous indications that at least some ellipticals were assembled late, after the hey-day of their star-formation. In addition, the small amount of star-formation that does occur in ellipticals seems to be similar in nature to that in spirals: molecular clouds in gas disks forming stars, at the same (low) efficiency found in spirals.

Among luminous ellipticals there are two discernible classes, those with and without cores (§5.3; Kormendy et al. 2009 and references therein). The ellipticals with nuclear cores, relative to those without, tend to be more luminous, have b/a closer to unity, have boxier isophotes, less rotational support, and more signs of triaxiality.

Among lower luminosity ellipticals there are at least three classes: low surface brightness, exponential galaxies typed as dE or sometimes Sph (such as NGC 205); high surface brightness, concentrated galaxies usually typed as cE (such as M32); and ultra-compact dwarfs with r_{50} as small as 10 pc (Drinkwater et al. 2004). Kormendy et al. (2009) reviews the distinction between the first two classes, arguing that the cE population is most similar to the giant elliptical population. Ferrarese et al. (2006) presents the alternative argument for dE galaxies.

Relative to S0s, the surface brightness profiles of ellipticals appear to have no “edge,” as S0s do. However, in their other properties — sizes, profile shapes, colors, symmetry, and smoothness — Es and S0s are very similar. Thus, the recent literature on very large samples is plagued with “elliptical” or “early-type” samples that actually include a fair number of S0s as well as early-type or edge-on spirals. Interestingly, these interlopers do not appear to affect many of the scaling relations we discuss here; nevertheless, they can be important in some circumstances and we emphasize again the importance of separating these two populations.

5.2. Structural trends

Although many astrophysicists typically think of ellipticals as de Vaucouleurs profile galaxies, in fact they have a range of Sérsic indices, whose values depend rather strongly on luminosity (as has been recognized for a long time; Caon, Capaccioli & D’Onofrio 1993; Prugniel & Simien 1997). The first row of Figure 6 shows this distribution, which reveals that selecting ellipticals using a strict cut in Sérsic index will exclude a significant (and luminosity-dependent) fraction of viable elliptical galaxy candidates. Kormendy et al. (2009) demonstrate this trend most clearly with a careful analysis of elliptical surface brightness profiles.

These structural trends are mostly independent of environment, as Figure 6 shows (Blanton et al. 2005a; Park et al. 2007). With the exception of the most luminous cases, red galaxies of a given luminosity are no more or less likely to be concentrated when they are found in dense regions. This result suggests that any process that turns spiral galaxies into ellipticals acts similarly in dense and underdense regions.

One shortcoming of the 2D Sérsic profile is that when examined carefully few ellipticals actually have precisely elliptical isophotes. One way of quantifying this non-ellipticity is to consider the residuals of the actual isophotes relative to perfect ellipses. If one Fourier transforms these residuals, the $\cos 4\theta$ term is of order 1% of the isophotal radius for many ellipticals (Bender & Moellenhoff 1987). The fractional amplitude of this term a_4/a is defined such that positive values are “diskier” than ellipses while negative values are “boxier.” Generally, boxy galaxies are more luminous than disk galaxies and more likely to exhibit a core (e.g., Kormendy & Djorgovski 1989; also see §5.4).

5.3. Nuclear properties

The structure of the central regions of ellipticals are now observable for large samples using *HST* imaging (Ferrarese et al. 2006; Lauer et al. 2007a; see in particular the review of Kormendy et al. 2009). Although these analyses have varied in their details, they all find that the central stellar mass surface density profiles can reasonably be modeled as a power law $\Sigma(r) \propto r^{-\gamma}$. As defined by Lauer et al. (1995), galaxies with $\gamma \sim 0.0$ – 0.3 are classified as “cores,” and galaxies with $\gamma \sim 0.5$ – 1.0 are classified as “cusps,” or sometimes “power-law,” “extra-light,” or just “coreless.” There are of course galaxies in between the extremes (Rest et al. 2001).

The ellipticals with cores are the most luminous galaxies, with $M_V - 5 \log_{10} h < -21$, and correspondingly have distinctly higher global Sérsic indices, boxier isophotes, slower rotation, and more triaxiality (Ferrarese et al. 2006; Lauer et al. 2007a; Kormendy et al. 2009). An oft-used model for the shapes of elliptical galaxy cores is the “Nuker” model introduced by Lauer et al. (1995), which is close to a broken power law. This model does not accurately reflect the surface brightness profiles of ellipticals at galactic radii larger than r_{50} , which tend to be closer to Sérsic profiles. Consequently, several researchers (e.g., Kormendy 1999; Trujillo et al. 2004; Ferrarese et al. 2006) have suggested the use of a Sérsic model altered to transition to a power law near the center. These cores are thought to be scoured by the gravitational effects of binary black holes during mergers (for a review see Kormendy et al. 2009).

For $-21 < M_V - 5 \log_{10} h < -18$, ellipticals tend to be cuspy (Ferrarese et al. 2006). Relative to the Sérsic models, these coreless galaxies often actually have an “extra light” component. The central light typically has isophotes that deviate from ellipses, being “diskier” ($a_4/a > 0$). If cuspy elliptical galaxies form in mergers, the diskiness of the central light components suggest that the last of these mergers should have been “wet,” with dissipative processes triggering star-formation and raising the central stellar surface density, and swamping the effects of black hole scouring (Kormendy et al. 2009).

5.4. Fundamental plane and dynamics

The SDSS survey has provided an unprecedented sample of galaxies with reliable spectroscopic velocity dispersions, allowing a detailed analysis of the fundamental plane (FP; Djorgovski & Davis 1987; Faber et al. 1987) — the tight relationship among r_{50} , half-light surface brightness I_{50} , and velocity dispersion σ . Bernardi et al. (2007) selected nearby early-types according to concentration, color and emission line strength and found that for a relationship like $r_{50} \propto \sigma^\alpha I_{50}^\beta$, the best fit is ($\alpha \sim 1.3$, $\beta \sim -0.76$), in only mild disagreement with the previous findings of Jørgensen, Franx & Kjaergaard (1996) based on more local samples ($\alpha \sim 1.25$, $\beta \sim -0.82$).

The FP differs from a naïve prediction based on the virial theorem. From dimensional analysis, $\mathcal{M} = c\sigma^2 R/G$, where c is a structural constant that depends on the orbital structure, the mass density profile, the surface brightness profile, and an appropriately weighted mass-to-light ratio, R is a characteristic radius, and G is the gravitational constant. Indeed, the rotation of these parameters into the κ -space of Bender, Burstein & Faber (1992) was motivated by this virial interpretation. In this case, for a constant mass-to-light ratio the FP parameters become ($\alpha = 2$, $\beta = -1$), rather different than the observed ones. Several possible explanations exist for the deviation from this relation: (a) a variation of the stellar mass to dynamical mass ratio; (b) a variation of the stellar mass-to-light ratio; or (c) “non-homology,” that is, a variation in the nature of ellipticals that changes c . Most analyses now favor the first explanation, with a dynamical to stellar mass ratio that scales as $(\mathcal{M}_{\text{dyn}}/\mathcal{M}_*) \propto \sigma^{0.86}$.

First, spectral synthesis modeling suggests that very little of that variation can be attributed to the stellar mass-to-light ratio (Padmanabhan et al. 2004; Bernardi et al. 2006; Trujillo, Burkert & Bell 2004; Proctor et al. 2008). Second, detailed modeling of the 2D dynamics using integral field measurements generally finds a variation of $\mathcal{M}_{\text{dyn}}/\mathcal{M}_*$ that is quantitatively similar to the virial estimates that assume homology (Cappellari et al. 2006; Thomas et al. 2007). Third, direct constraints on mass density profiles with strong gravitational lensing indicate that the dynamical mass to light ratio is changing (Bolton et al. 2008).

Nevertheless, as Cappellari et al. (2006) notes, it is curious that the simple virial estimate yields the same mass-to-light ratio trends as more complex and direct modelling. After all, the assumptions of homology must be wrong in detail, as Trujillo et al. (2004) point out. Cappellari et al. (2006) further caution that the virial estimate only works if the de Vaucouleurs estimate of r_{50} is used — notwithstanding the fact that the de Vaucouleurs model is incorrect for many of these galaxies!

The FP is a weak function of environment, as with all other scaling relationships. For example, Park et al. (2007) shows that the Faber-Jackson relationship does not vary significantly. The FP analysis of Bernardi et al. (2006) detected a 0.1 mag surface brightness shift between the highest and lowest density subsamples, which they estimated was consistent with an age difference of 1 Gyr between cluster and field ellipticals (see §5.7).

The apparent simplicity of the FP relationship masks a good deal of variability and complexity in elliptical dynamics. For example, ellipticals are known to occasionally contain multiple kinematically distinct components (Efsthathiou, Ellis & Carter 1982), often in the form of rotating disks around the core (Bender 1988). In addition, the kinematics is often misaligned with the photometry or twists as a function of radius, often interpreted as a sign of triaxiality (e.g., Binney 1978; Schechter & Gunn 1979). The recent analysis of SAURON data has greatly increased our understanding of the variety and incidence of kinematic substructures and other features (e.g., Krajnović et al. 2008).

The FP also masks the importance of rotation to the global dynamics of many ellipticals. Tradition-

ally, this importance has been quantified by the ratio of rotation speed to central velocity dispersion, V/σ (originally due to Illingworth 1977, but see the latest discussion of Binney 2005). Using SAURON data, Cappellari et al. (2007) argue for a different estimator $\lambda_R = \langle R|V| \rangle / \langle R\sqrt{V^2 + \sigma^2} \rangle$, where the averages are weighted by flux. This measurement requires 2D velocity maps but is apparently a better tracer of the angular momentum content than V/σ , which is more significantly affected by kinematically decoupled cores as well as projection effects.

Figure 14 shows the distribution of λ_R from Emsellem et al. (2007), for the SAURON sample of Es and S0s. The upper left panel shows the relationship between angular momentum content and virial mass M_{vir} . The red points are the “slow rotators” according to the SAURON definition ($\lambda_R < 0.1$). For comparison, in the bottom two panels we also show the distribution of the isophotal shape parameter a_4/a (§5.2) as a function of both M_{vir} and λ_R . The upper right panel of Figure 14 shows λ_R versus the observed ellipticity ϵ within r_{50} . Overplotted is the approximate curve for an oblate rotator with an isotropic velocity dispersion, seen edge-on.

The most massive systems have a strong tendency to be the slowest rotators, the closest to perfect ellipsoids, and the most axisymmetric. Relative to the “fast rotators,” these slow rotators tend to have higher masses, flat or falling λ_R profiles, less cuspy centers (§5.2), more boxy isophotes, more kinematically decoupled cores, and greater kinematic misalignments (indicating triaxiality). It is difficult to tell with the available data whether there are some independent relationships among these properties that are responsible for the others. However, the overall trend is suggestive of the importance of major dry mergers in the formation of these systems (e.g., Hernquist 1993), but perhaps not minor dry mergers (Burkert et al. 2008).

The lower mass systems have a stronger tendency to be “disky” and are faster rotators. They tend to have disk-like isophotes as well as aligned kinematics and photometry without twists (consistent with the importance of rotation; Cappellari et al. 2007). Detailed analysis of their 2D dynamics suggests that they tend to have anisotropic velocity dispersions, as their positions in the upper right panel of Figure 14 suggests (Cappellari et al. 2007). Interestingly, the S0s, while always fast rotators, do not appear to be particularly distinct from fast rotator ellipticals in their dynamics (though the SAURON analysis is limited to radii $\lesssim r_{50}$).

Thus, though the FP is simple and appears to remain relatively constant with environment, there are still only small samples available with truly detailed 2D dynamics ($\lesssim 100$ nearby ellipticals total). Thus, nobody has explored whether these more detailed properties vary with environment even as the FP remains relatively constant; such a detection would be an important constraint on formation mechanisms.

In this section (as in this review as a whole) we have focused mainly on the properties of the luminous galaxies. Just as dwarf disk galaxies deviate from the Tully-Fisher relation, the dE galaxies deviate from extrapolations of the FP (Geha, Guhathakurta & van der Marel 2003; van Zee, Skillman & Haynes 2004), while cE galaxies do not (Kormendy et al. 2009). However, low luminosity ellipticals do follow a more general, but still regular, relationship described by Zaritsky, Gonzalez & Zabludoff (2006), a “fundamental manifold” for spheroids.

5.5. Brightest cluster galaxies and cD galaxies

Among ellipticals, brightest cluster galaxies (BCGs) and cD galaxies form a special class (Morgan & Lesh 1965; Sandage 1972). BCGs are usually defined as the highest optical luminosity galaxy in any reasonably

massive cluster ($> 10^{14} \mathcal{M}_\odot$). A large fraction of BCGs have a larger associated distribution of stars that extends out into the host cluster, called the “cD” envelope for historical reasons, but sometimes referred to as the “intracluster light” (ICL).

In Figure 12, BCGs and galaxies with cD envelopes are shown as the magenta dots. BCGs are luminous and massive, with a log-normal distribution of stellar mass with a mean of $\mathcal{M}_* \sim 2 \times 10^{11} h^{-2} \mathcal{M}_\odot$ and dispersion $\sigma_{\ln \mathcal{M}} \sim 0.4$ (Lin & Mohr 2004; Hansen et al. 2009; Yang, Mo & van den Bosch 2008). These luminosities are a function of the host cluster mass, with $L_K \propto \mathcal{M}_h^{0.2-0.3}$ for massive clusters (Lin et al. 2004; Hansen et al. 2009) and a steeper relationship at lower masses (Yang et al. 2007; Brough et al. 2008). Thus, as the total halo mass and luminosity rises, the fractional contribution of the BCG decreases.

Tremaine & Richstone (1977) found hints that BCGs were not merely the brightest members of a randomly sampled luminosity function for each cluster. In particular, the second brightest galaxy is normally at least 0.8 mag fainter than the first. In contrast, if the luminosities randomly sampled almost any conceivable distribution, then the expected magnitude “gap” between the first and second ranked cluster galaxies would be about the same or less than $\sigma_{\ln \mathcal{M}}$, or about 0.4 mag (Vale & Ostriker 2008; Loh & Strauss 2006). This “gap” in magnitude suggests an anti-correlation among galaxy luminosities within the same cluster.

The dry merger, or cannibalism, scenario for the growth of BCGs is consistent with the last two results. First, the dynamical friction time scales for galaxies tends to increase as the host cluster mass increases, explaining why a smaller fraction of the cluster luminosity is accreted onto the central galaxy as mass increases (Cooray & Cen 2005). Second, if the second ranked galaxy is close in mass to the BCG, it is drawn preferentially to the BCG and will merge with it. This process will open a gap between the masses and luminosities of the first and second ranked galaxies (for recent analyses see Loh & Strauss 2006; Milosavljević et al. 2006).

Other hints that BCGs are special come from comparing their fundamental plane relation to that of other ellipticals. This comparison is complicated by the fact that BCGs are much brighter than the typical elliptical. Oegerle & Hoessel (1991) reported that BCGs roughly followed the fundamental plane defined by lower luminosity galaxies. However, above $M_r - 5 \log_{10} h \sim -22.3$ and $\sigma \sim 280 \text{ km s}^{-1}$, the velocity dispersion of BCGs becomes a weaker function of luminosity, causing a deviation from the extrapolation of the fundamental plane. This weakening has been verified in modern data sets (Lauer et al. 2007b; von der Linden et al. 2007; Bernardi et al. 2007; Desroches et al. 2007). However, at luminosities where BCGs and elliptical populations overlap, the differences in their velocity dispersions are $< 5\%$ (von der Linden et al. 2007; Desroches et al. 2007).

Several large studies based on SDSS also indicate that the most luminous BCGs typically are larger than the radius-luminosity relation for typical ellipticals would predict ($r_{50} \propto L^\alpha$, with $\alpha \sim 0.6$). Either BCGs and other ellipticals lie on different loci in r_{50} - L space, or the locus they both live on is curved such that r_{50} is a stronger function of L at high luminosity. In fact, there is evidence that both effects exist. At higher luminosities, the non-BCG ellipticals appear to deviate from a power-law relation (Desroches et al. 2007; von der Linden et al. 2007), with a local power law α varying from 0.5 at $M_r - 5 \log_{10} h \sim -20$ to 0.7 at $M_r - 5 \log_{10} h \sim -24$. Simultaneously, BCGs appear to be larger than non-BCGs at a given magnitude, but the literature has not converged on the details. von der Linden et al. (2007) find that the BCGs are all 10% larger on average than non-BCG ellipticals, constant with luminosity, defining a slightly different fundamental plane. Desroches et al. (2007), meanwhile, find that the BCGs define a steeper relationship than the ellipticals, and that at $M_r - 5 \log_{10} h \sim -22$ the typical BCG is smaller than the typical elliptical. Bernardi et al. (2007) also find a steeper slope for BCGs, but that the relationships converge near $M_r - 5 \log_{10} h \sim -22$.

These results suffer from two major systematic effects. First, there are some significant ambiguities in defining a “BCG”, particularly for cluster catalogs (e.g., Miller et al. 2005) based on an incomplete redshift survey like the SDSS (even 5%–10% incompleteness matters; see von der Linden et al. 2007). Second, BCGs are large objects on the sky, and their photometry is not handled correctly by the SDSS (§3; Lauer et al. 2007b). All of the work cited here either reanalyzes the images (Bernardi et al. 2007; Desroches et al. 2007) or corrects the catalog parameters in an ad hoc way (von der Linden et al. 2007). No cross-comparison of their analyses has been published.

Many BCGs have an extended distribution of stars that is inconsistent with a single de Vaucouleurs profile extrapolated from small radii, or even with a more general Sérsic profile, known as a cD envelope or the ICL. Mihos et al. (2005) found that the Virgo Cluster has a particularly dramatic ICL component, with visible streams and other features that might suggest a tidal stripping or merging scenario for its formation. For a large sample of clusters, Gonzalez, Zabludoff & Zaritsky (2005) recently showed that detected ICL components are often discernably separate entities from the host BCGs, with well defined transitions in the surface brightness profile, axis ratio, and position angle. Zibetti et al. (2005) stacked images of many different SDSS clusters and statistically detected the ICL component. Zibetti et al. (2005) and a study of individual detections by Krick & Bernstein (2007) both conclude that of order 5%–20% of the total cluster optical light within 500 kpc or so comes from the ICL; the results of Gonzalez, Zabludoff & Zaritsky (2005) imply even more. If so, the stellar mass in the ICL is comparable to that in the BCG itself (or possibly 4–5 times the BCG mass if the analysis of Gonzalez, Zabludoff & Zaritsky 2005 is correct). Its existence appears consistent with the merger hypothesis for BCGs themselves.

The dynamics of the ICL component is poorly known in most cases, and it is unclear to what degree it represents the dynamics of the cluster as a whole. Some BCGs show the rising velocity dispersion profile at large radius expected from the cluster dark matter distribution (most notably those found in Dressler 1979; Kelson et al. 2002). However, the large studies of Fisher, Illingworth & Franx (1995) and Loubser et al. (2008) find that only a minority of cD envelopes have such a profile. Interestingly, detectable rotation is seen in a number of cD envelopes, with $V/\sigma \sim 0.3$.

5.6. Deviations from smooth profiles

In addition to boxiness and diskiness, elliptical galaxies often show other deviations from smooth elliptical isophotes, at least at very faint levels (Kormendy & Djorgovski 1989). The most common deviation from smoothness is due to dust features; as we outline in §5.8, many elliptical galaxies have a small but detectable amount of cold gas and associated dust. For example, Colbert, Mulchaey & Zabludoff (2001) find that about 75% of ellipticals have detectable dust extinction in the optical, irrespective of environment.

Elliptical galaxy profiles also often reveal shells or ripples, and other signs of recent interaction (Athanasoula & Bosma 1985). While Malin & Carter (1983) found that about 10% of all ellipticals had detectable features, perhaps unsurprisingly it appears that deeper observations reveal structure in a larger fraction. van Dokkum (2005) find that 70% of ellipticals have detectable tidal features down to 27–28 mag arcsec⁻². For about 20% of those detections, a secondary object that appears responsible for the features is observed. These observations suggest that some growth of elliptical galaxies occurs through merging; however, precisely how much is difficult to infer from such observations. Colbert, Mulchaey & Zabludoff (2001) also searched their sample for tidal features, finding that the fraction of disturbed ellipticals is a strong function of environment, more common in isolated regions than in groups and clusters. Finally, ellipticals with more fine structure tend to

be slightly bluer than those with less (Schweizer & Seitzer 1992) and perhaps lie on the bright side of the fundamental plane (Michard & Prugniel 2004).

A final deviation from a purely elliptical profile is that of isophotal twists. These features, which can be caused by triaxiality or by tidal effects, appear to be rare: a survey of Virgo ellipticals using *HST*/ACS reported only seven cases of isophotal twisting (some of these very marginal or related to central disks) out of 100 observed early-type galaxies (Ferrarese et al. 2006).

5.7. Stellar populations

The spectra of elliptical galaxies are dominated by emission from the surfaces of stars, typically K giants but comprising some mixture of stellar types depending on the age, metallicity, and metal abundances of the stellar population. For this reason ellipticals all have nearly the same optical broad-band color, with a weak dependence of color on galaxy luminosity (and equivalently, stellar mass or velocity dispersion). This dependence is due to both age and metallicity trends as a function of mass, as detailed spectroscopic analyses reveal. Renzini (2006) review the subject in detail. However, in brief, Balmer absorption lines such as $H\gamma$, $H\delta$ and $H\beta$ tend to trace age in old stellar populations, while metal-line indices such as $\langle Fe \rangle$ and Mg b yield information about the metallicity and α abundances in the stellar atmospheres.

Based on high signal-to-noise optical spectroscopy of morphologically selected E and S0 galaxies, Thomas et al. (2005) show that the metallicity (or iron abundance) and $[\alpha/Fe]$ ratio are both correlated with velocity dispersion (or mass). As found previously, the Mg b indicator is much more tightly correlated to mass than $\langle Fe \rangle$ (e.g. Worthey 1998 and references therein). Similar results have also been found with large samples of (lower signal-to-noise) SDSS galaxies (e.g., Eisenstein et al. 2003; Bernardi et al. 2006; Gallazzi et al. 2006; Jimenez et al. 2007).

Many ellipticals show evidence for recent star formation in their optical spectra, and the incidence is higher in lower-mass galaxies (Trager et al. 2000; Thomas et al. 2005). These conclusions have been strengthened by recent observations with *GALEX*. Yi et al. (2005), Kaviraj et al. (2007), and Schawinski et al. (2007) have all found evidence for recent ($\lesssim 1$ Gyr) star formation in 15%–30% of morphologically selected elliptical galaxies, which accounts for 1%–3% of the stellar mass of the galaxy.

There appears to be some variation of these star-formation histories with environment. Figure 15 shows $H\beta$, $\langle Fe \rangle$ and Mg b as a function of velocity dispersion σ for E/S0 galaxies from Thomas et al. (2005). Filled symbols correspond to galaxies in dense regions, while unfilled symbols are for galaxies in underdense regions. They appear to lie on somewhat different loci. According to Thomas et al. (2005), based on these results the field early-type galaxies are on average ~ 2 Gyr younger and slightly more metal-rich, while both populations show comparable $[\alpha/Fe]$ ratios. Bernardi et al. (2006) found qualitatively similar results, though with a rather different analysis technique. Schawinski et al. (2007) further found that early-types with recent star formation were more prevalent in low density environments, even after controlling for the fact that lower-mass (massive) galaxies are found preferentially in underdense (dense) regions.

The nature of elliptical galaxy stellar populations is an old, storied, and quite controversial one, and the limited space here cannot do it justice. However, we do note several investigations that have reached conclusions in conflict with those described above. First, recent *Spitzer* observations of the mid-IR (9–12 μm) spectra of ellipticals in nearby clusters have found that the vast majority are consistent with being purely passively evolving systems (Bressan et al. 2006; Bregman, Temi & Bregman 2006). Second, Trager, Faber & Dressler

(2008) find that early-type galaxies in the Coma cluster show the same mean age as field ellipticals (though less scatter). The exact nature of the recent star formation in ellipticals, and its variation with environment, therefore appears to be in some doubt.

5.8. Cold gas content

Elliptical galaxies contain a small amount of cold atomic and molecular interstellar gas (Faber & Gallagher 1976). When detected, the gas comprises $\lesssim 1\%$ of the total mass of the system (Knapp, Turner & Cunniffe 1985), so it is not a dominant baryonic component.

Early observations showed that the H I detection rates in ellipticals are several times higher in objects with morphological fine structure such as visible dust lanes, shells, and ripples (Bregman, Hogg & Roberts 1992; van Gorkom & Schiminovich 1997), which themselves occur more frequently in field ellipticals (Malin & Carter 1983; Schweizer et al. 1990). This result indicates a close connection between the gas properties of a galaxy and visible signs of interaction.

The morphology of the H I gas in early-type galaxies generally falls into two categories: most have disk- or ring-like structures with regular kinematics, extending up to ~ 200 kpc in diameter, while in others the H I appears in an irregular, tail-like structure or in individual clouds that are offset from the center of the galaxy (Morganti et al. 2006; Oosterloo et al. 2007). Morganti et al. (2006) surveyed a representative subset of the SAURON galaxies and detected H I emission in 70% of the sample, with gas masses ranging from 10^6 to $10^9 M_\odot$. They found that galaxies with H I disks had the most ionized gas emission (see also Serra et al. 2008), but that the H I properties were uncorrelated with either the age of the stellar population or the stellar kinematics (fast vs. slow rotators). Thus, most early-types seem to accumulate at least some gas, irrespective of their evolutionary past.

Surveys of molecular gas in elliptical galaxies have also rapidly advanced, although the samples remain relatively sparse. Combes, Young & Bureau (2007) reported that 28% of the SAURON sample has detectable CO. Similarly, Sage, Welch & Young (2007) detected CO emission in 33% of a volume-limited sample of field ellipticals; their survey was designed to detect at least 1% of the gas expected to have been returned to the interstellar medium by evolved stars in a Hubble time. From interferometric mapping, the molecular gas is typically in a rotationally supported disk 2 – 12 kpc in diameter (Young 2002, 2005). In many cases these gas disks contain higher specific angular momentum than the stars, or are counter-rotating with respect to the stars, suggesting an external origin (Young, Bureau & Cappellari 2008).

The analysis by Combes, Young & Bureau (2007) of CO-rich early-type galaxies also found that their sample obeyed the Kennicutt-Schmidt relation (§3.5; Kennicutt 1998b) for disk and starburst galaxies, but at gas and star formation rate surface densities two orders of magnitudes lower. Further evidence for ongoing star formation in early-type galaxies was presented by Young, Bendo & Lucero (2008), who studied a sample of CO-rich E/S0 galaxies and found good spatial correspondence between the CO, 24 μm , and radio continuum emission, from which they concluded that the 24 μm emission is predominantly due to star formation (rather than AGN or circumstellar in origin).

The nature of the gas in ellipticals is mysterious. Stellar recycling arguments suggest that they should contain about ten times the atomic hydrogen mass that they actually do. Additionally, the gas mass is not correlated with the stellar mass, which it would be if recycling were an important source (Ciotti et al. 1991; Sage, Welch & Young 2007). Where the recycled gas goes is an unsolved problem.

6. Interactions, mergers, starbursts, and post-starbursts

Galaxy mergers are easily visible in about 1%–2% of all luminous galaxies — frequent enough to suggest that they could be important to galaxy evolution, but also infrequent enough that real statistical samples of mergers are only becoming available today. Figure 16 shows a subset of a sample of merging galaxies selected from SDSS DR6 by eye (Christina Ignarra 2008, private communication). A wide variety of merger types and tidal features are evident, including “dry mergers” between pairs of red galaxies, minor mergers, merger-driven starbursts, and large tidal tails. Although Struck (1999) present a detailed classification of merging systems that attempts to characterize their physical nature, it has not been applied to any of the newly available large samples.

There are two general ways of counting “mergers”: searching for signs in the images, and counting close pairs. For example, in Figure 16, we have simply searched for merger signs in the galaxies by eye. More objective samples have been created by measuring asymmetry and/or using unsharp-masking techniques (De Propris et al. 2007; McIntosh et al. 2008). Though such perturbation-based samples are pure in the sense of essentially containing only real physical pairs, they are biased because they require signs of interaction to be detectable. An alternative technique is to search for close pairs within about 50 kpc or so. Close pair samples are closer to unbiased but even when chosen from redshift surveys include non-physical pairs (Barton, Geller & Kenyon 2000; Smith et al. 2007). Although the distance to the nearest neighbor and the degree of perturbation are correlated, when De Propris et al. (2007) performed a careful comparison of the two approaches, they found generally non-overlapping samples. This result may indicate that close pair samples reveal the pre-merger population whereas searching for perturbations reveals a later stage.

Using large samples from the SDSS, several groups have studied the relationship between mergers and star-formation. As the results of Barton, Geller & Kenyon (2000) and others had previously indicated (Kennicutt et al. 1987, 1998), close pairs of galaxies show a factor of 1.5 – 2 enhancement in their star-formation rate relative to a control sample. Equal mass mergers show the clearest signatures (Li et al. 2008; Ellison et al. 2008). Barton et al. (2007) use a carefully calibrated isolation criterion to select pairs that are not part of larger groups, finding a clearer signature of star-formation enhancement for such isolated pairs.

Although close neighbors are associated with true starbursts only rarely, those rare cases still account for about 40% of the existing starbursts in the Universe. Theory suggests that major gas-rich mergers would create such starbursts — a consequence of the large amount of gas that is driven to the center of the merging system (e.g., Mihos, Richstone & Bothun 1992; Cox et al. 2006). For these reasons, the most luminous infrared galaxies, whose luminosity is powered by dust-obscured star formation, are often associated with major mergers (Sanders & Mirabel 1996).

A class of mergers that do not have associated star-formation are the so-called “dry mergers” — red, gas-poor galaxies merging with other red, gas-poor galaxies. A classic example of such a merger is the infall through dynamical friction of an elliptical galaxy in a cluster onto the central system, building up its stellar mass and perhaps helping to create a cD envelope (§5.5). Indeed, surveys at higher redshift indicate that these sorts of mergers play some role for galaxies on the red sequence (e.g., Bell et al. 2006; Masjedi, Hogg & Blanton 2008). However, at least occasionally mergers of red galaxies turn out to not be quite “dry,” and indeed have substantial gas content (Donovan, Hibbard & van Gorkom 2007).

A very rare but oft-studied subset of galaxies that may be related to mergers are the “post-starbursts.” Such galaxies can be identified by their lack of ionized gas producing $H\alpha$ or other emission lines, indicating no O and B stars, but strong Balmer lines in their spectra, indicating the presence of A stars. They are often

referred to as “K+A” or “E+A” galaxies because of their distinct spectral characteristics (Dressler & Gunn 1983; Zabludoff et al. 1996). Because of the life-times of A stars, they must have ended star-formation within the last Gyr or so, and may be undergoing a transformation. It is unknown whether such transformations result from ram pressure stripping events, mergers, or something else. Indeed, post-starburst galaxies may have more than one formation mechanism.

In Figure 17, we show one method for selecting such galaxies, used by Quintero et al. (2004). They fit the full SDSS spectrum to a sum of an A star template and an old galaxy template, which results in an arbitrarily normalized ratio of A stars to old stars, denoted A/K . By comparing this ratio to $H\alpha$ equivalent width they can identify galaxies with no recent star-formation but a significant contribution of A stars to the integrated spectrum. Indeed, they observe a spur of such galaxies.

This method of selection differs from previous methods in two ways. First, they use the $H\alpha$ emission line rather than $[O II] \lambda 3727$ (e.g., Blake et al. 2004) or a combination of multiple lines (e.g., Poggianti et al. 2004). As Yan et al. (2006) show, using $[O II] \lambda 3727$ alone can easily exclude half or more of the K+A sample, which commonly have weak AGN (Yang et al. 2006). Any method using $H\alpha$ is preferable in this respect. Second, they use full spectral fits rather than Balmer line equivalent widths (e.g., Balogh et al. 2005). This selection alters slightly the “purity” of the sample, as any sufficiently blue continuum will lead to a K+A classification, regardless of A star content.

These galaxies tend to be high in surface brightness and to be highly concentrated, yet blue (Norton et al. 2001; Quintero et al. 2004), with a strong possibility that as their stellar population fades they will become consistent with the red sequence, and become elliptical galaxies. *HST* imaging and optical spectroscopy by Yang et al. (2008) suggests that currently they are discrepant from the fundamental plane of ellipticals — that is, they are consistent with having the lower mass-to-light ratios appropriate to their young stellar populations, and may fade onto the fundamental plane. Most appear considerably more disturbed than the typical elliptical (Zabludoff et al. 1996), though those disturbances may disappear over time.

Interestingly, there is very little evidence that these galaxies occur more frequently in any particular environment, generally following the environmental trends of late-type galaxies (Quintero et al. 2004; Blake et al. 2004; Hogg et al. 2006; Yan et al. 2009). Poggianti et al. (2004) claim that in the Coma cluster there is a population of low luminosity ($M_V > -18.5$) K+A galaxies associated with dense areas in the hot intracluster medium. As Yan et al. (2009) point out, some K+As may be explained by interaction with the ICM, but most cannot; the distribution of most K+As across environment is more consistent with a merger scenario (Zabludoff et al. 1996).

7. Discussion

Over the past decade, astronomers have gathered a huge amount of information about nearby galaxies. In some cases these data have confirmed and made more precise previously known correlations — such as the fundamental plane. In others, they have broken newer ground — such as the refinement of infrared indicators of star-formation and full dynamical modeling of galaxy centers. An overarching theme has been that the size of the new data sets has allowed us to ask more sophisticated statistical questions of the galaxy population. In particular, our understanding of the effect of galaxy environment on galaxy properties is now highly refined.

One clear result from these studies is that while a galaxy’s surroundings affect its probability of being

a “late type” or “early type” galaxy, they only secondarily affect the scaling relations of those types. That is, whereas elliptical galaxies are more common in groups and clusters than in the field, the processes that produce them are likely to have been similar no matter where they are found today. Galaxy formation theorists ought to be trying to explain this general rule.

Nevertheless, there are several notable exceptions to the rule. In particular, the central galaxies in groups and clusters appear to be a special class (§5.5). Very close neighbors (< 50 kpc) seem to affect each other substantially (§2.5, §6). Galaxies in dense regions are at least 0.02 dex more metal rich than those in the field (§3.7). Elliptical galaxies in dense regions may be slightly older (§5.7, §5.8), and have a slightly different fundamental plane relationship (§5.4). Ellipticals in the field may also have had a more active recent merger history (§5.6). In addition, while the fundamental plane and Tully-Fisher relations, and the relationship between luminosity and Sérsic index, might be constant with environment, each of those relationships mask more complex structures — be they kinematic complexities, bars, or other features. It may yet be that these more detailed properties depend on environment in some revealing fashion, even while maintaining the gross relations. While the theoretical galaxy formation community has yet to come to agreement on how the broad trends come to be, the observers ought still to work on teasing out these intriguing deviations.

Another trend that has recently come into focus is the dependence of mass-to-light ratio on mass. For galaxies around L_* , there is generally only a weak relationship; the Tully-Fisher and fundamental plane relationships are (approximately) constant mass-to-light ratio. But clearly the fundamental plane relationship shows a slow increase to high masses, which for the BCGs becomes even more extreme (§5.5). Meanwhile, at low masses the dwarf disk galaxies deviate from the Tully-Fisher relationship, again showing high mass-to-light ratios; in this case, because they appear to not have converted much of their cold gas into stars (§3.4). Thus, the halos that seem to produce the most stellar mass per unit dark matter mass are somewhere around L_* . Interestingly, such a trend is exactly what is required for the Λ CDM mass function, with its slow cutoff at high mass and steep faint-end slope, to successfully produce the observed luminosity function (§2.3; Tasitsiomi et al. 2004; Seljak et al. 2005). The best quantification of this trend is that of Zaritsky, Zabludoff & Gonzalez (2008), who attempt to construct a dynamical relationship that applies to all galaxy classes.

What is even more clear, however, is that even with the vast number of papers written, the available information in the new data sets is nowhere near being exhausted. Progress is possible because much (though not all) of the new data is amenable to the sophisticated techniques that have been used on smaller, less homogeneous surveys. In particular, a few interesting questions have barely been touched with the modern data sets and bear further discussion:

1. The lenticular population has received far too little attention, either being tossed in along with the elliptical galaxies or ignored altogether. The E/S0 separation is not an arbitrary one — the edges, rings and bars are clear indications of type — we need well-defined and consistent methods of identifying S0s in the new massive surveys.
2. The nature and existence of breaks in the stellar profile of disks, and the incidence of extended UV disks, seem topics ripe for study in the new massive surveys. While there is now a real census of these galactic features, there has been no study of how they vary with environment or with other galaxy properties. Similarly, there are now reasonably large data sets of bulges, pseudobulges, and bars, as well as other detailed properties, whose relationship with close neighbors and the larger scale environment are largely unknown.

3. The cores of elliptical galaxies are complex and interesting places. Evaluating the recently proposed role of AGN in these cores to the shut-off of star-formation in massive galaxies (e.g. Croton et al. 2006) may require understanding these cores much better. Photometric information alone does not disentangle the effects of dust and stellar populations, and the stellar population and dynamical studies available with larger sets of IFU observations may yield a less ambiguous set of models for elliptical cores.
4. More generally, while some crude measures of galaxy structural properties exist, there are few efforts to quantify classical morphological features like spiral arm organization and pitch angle. Modern techniques in inference applied to modern data sets should allow such a quantification. Classical morphology clearly is important and relevant — witness its continued popularity among astronomers studying the detailed properties of galaxies even as “large data set” astronomers eschew it. We can and ought to measure quantitatively the properties it is putatively based upon.
5. New surveys allow us to connect the radio properties of galaxies (such as neutral and molecular gas content) with their optical properties (such as stellar mass and age) with large statistical samples. Although many interesting findings have resulted from such comparisons, a comprehensive analysis has not yet been completed. The stellar populations are intimately tied to the interstellar gas, without which our understanding is at best incomplete. With upcoming blind H I surveys such as ALFALFA, hopefully this gap will be filled with respect to atomic gas at least.

During the course of writing this review, we benefited from conversations with Adam Bolton, Marla C. Geha, David W. Hogg, Dušan Kereš, Michael Hudson, Jill Knapp, and David Schiminovich. We would like to thank Christina Ignarra and Alejandro Quintero for providing some of the data necessary for the Figures 16 and 17. Finally, we thank our scientific editor John Kormendy for his extremely useful and challenging comments.

This research has made use of NASA’s Astrophysics Data System and of the NASA/IPAC Extragalactic Database (NED) which is operated by the Jet Propulsion Laboratory, California Institute of Technology, under contract with the National Aeronautics and Space Administration.

Funding for the creation and distribution of the SDSS Archive has been provided by the Alfred P. Sloan Foundation, the Participating Institutions, the National Aeronautics and Space Administration, the National Science Foundation, the U.S. Department of Energy, the Japanese Monbukagakusho, and the Max Planck Society. The SDSS Web site is <http://www.sdss.org/>.

The SDSS is managed by the Astrophysical Research Consortium (ARC) for the Participating Institutions. The Participating Institutions are The University of Chicago, Fermilab, the Institute for Advanced Study, the Japan Participation Group, The Johns Hopkins University, the Korean Scientist Group, Los Alamos National Laboratory, the Max-Planck-Institute for Astronomy (MPIA), the Max-Planck-Institute for Astrophysics (MPA), New Mexico State University, University of Pittsburgh, University of Portsmouth, Princeton University, the United States Naval Observatory, and the University of Washington.

The Galaxy Evolution Explorer (GALEX) is a NASA Small Explorer. The mission was developed in cooperation with the Centre National d’Etudes Spatiales of France and the Korean Ministry of Science and Technology.

REFERENCES

- Abraham RG, Valdes F, Yee HKC, van den Bergh S. 1994. *ApJ* 432:75–90
- Adelman-McCarthy JK, Agüeros MA, Allam SS, Prieto CA, Anderson KSJ, et al. 2008. *The Astrophysical Journal Supplement Series* 175:297. (c) 2008: The American Astronomical Society
- Allen PD, Driver SP, Graham AW, Cameron E, Liske J, de Propris R. 2006. *MNRAS* 371:2–18
- Athanassoula E. 1992. *MNRAS* 259:345–364
- Athanassoula E. 2003. *MNRAS* 341:1179–1198
- Athanassoula E. 2005. *MNRAS* 358:1477–1488
- Athanassoula E, Bosma A. 1985. *IN: Annual review of astronomy and astrophysics. Volume 23 (A86-14507 04-90). Palo Alto* 23:147
- Bacon R, Copin Y, Monnet G, Miller BW, Allington-Smith JR, et al. 2001. *MNRAS* 326:23–35
- Balcells M, Graham AW, Domínguez-Palmero L, Peletier RF. 2003. *ApJ* 582:L79–L82
- Baldry IK, Glazebrook K, Brinkmann J, Ivezić Ž, Lupton RH, et al. 2004. *ApJ* 600:681–694
- Baldry IK, Glazebrook K, Driver SP. 2008. *MNRAS* 388:945–959
- Baldwin JA, Phillips MM, Terlevich R. 1981. *PASP* 93:5–19
- Ball NM, Loveday J, Brunner RJ. 2008. *MNRAS* 383:907–922
- Ball NM, Loveday J, Fukugita M, Nakamura O, Okamura S, et al. 2004. *MNRAS* 348:1038–1046
- Balogh M, et al. 2004. *MNRAS* 348:1355–1372
- Balogh ML, Miller C, Nichol R, Zabludoff A, Goto T. 2005. *MNRAS* 360:587–609
- Balogh ML, Morris SL, Yee HKC, Carlberg RG, Ellingson E. 1999. *ApJ* 527:54–79
- Bamford SP, Nichol RC, Baldry IK, Land K, Lintott CJ, et al. 2009. *Monthly Notices of the Royal Astronomical Society* 393:1324
- Barazza FD, Joglee S, Marinova I. 2008. *ApJ* 675:1194–1212
- Barnes EI, Sellwood JA, Kosowsky A. 2004. *AJ* 128:2724–2742
- Barr JM, Bedregal AG, Aragón-Salamanca A, Merrifield MR, Bamford SP. 2007. *A&A* 470:173–178
- Barton EJ, Arnold JA, Zentner AR, Bullock JS, Wechsler RH. 2007. *ApJ* 671:1538–1549
- Barton EJ, Geller MJ, Kenyon SJ. 2000. *ApJ* 530:660–679
- Bedregal AG, Aragón-Salamanca A, Merrifield MR. 2006. *MNRAS* 373:1125–1140
- Begum A, Chengalur JN, Karachentsev ID, Sharina ME. 2008. *MNRAS* 386:138–144
- Bell EF, de Jong RS. 2001. *ApJ* 550:212–229

- Bell EF, McIntosh DH, Katz N, Weinberg MD. 2003. *ApJS* 149:289–312
- Bell EF, et al. 2006. *ApJ* 640:241–251
- Bender R. 1988. *A&A* 202:L5–L8
- Bender R, Burstein D, Faber SM. 1992. *ApJ* 399:462–477
- Bender R, Moellenhoff C. 1987. *A&A* 177:71–83
- Berentzen I, Athanassoula E, Heller CH, Fricke KJ. 2004. *MNRAS* 347:220–236
- Berlind AA, Kazin E, Blanton MR, Pueblas S, Scoccimarro R, Hogg DW. 2006. *ApJ* submitted (astro-ph/0610524)
- Bernardi M, Hyde JB, Sheth RK, Miller CJ, Nichol RC. 2007. *AJ* 133:1741–1755
- Bernardi M, Nichol RC, Sheth RK, Miller CJ, Brinkmann J. 2006. *AJ* 131:1288–1317
- Best PN, Kaiser CR, Heckman TM, Kauffmann G. 2006. *Monthly Notices of the Royal Astronomical Society: Letters* 368:L67
- Bigiel F, Leroy A, Walter F, Brinks E, de Blok WJG, et al. 2008. *The Astronomical Journal* 136:2846
- Binggeli B, Sandage A, Tammann GA. 1988. *ARA&A* 26:509–560
- Binney J. 1978. *MNRAS* 183:501–514
- Binney J. 2005. *MNRAS* 363:937–942
- Blake C, et al. 2004. *MNRAS* 355:713–727
- Bland-Hawthorn J, Vlajić M, Freeman KC, Draine BT. 2005. *ApJ* 629:239–249
- Blanton MR. 2006. *ApJ* 648:268–280
- Blanton MR, Berlind AA. 2007. *ApJ* 664:791–803
- Blanton MR, Eisenstein D, Hogg DW, Schlegel DJ, Brinkmann J. 2005a. *ApJ* 629:143–157
- Blanton MR, Geha M, West AA. 2008. *The Astrophysical Journal* 682:861
- Blanton MR, Lupton RH, Schlegel DJ, Strauss MA, Brinkmann J, et al. 2005b. *ApJ* 631:208–230
- Blanton MR, Roweis S. 2007. *AJ* 133:734–754
- Blanton MR, et al. 2001. *AJ* 121:2358–2380
- Blanton MR, et al. 2003. *ApJ* 594:186–207
- Blanton MR, et al. 2005c. *AJ* 129:2562–2578
- Blitz L, Rosolowsky E. 2006. *ApJ* 650:933–944
- Boissier S, de Paz AG, Boselli A, Madore BF, Buat V, et al. 2007. *The Astrophysical Journal Supplement Series* 173:524. (c) 2007: The American Astronomical Society

- Bolton AS, Treu T, Koopmans LVE, Gavazzi R, Moustakas LA, et al. 2008. *ApJ* 684:248–259
- Boselli A, Gavazzi G. 2006. *PASP* 118:517–559
- Boselli A, Gavazzi G, Combes F, Lequeux J, Casoli F. 1994. *Astron. Astrophys.* 285 285:69
- Boselli A, Gavazzi G, Donas J, Scodreggio M. 2001. *AJ* 121:753–767
- Bregman JN, Hogg DE, Roberts MS. 1992. *ApJ* 387:484–502
- Bregman JN, Temi P, Bregman JD. 2006. *ApJ* 647:265–275
- Bressan A, Panuzzo P, Buson L, Clemens M, Granato GL, et al. 2006. *ApJ* 639:L55–L58
- Brinchmann J, Charlot S, White SDM, Tremonti C, Kauffmann G, et al. 2004. *MNRAS* 351:1151–1179
- Brough S, Couch WJ, Collins CA, Jarrett T, Burke DJ, Mann RG. 2008. *MNRAS* 385:L103–L107
- Brown MJI, Dey A, Jannuzi BT, Brand K, Benson AJ, et al. 2007. *ApJ* 654:858–877
- Bureau M, Aronica G, Athanassoula E, Dettmar RJ, Bosma A, Freeman KC. 2006. *MNRAS* 370:753–772
- Burkert A, Naab T, Johansson PH, Jesseit R. 2008. *ApJ* 685:897–903
- Burstein D, Ho LC, Huchra JP, Macri LM. 2005. *ApJ* 621:246–255
- Buta R, Vasylyev S, Salo H, Laurikainen E. 2005. *The Astronomical Journal* 130:506. (c) 2005: The American Astronomical Society
- Caldwell N, Rose JA, Sharples RM, Ellis RS, Bower RG. 1993. *AJ* 106:473–492
- Calzetti D. 2008. In *Pathways Through an Eclectic Universe*, eds. JH Knapen, TJ Mahoney, A Vazdekis, vol. 390 of *Astronomical Society of the Pacific Conference Series*
- Calzetti D, Kennicutt RC, Engelbracht CW, Leitherer C, Draine BT, et al. 2007. *ApJ* 666:870–895
- Caon N, Capaccioli M, D’Onofrio M. 1993. *MNRAS* 265:1013–1021
- Cappellari M, Bacon R, Bureau M, Damen MC, Davies RL, et al. 2006. *MNRAS* 366:1126–1150
- Cappellari M, Emsellem E, Bacon R, Bureau M, Davies RL, et al. 2007. *MNRAS* 379:418–444
- Casoli F, Sauty S, Gerin M, Boselli A, Fouque P, et al. 1998. *Astronomy and Astrophysics* 331:451
- Cayatte V, Kotanyi C, Balkowski C, van Gorkom JH. 1994. *AJ* 107:1003–1017
- Chabrier G. 2003. *PASP* 115:763–795
- Choi YY, Park C, Vogeley MS. 2007. *ApJ* 658:884–897
- Christlein D, Zabludoff AI. 2004. *The Astrophysical Journal* 616:192. (c) 2004: The American Astronomical Society
- Christlein D, Zabludoff AI. 2005. *ApJ* 621:201–214
- Christlein D, Zaritsky D. 2008. *ApJ* 680:1053–1071

- Chung A, van Gorkom JH, Crowl H, Kenney JDP, Vollmer B. 2008. In *Frontiers of Astrophysics: A Celebration of NRAO's 50th Anniversary*, eds. AH Bridle, JJ Condon, GC Hunt, vol. 395 of *Astronomical Society of the Pacific Conference Series*
- Chung A, van Gorkom JH, Kenney JDP, Vollmer B. 2007. *The Astrophysical Journal* 659:L115. (c) 2007: The American Astronomical Society
- Cid Fernandes R, Asari NV, Sodr e L, Stasi nska G, Mateus A, et al. 2007. *MNRAS* 375:L16–L20
- Ciotti L, D'Ercole A, Pellegrini S, Renzini A. 1991. *ApJ* 376:380–403
- Colbert JW, Mulchaey JS, Zabludoff AI. 2001. *AJ* 121:808–819
- Cole S, Norberg P, Baugh CM, Frenk CS, Bland-Hawthorn J, et al. 2001. *MNRAS* 326:255–273
- Colless M, et al. 2001. *MNRAS* 328:1039–1063
- Combes F, Sanders RH. 1981. *Astronomy and Astrophysics* 96:164. A&AA ID. AAA029.151.040
- Combes F, Young LM, Bureau M. 2007. *MNRAS* 377:1795–1807
- Conselice CJ. 2003. *ApJS* 147:1–28
- Cooper MC, Tremonti CA, Newman JA, Zabludoff AI. 2008. *MNRAS* 390:245–256
- Cooray A, Cen R. 2005. *ApJ* 633:L69–L72
- Courteau S, Dutton AA, van den Bosch FC, MacArthur LA, Dekel A, et al. 2007. *ApJ* 671:203–225
- Cox TJ, Jonsson P, Primack JR, Somerville RS. 2006. *MNRAS* 373:1013–1038
- Crook AC, Huchra JP, Martimbeau N, Masters KL, Jarrett T, Macri LM. 2007. *ApJ* 655:790–813
- Croton DJ, et al. 2006. *MNRAS* 365:11–28
- Dalcanton JJ. 2007. *ApJ* 658:941–959
- Dalcanton JJ, Yoachim P, Bernstein RA. 2004. *ApJ* 608:189–207
- Dale DA, Gil de Paz A, Gordon KD, Hanson HM, Armus L, et al. 2007. *ApJ* 655:863–884
- de Jong RS. 1996. *A&AS* 118:557–573
- de Jong RS, Simard L, Davies RL, Saglia RP, Burstein D, et al. 2004. *MNRAS* 355:1155–1170
- De Propris R, Conselice CJ, Liske J, Driver SP, Patton DR, et al. 2007. *ApJ* 666:212–221
- de Souza RE, Gadotti DA, dos Anjos S. 2004. *ApJS* 153:411–427
- de Vaucouleurs G. 1948. *Annales d'Astrophysique* 11:247
- de Vaucouleurs G. 1959. *Handbuch der Physik* 53:275–+
- de Vaucouleurs G. 1963. *ApJS* 8:31–+
- de Vaucouleurs G, de Vaucouleurs A, Corwin Jr. HG, Buta RJ, Paturel G, Fouque P. 1991. *Third Reference Catalogue of Bright Galaxies*. Berlin: Springer-Verlag

- Desroches LB, Quataert E, Ma CP, West AA. 2007. *MNRAS* 377:402–414
- Djorgovski S, Davis M. 1987. *ApJ* 313:59–68
- Donovan JL, Hibbard JE, van Gorkom JH. 2007. *AJ* 134:1118–1123
- Draine BT. 2003. *ARA&A* 41:241–289
- Draine BT, Dale DA, Bendo G, Gordon KD, Smith JDT, et al. 2007. *ApJ* 663:866–894
- Dressler A. 1979. *Astrophysical Journal* 231:659. A&AA ID. AAA026.158.013
- Dressler A. 1980. *ApJ* 236:351–365
- Dressler A, Gunn JE. 1983. *ApJ* 270:7–19
- Dressler A, Oemler Jr. A, Couch WJ, Smail I, Ellis RS, et al. 1997. *ApJ* 490:577–591
- Dressler A, Sandage A. 1983. *ApJ* 265:664–680
- Drinkwater MJ, Gregg MD, Couch WJ, Ferguson HC, Hilker M, et al. 2004. *Publications of the Astronomical Society of Australia* 21:375–378. (c) 2004 Astronomical Society of Australia
- Driver SP, Allen PD, Liske J, Graham AW. 2007. *ApJ* 657:L85–L88
- Dutton AA, Courteau S, de Jong R, Carignan C. 2005. *ApJ* 619:218–242
- Efstathiou G, Ellis RS, Carter D. 1982. *MNRAS* 201:975–990
- Efstathiou G, Ellis RS, Peterson BA. 1988. *MNRAS* 232:431–461
- Eisenstein DJ, et al. 2003. *ApJ* 585:694–713
- Ellis SC, Driver SP, Allen PD, Liske J, Bland-Hawthorn J, De Propris R. 2005. *MNRAS* 363:1257–1271
- Ellison SL, Patton DR, Simard L, McConnachie AW. 2008. *ApJ* 672:L107–L110
- Elmegreen BG, Elmegreen DM. 1985. *ApJ* 288:438–455
- Elmegreen DM, Elmegreen BG. 1984. *ApJS* 54:127–149
- Elmegreen DM, Elmegreen BG. 1987. *ApJ* 314:3–9
- Elmegreen DM, Elmegreen BG, Frogel JA, Eskridge PB, Pogge RW, et al. 2002. *AJ* 124:777–781
- Emsellem E, Cappellari M, Krajnović D, van de Ven G, Bacon R, et al. 2007. *MNRAS* 379:401–417
- Erwin P, Beckman JE, Pohlen M. 2005. *ApJ* 626:L81–L84
- Eskridge PB, Frogel JA, Pogge RW, Quillen AC, Davies RL, et al. 2000. *AJ* 119:536–544
- Faber SM, Dressler A, Davies RL, Burstein D, Lynden-Bell D. 1987. *IN: Nearly normal galaxies: From the Planck time to the present; Proceedings of the Eighth Santa Cruz Summer Workshop in Astronomy and Astrophysics* :175
- Faber SM, Gallagher JS. 1976. *ApJ* 204:365–375

- Faber SM, Jackson RE. 1976. *ApJ* 204:668–683
- Ferrarese L, Côté P, Jordán A, Peng EW, Blakeslee JP, et al. 2006. *ApJS* 164:334–434
- Fisher D, Illingworth G, Franx M. 1995. *ApJ* 438:539–562
- Fisher DB, Drory N. 2008. *AJ* 136:773–839
- Friedli D, Benz W. 1993. *A&A* 268:65–85
- Fujita Y. 2004. *PASJ* 56:29–43
- Gadotti DA. 2008a. *ArXiv e-prints*
- Gadotti DA. 2008b. *MNRAS* 384:420–439
- Gadotti DA. 2009. *Monthly Notices of the Royal Astronomical Society* 393:1531. (c) Journal compilation © 2009 RAS
- Gadotti DA, de Souza RE. 2005. *ApJ* 629:797–815
- Gadotti DA, de Souza RE. 2006. *ApJS* 163:270–281
- Gallazzi A, Charlot S, Brinchmann J, White SDM. 2006. *MNRAS* 370:1106–1124
- Ganda K, Falcón-Barroso J, Peletier RF, Cappellari M, Emsellem E, et al. 2006. *MNRAS* 367:46–78
- Ganda K, Peletier RF, McDermid RM, Falcón-Barroso J, de Zeeuw PT, et al. 2007. *MNRAS* 380:506–540
- Garnett DR. 2002. *ApJ* 581:1019–1031
- Geha M, Blanton MR, Masjedi M, West AA. 2006. *ApJ* 653:240–254
- Geha M, Guhathakurta P, van der Marel RP. 2003. *AJ* 126:1794–1810
- Gil de Paz A, Madore BF, Boissier S, Thilker D, Bianchi L, et al. 2007. *ApJ* 661:115–134
- Giovanelli R, Haynes MP. 1983. *AJ* 88:881–908
- Giovanelli R, Haynes MP, Kent BR, Saintonge A, Stierwalt S, et al. 2007. *AJ* 133:2569–2583
- Giuricin G, Samurović S, Girardi M, Mezzetti M, Marinoni C. 2001. *ApJ* 554:857–872
- Gomez P, et al. 2003. *ApJ* 584:210–227
- Gonzalez AH, Zabludoff AI, Zaritsky D. 2005. *ApJ* 618:195–213
- Gordon KD, Clayton GC, Witt AN, Misselt KA. 2000. *ApJ* 533:236–244
- Graham AW. 2001. *AJ* 121:820–840
- Graham AW, Driver SP. 2005. *Publications of the Astronomical Society of Australia* 22:118. (c) 2005 Astronomical Society of Australia
- Gunn JE, Gott JRI. 1972. *ApJ* 176:1–+
- Guzzo L, Strauss MA, Fisher KB, Giovanelli R, Haynes MP. 1997. *ApJ* 489:37–48

- Hameed S, Devereux N. 2005. *AJ* 129:2597–2616
- Hansen SM, Sheldon ES, Wechsler RH, Koester BP. 2009. *The Astrophysical Journal* 699:1333
- Hashimoto Y, Oemler AJ. 1999. *ApJ* 510:609–613
- Haynes MP, Giovanelli R, Chincarini GL. 1984. *ARA&A* 22:445–470
- Heckman TM. 1980. *A&A* 87:152–164
- Hernquist L. 1993. *ApJ* 409:548–562
- Hinz JL, Rieke GH, Caldwell N. 2003. *AJ* 126:2622–2634
- Ho LC. 2008. *ARA&A* 46:475–539
- Ho LC, Filippenko AV, Sargent WLW. 1997. *ApJ* 487:591–+
- Hogg DW, Masjedi M, Berlind AA, Blanton MR, Quintero AD, Brinkmann J. 2006. *ApJ* 650:763–769
- Holmberg E. 1958. *Meddelanden fran Lunds Astronomiska Observatorium Serie II* 136:1–+
- Hopkins AM, Miller CJ, Nichol RC, Connolly AJ, Bernardi M, et al. 2003. *ApJ* 599:971–991
- Hoyle F, Rojas RR, Vogeley MS, Brinkmann J. 2005. *ApJ* 620:618–628
- Hubble EP. 1936. *The Realm of the Nebulae*. New Haven: Yale University Press
- Illingworth G. 1977. *ApJ* 218:L43–L47
- Jansen RA, Fabricant D, Franx M, Caldwell N. 2000. *ApJS* 126:331–397
- Jimenez R, Bernardi M, Haiman Z, Panter B, Heavens AF. 2007. *ApJ* 669:947–951
- Jones DH, Saunders W, Colless M, Read MA, Parker QA, et al. 2004. *MNRAS* 355:747–763
- Jørgensen I, Franx M, Kjaergaard P. 1996. *MNRAS* 280:167–185
- Kannappan SJ, Fabricant DG, Franx M. 2002. *AJ* 123:2358–2386
- Kannappan SJ, Jansen RA, Barton EJ. 2004. *AJ* 127:1371–1385
- Kassin SA, de Jong RS, Weiner BJ. 2006. *ApJ* 643:804–824
- Kauffmann G, Heckman TM, White SDM, Charlot S, Tremonti C, et al. 2003. *Monthly Notice of the Royal Astronomical Society* 341:54. (c) 2003 RAS
- Kauffmann G, White SDM, Heckman TM, Ménard B, Brinchmann J, et al. 2004. *MNRAS* 353:713–731
- Kauffmann G, et al. 2003a. *MNRAS* 346:1055–1077
- Kauffmann G, et al. 2003b. *MNRAS* 341:33–53
- Kaviraj S, Schawinski K, Devriendt JEG, Ferreras I, Khochfar S, et al. 2007. *ApJS* 173:619–642
- Kelly BC, McKay TA. 2004. *AJ* 127:625–645

- Kelson DD, Zabludoff AI, Williams KA, Trager SC, Mulchaey JS, Bolte M. 2002. *ApJ* 576:720–737
- Kendall S, Kennicutt RC, Clarke C, Thornley MD. 2008. *MNRAS* 387:1007–1020
- Kenney JD, Young JS. 1988. *Astrophysical Journal Supplement Series (ISSN 0067-0049)* 66:261
- Kennicutt RC. 1989. *ApJ* 344:685–703
- Kennicutt RC. 1992. *ApJ* 388:310–327
- Kennicutt RC. 1998a. *ApJ* 498:541–+
- Kennicutt RC, Bresolin F, French H, Martin P. 2000. *The Astrophysical Journal* 537:589. (c) 2000: The American Astronomical Society
- Kennicutt RC, Lee JC, Akiyama S, Funes JG, Sakai S. 2005. In *The Evolution of Starbursts*, eds. S Hüttmeister, E Manthey, D Bomans, K Weis, vol. 783 of *American Institute of Physics Conference Series*
- Kennicutt RC, Tamblyn P, Congdon CE. 1994. *ApJ* 435:22–36
- Kennicutt Jr. RC. 1983. *ApJ* 272:54–67
- Kennicutt Jr. RC. 1998b. *ARA&A* 36:189–232
- Kennicutt Jr. RC, Armus L, Bendo G, Calzetti D, Dale DA, et al. 2003. *PASP* 115:928–952
- Kennicutt Jr. RC, Calzetti D, Walter F, Helou G, Hollenbach DJ, et al. 2007. *ApJ* 671:333–348
- Kennicutt Jr. RC, Roettiger KA, Keel WC, van der Hulst JM, Hummel E. 1987. *AJ* 93:1011–1023
- Kennicutt Jr. RC, Schweizer F, Barnes JE, Friedli D, Martinet L, Pfenniger D, eds. 1998. *Galaxies: Interactions and Induced Star Formation*
- Kewley LJ, Groves B, Kauffmann G, Heckman T. 2006. *MNRAS* 372:961–976
- Khalatyan A, Cattaneo A, Schramm M, Gottlöber S, Steinmetz M, Wisotzki L. 2008. *Monthly Notices of the Royal Astronomical Society* 387:13. (c) Journal compilation © 2008 RAS
- Kilborn VA, Koribalski BS, Forbes DA, Barnes DG, Musgrave RC. 2005. *MNRAS* 356:77–88
- Knapp GR, Turner EL, Cunniffe PE. 1985. *AJ* 90:454–468
- Kochanek CS, Pahre MA, Falco EE, Huchra JP, Mader J, et al. 2001. *ApJ* 560:566–579
- Koopmann RA, Haynes MP, Catinella B. 2006. *AJ* 131:716–735
- Koopmann RA, Kenney JDP. 1998. *ApJ* 497:L75+
- Köppen J, Weidner C, Kroupa P. 2007. *MNRAS* 375:673–684
- Kormendy J. 1979. *ApJ* 227:714–728
- Kormendy J. 1982. In *Saas-Fee Advanced Course 12: Morphology and Dynamics of Galaxies*, eds. L Martinet, M Mayor

- Kormendy J. 1999. *Galaxy Dynamics* 182:124
- Kormendy J. 2004. In *Coevolution of Black Holes and Galaxies*, ed. LC Ho
- Kormendy J, Djorgovski S. 1989. *ARA&A* 27:235–277
- Kormendy J, Fisher DB, Cornell ME, Bender R. 2009. *The Astrophysical Journal Supplement* 182:216
- Kormendy J, Kennicutt Jr. RC. 2004. *ARA&A* 42:603–683
- Krajnović D, Bacon R, Cappellari M, Davies RL, de Zeeuw PT, et al. 2008. *MNRAS* 390:93–117
- Krick JE, Bernstein RA. 2007. *AJ* 134:466–493
- Kroupa P. 2001. *MNRAS* 322:231–246
- Lauer TR, Ajhar EA, Byun YI, Dressler A, Faber SM, et al. 1995. *AJ* 110:2622–+
- Lauer TR, Gebhardt K, Faber SM, Richstone D, Tremaine S, et al. 2007a. *ApJ* 664:226–256
- Lauer TR, et al. 2007b. *ApJ* 662:808–834
- Laurikainen E, Salo H, Buta R. 2005. *Monthly Notices of the Royal Astronomical Society* 362:1319. (c) 2005 RAS
- Laurikainen E, Salo H, Buta R, Knapen JH. 2007. *MNRAS* 381:401–417
- Leroy AK, Walter F, Brinks E, Bigiel F, de Blok WJG, et al. 2008. *The Astronomical Journal* 136:2782
- Levy L, Rose JA, van Gorkom JH, Chaboyer B. 2007. *The Astronomical Journal* 133:1104. (c) 2007: The American Astronomical Society
- Lewis I, et al. 2002. *MNRAS* 334:673–683
- Li C, Kauffmann G, Heckman TM, White SDM, Jing YP. 2008. *MNRAS* 385:1915–1922
- Lin L, et al. 2004. *ApJ* 617:L9–L12
- Lin YT, Mohr JJ. 2004. *The Astrophysical Journal* 617:879. (c) 2004: The American Astronomical Society
- Loh YS, Strauss MA. 2006. *MNRAS* 366:373–386
- Lotz JM, Primack J, Madau P. 2004. *AJ* 128:163–182
- Loubser SI, Sansom AE, Sanchez-Blazquez P, Soechting IK, Bromage GE. 2008. *ArXiv e-prints*
- Mac Low MM, Ferrara A. 1999. *ApJ* 513:142–155
- Malin DF, Carter D. 1983. *ApJ* 274:534–540
- Maller AH, Berlind AA, Blanton MR, Hogg DW. 2009. *The Astrophysical Journal* 691:394
- Mandelbaum R, Seljak U, Cool RJ, Blanton M, Hirata CM, Brinkmann J. 2006. *MNRAS* 372:758–776
- Marinova I, Jogee S. 2007. *ApJ* 659:1176–1197
- Martin CL, Kennicutt RC. 2001. *ApJ* 555:301–321

- Martin CL, Kobulnicky HA, Heckman TM. 2002. *ApJ* 574:663–692
- Martin DC, et al. 2005. *ApJ* 619:L1–L6
- Martin P, Roy JR. 1994. *ApJ* 424:599–614
- Masjedi M, Hogg DW, Blanton MR. 2008. *ApJ* 679:260–268
- Masters KL, Springob CM, Haynes MP, Giovanelli R. 2006. *ApJ* 653:861–880
- Mathews WG, Brighenti F. 2003. *Annual Review of Astronomy & Astrophysics* 41:191
- McGaugh SS. 2005. *ApJ* 632:859–871
- McIntosh DH, Guo Y, Hertzberg J, Katz N, Mo HJ, et al. 2008. *MNRAS* 388:1537–1556
- Meléndez J, Asplund M. 2008. *Astronomy and Astrophysics* 490:817
- Menéndez-Delmestre K, Sheth K, Schinnerer E, Jarrett TH, Scoville NZ. 2007. *ApJ* 657:790–804
- Meyer MJ, et al. 2004. *MNRAS* 350:1195–1209
- Michard R, Prugniel P. 2004. *Astronomy and Astrophysics* 423:833
- Mihos JC. 2004. In *Clusters of Galaxies: Probes of Cosmological Structure and Galaxy Evolution*, eds. JS Mulchaey, A Dressler, A Oemler
- Mihos JC, Harding P, Feldmeier J, Morrison H. 2005. *ApJ* 631:L41–L44
- Mihos JC, Richstone DO, Bothun GD. 1992. *ApJ* 400:153–162
- Miller CJ, Nichol RC, Reichart D, Wechsler RH, Evrard AE, et al. 2005. *AJ* 130:968–1001
- Milosavljević M, Miller CJ, Furlanetto SR, Cooray A. 2006. *ApJ* 637:L9–L12
- Moore B, Lake G, Katz N. 1998. *Astrophysical Journal v.495* 495:139. (c) 1998: The American Astronomical Society
- Moorthy BK, Holtzman JA. 2006. *MNRAS* 371:583–608
- Morgan WW, Lesh JR. 1965. *Astrophysical Journal* 142:1364
- Morganti R, de Zeeuw PT, Oosterloo TA, McDermid RM, Krajnović D, et al. 2006. *MNRAS* 371:157–169
- Mouhcine M, Baldry IK, Bamford SP. 2007. *MNRAS* 382:801–808
- Moustakas J, Kennicutt Jr. RC, Tremonti CA. 2006. *ApJ* 642:775–796
- Mulchaey JS. 2000. *ARA&A* 38:289–335
- Norberg P, et al. 2002. *MNRAS* 332:827–838
- Norton SA, Gebhardt K, Zabludoff AI, Zaritsky D. 2001. *ApJ* 557:150–164
- Obrić M, Ivezić Ž, Best PN, Lupton RH, Tremonti C, et al. 2006. *MNRAS* 370:1677–1698
- Odehahn SC, Cohen SH, Windhorst RA, Philip NS. 2002. *ApJ* 568:539–557

- Oegerle WR, Hoessel JG. 1991. *ApJ* 375:15–24
- O’Neil K, Bothun G, van Driel W, Monnier Raguaine D. 2004. *A&A* 428:823–835
- Oosterloo TA, Morganti R, Sadler EM, van der Hulst T, Serra P. 2007. *A&A* 465:787–798
- Padmanabhan N, Seljak U, Strauss MA, Blanton MR, Kauffmann G, et al. 2004. *New Astronomy* 9:329–342
- Pagel BEJ. 1997. *Nucleosynthesis and Chemical Evolution of Galaxies*. Nucleosynthesis and Chemical Evolution of Galaxies, by Bernard E. J. Pagel, pp. 392. ISBN 0521550610. Cambridge, UK: Cambridge University Press, October 1997.
- Panther B, Jimenez R, Heavens AF, Charlot S. 2007. *MNRAS* 378:1550–1564
- Park C, Choi YY, Vogeley MS, Gott JRI, Blanton MR. 2007. *ApJ* 658:898–916
- Park C, Gott JRI, Choi YY. 2008. *ApJ* 674:784–796
- Peletier RF, Falcón-Barroso J, Bacon R, Cappellari M, Davies RL, et al. 2007. *MNRAS* 379:445–468
- Peng CY, Ho LC, Impey CD, Rix HW. 2002. *AJ* 124:266–293
- Petrosian V. 1976. *ApJ* 209:L1–L5
- Pilyugin LS, Vílchez JM, Contini T. 2004. *A&A* 425:849–869
- Pizagno J, Prada F, Weinberg DH, Rix HW, Pogge RW, et al. 2007. *AJ* 134:945–972
- Poggianti BM, Bridges TJ, Komiyama Y, Yagi M, Carter D, et al. 2004. *ApJ* 601:197–213
- Pohlen M, Beckman JE, Hüttemeister S, Knapen JH, Erwin P, Dettmar RJ. 2004. In *Penetrating Bars Through Masks of Cosmic Dust*, eds. DL Block, I Puerari, KC Freeman, R Groess, EK Block, vol. 319 of *Astrophysics and Space Science Library*
- Pohlen M, Trujillo I. 2006. *A&A* 454:759–772
- Popesso P, Böhringer H, Romaniello M, Voges W. 2005. *A&A* 433:415–429
- Postman M, Geller M. 1984. *ApJ* 281:95–99
- Proctor RN, Lah P, Forbes DA, Colless M, Couch W. 2008. *MNRAS* 386:1781–1796
- Prugniel P, Simien F. 1997. *A&A* 321:111–122
- Quintero AD, Berlind AA, Blanton MR, Hogg DW. 2006. *ApJ* submitted (astro-ph/0611361)
- Quintero AD, et al. 2004. *ApJ* 602:190–199
- Read JI, Trentham N. 2005. *Royal Society of London Philosophical Transactions Series A* 363:2693–+
- Reese AS, Williams TB, Sellwood JA, Barnes EI, Powell BA. 2007. *AJ* 133:2846–2858
- Renzini A. 2006. *ARA&A* 44:141–192
- Rest A, van den Bosch FC, Jaffe W, Tran H, Tsvetanov Z, et al. 2001. *AJ* 121:2431–2482
- Rieke GH, Alonso-Herrero A, Weiner BJ, Perez-Gonzalez PG, Blaylock M, et al. 2008. *ArXiv e-prints*

- Rix HW, Zaritsky D. 1995. *ApJ* 447:82–+
- Roberts MS, Haynes MP. 1994. *ARA&A* 32:115–152
- Rosati P, Borgani S, Norman C. 2002. *ARA&A* 40:539–577
- Rownd BK, Young JS. 1999. *AJ* 118:670–704
- Sage LJ, Welch GA, Young LM. 2007. *ApJ* 657:232–240
- Sakamoto K, Okumura SK, Ishizuki S, Scoville NZ. 1999. *ApJ* 525:691–701
- Salim S, Rich RM, Charlot S, Brinchmann J, Johnson BD, et al. 2007. *The Astrophysical Journal Supplement Series* 173:267. (c) 2007: The American Astronomical Society
- Sandage A. 1961. *The Hubble Atlas of Galaxies*. Washington: Carnegie Institution
- Sandage A. 1972. *ApJ* 178:1–24
- Sandage A. 2005. *Annual Review of Astronomy & Astrophysics* 43:581
- Sandage A, Tammann GA. 1981. *Carnegie Inst. of Washington* :0000
- Sanders DB, Mirabel IF. 1996. *ARA&A* 34:749–792
- Scarlata C, Carollo CM, Lilly S, Sargent MT, Feldmann R, et al. 2007. *ApJS* 172:406–433
- Schade D, Lilly SJ, Crampton D, Hammer F, Le Fevre O, Tresse L. 1995. *ApJ* 451:L1–L4
- Schawinski K, Kaviraj S, Khochfar S, Yoon SJ, Yi SK, et al. 2007. *ApJS* 173:512–523
- Schaye J. 2004. *ApJ* 609:667–682
- Schechter P. 1976. *ApJ* 203:297–306
- Schechter PL, Gunn JE. 1979. *ApJ* 229:472–484
- Schiminovich D, Wyder TK, Martin DC, Johnson BD, Salim S, et al. 2007. *ApJS* 173:315–341
- Schmidt M. 1959. *Astrophysical Journal* 129:243
- Schmidt M. 1968. *ApJ* 151:393–+
- Schweizer F, Seitzer P. 1992. *Astronomical Journal (ISSN 0004-6256)* 104:1039
- Schweizer F, Seitzer P, Faber SM, Burstein D, Dalle Ore CM, Gonzalez JJ. 1990. *ApJ* 364:L33–L36
- Seigar MS, James PA. 2002. *MNRAS* 337:1113–1117
- Seljak U, Makarov A, Mandelbaum R, Hirata CM, Padmanabhan N, et al. 2005. *Phys. Rev. D* 71:043511–+
- Sellwood JA. 2000. *Dynamics of Galaxies: from the Early Universe to the Present* 197:3. ISBN: 1-58381-024-2
- Sellwood JA, Wilkinson A. 1993. *Reports on Progress in Physics* 56:173–256
- Serra P, Trager SC, Oosterloo TA, Morganti R. 2008. *A&A* 483:57–69

- Sérsic JL. 1968. *Atlas de Galaxias Australes*. Cordoba: Obs. Astronómico
- Shen S, Mo HJ, White SDM, Blanton MR, Kauffmann G, et al. 2003. *MNRAS* 343:978–994
- Sheth K, Elmegreen DM, Elmegreen BG, Capak P, Abraham RG, et al. 2008. *ApJ* 675:1141–1155
- Sheth K, Vogel SN, Regan MW, Thornley MD, Teuben PJ. 2005. *ApJ* 632:217–226
- Simard L. 1998. In *Astronomical Data Analysis Software and Systems VII*, eds. R Albrecht, RN Hook, HA Bushouse, vol. 145 of *Astronomical Society of the Pacific Conference Series*
- Skrutskie MF, Cutri RM, Stiening R, Weinberg MD, Schneider S, et al. 2006. *AJ* 131:1163–1183
- Smith BJ, Struck C, Hancock M, Appleton PN, Charmandaris V, Reach WT. 2007. *AJ* 133:791–817
- Sofue Y, Rubin V. 2001. *ARA&A* 39:137–174
- Spano M, Marcelin M, Amram P, Carignan C, Epinat B, Hernandez O. 2008. *MNRAS* 383:297–316
- Springob CM, Haynes MP, Giovanelli R. 2005. *ApJ* 621:215–226
- Springob CM, Haynes MP, Giovanelli R, Kent BR. 2005. *ApJS* 160:149–162
- Stevens JB, Webster RL, Barnes DG, Pisano DJ, Drinkwater MJ. 2004. *Publications of the Astronomical Society of Australia* 21:318–333
- Storrie-Lombardi MC, Lahav O, Sodre Jr. L, Storrie-Lombardi LJ. 1992. *MNRAS* 259:8P–+
- Strateva I, et al. 2001. *AJ* 122:1861–1874
- Strauss MA, Willick JA. 1995. *Phys. Rep.* 261:271–431
- Strauss MA, et al. 2002. *AJ* 124:1810–1824
- Struck C. 1999. *Phys. Rep.* 321:1–3
- Swaters RA, van Albada TS, van der Hulst JM, Sancisi R. 2002. *A&A* 390:829–861
- Takeuchi TT, Yoshikawa K, Ishii TT. 2000. *The Astrophysical Journal Supplement Series* 129:1. (c) 2000: The American Astronomical Society
- Tasitsiomi A, Kravtsov AV, Wechsler RH, Primack JR. 2004. *ApJ* 614:533–546
- Thilker DA, Bianchi L, Meurer G, Gil de Paz A, Boissier S, et al. 2007. *ApJS* 173:538–571
- Thomas D, Maraston C, Bender R, Mendes de Oliveira C. 2005. *ApJ* 621:673–694
- Thomas J, Saglia RP, Bender R, Thomas D, Gebhardt K, et al. 2007. *MNRAS* 382:657–684
- Tinsley BM. 1980. *Fundamentals of Cosmic Physics* 5:287–388
- Toomre A. 1964. *ApJ* 139:1217–1238
- Trager SC, Faber SM, Dressler A. 2008. *MNRAS* 386:715–747
- Trager SC, Faber SM, Worthey G, González JJ. 2000. *AJ* 120:165–188

- Tremaine SD, Richstone DO. 1977. *ApJ* 212:311–316
- Tremonti CA, et al. 2004. *ApJ* 613:898–913
- Trujillo I, Burkert A, Bell EF. 2004. *ApJ* 600:L39–L42
- Trujillo I, Rudnick G, Rix H, Labbé I, Franx M, et al. 2004. *ApJ* 604:521–533
- Tully RB, Fisher JR. 1977. *A&A* 54:661–673
- Tully RB, Pierce MJ, Huang JS, Saunders W, Verheijen MAW, Witchalls PL. 1998. *AJ* 115:2264–2272
- Vale A, Ostriker JP. 2008. *MNRAS* 383:355–368
- van den Bergh S. 1976. *Astrophysical Journal* 206:883. A&AA ID. AAA017.158.120
- van den Bergh S. 1991. *PASP* 103:390–+
- van den Bergh S. 2002a. *AJ* 124:782–785
- van den Bergh S. 2002b. *AJ* 124:786–787
- van den Bergh S, Abraham RG, Whyte LF, Merrifield MR, Eskridge PB, et al. 2002. *AJ* 123:2913–2924
- van der Kruit PC. 2001. In *Galaxy Disks and Disk Galaxies*, eds. JG Funes, EM Corsini, vol. 230 of *Astronomical Society of the Pacific Conference Series*
- van Dokkum PG. 2005. *AJ* 130:2647–2665
- van Gorkom J, Schiminovich D. 1997. In *The Nature of Elliptical Galaxies; 2nd Stromlo Symposium*, eds. M Arnaboldi, GS Da Costa, P Saha, vol. 116 of *Astronomical Society of the Pacific Conference Series*
- van Zee L, Skillman ED, Haynes MP. 2004. *AJ* 128:121–136
- Varela J, Moles M, Márquez I, Galletta G, Masegosa J, Bettoni D. 2004. *A&A* 420:873–879
- Veilleux S, Cecil G, Bland-Hawthorn J. 2005. *ARA&A* 43:769–826
- Verheijen MAW. 2001. *ApJ* 563:694–715
- Vogt NP, Haynes MP, Giovanelli R, Herter T. 2004. *AJ* 127:3300–3324
- von der Linden A, Best PN, Kauffmann G, White SDM. 2007. *MNRAS* 379:867–893
- Wadadekar Y, Robbason B, Kembhavi A. 1999. *AJ* 117:1219–1228
- Walter F, Brinks E, de Blok WJG, Bigiel F, Kennicutt RC, et al. 2008. *The Astronomical Journal* 136:2563
- Walter F, Cannon JM, Roussel H, Bendo GJ, Calzetti D, et al. 2007. *The Astrophysical Journal* 661:102.
(c) 2007: The American Astronomical Society
- Warmels RH. 1988. *A&AS* 72:19–87
- Weinmann SM, van den Bosch FC, Yang X, Mo HJ. 2006. *MNRAS* 366:2–28
- Weinzirl T, Jogee S, Khochfar S, Burkert A, Kormendy J. 2009. *The Astrophysical Journal* 696:411

- Whyte LF, Abraham RG, Merrifield MR, Eskridge PB, Frogel JA, Pogge RW. 2002. *MNRAS* 336:1281–1286
- Witt AN, Gordon KD. 2000. *ApJ* 528:799–816
- Wong T, Blitz L. 2002. *The Astrophysical Journal* 569:157
- Worthey G. 1998. *PASP* 110:888–899
- Wyse RFG, Gilmore G, Franx M. 1997. *ARA&A* 35:637–675
- Yamauchi C, Ichikawa Si, Doi M, Yasuda N, Yagi M, et al. 2005. *AJ* 130:1545–1557
- Yan R, Newman JA, Faber SM, Coil AL, Cooper MC, et al. 2009. *Monthly Notices of the Royal Astronomical Society* :1040(c) Journal compilation © 2009 RAS
- Yan R, Newman JA, Faber SM, Konidaris N, Koo D, Davis M. 2006. *ApJ* 648:281–298
- Yang X, Mo HJ, van den Bosch FC. 2006. *ApJ* 638:L55–L58
- Yang X, Mo HJ, van den Bosch FC. 2008. *ApJ* 676:248–261
- Yang X, Mo HJ, van den Bosch FC, Pasquali A, Li C, Barden M. 2007. *ApJ* 671:153–170
- Yang Y, Tremonti CA, Zabludoff AI, Zaritsky D. 2006. *The Astrophysical Journal* 646:L33. (c) 2006: The American Astronomical Society
- Yang Y, Zabludoff AI, Zaritsky D, Mihos JC. 2008. *The Astrophysical Journal* 688:945. (c) 2008: The American Astronomical Society
- Yi SK, Yoon SJ, Kaviraj S, Deharveng JM, Rich RM, et al. 2005. *ApJ* 619:L111–L114
- York DG, et al. 2000. *AJ* 120:1579–1587
- Young JS, Scoville NZ. 1991. *IN: Annual review of astronomy and astrophysics. Vol. 29 (A92-18081 05-90). Palo Alto* 29:581
- Young JS, Xie S, Tacconi L, Knezek P, Viscuso P, et al. 1995. *ApJS* 98:219–+
- Young LM. 2002. *AJ* 124:788–810
- Young LM. 2005. *ApJ* 634:258–271
- Young LM, Bendo GJ, Lucero DM. 2008. *ArXiv e-prints*
- Young LM, Bureau M, Cappellari M. 2008. *ApJ* 676:317–334
- Zabludoff AI, Zaritsky D, Lin H, Tucker D, Hashimoto Y, et al. 1996. *ApJ* 466:104–113
- Zamojski MA, Schiminovich D, Rich RM, Mobasher B, Koekemoer AM, et al. 2007. *The Astrophysical Journal Supplement Series* 172:468. (c) 2007: The American Astronomical Society
- Zaritsky D, Gonzalez AH, Zabludoff AI. 2006. *ApJ* 638:725–738
- Zaritsky D, Kennicutt RC, Huchra JP. 1994. *ApJ* 420:87–109
- Zaritsky D, Zabludoff AI, Gonzalez AH. 2008. *ApJ* 682:68–80

Zibetti S, White SDM, Schneider DP, Brinkmann J. 2005. *MNRAS* 358:949–967

Zwaan MA, Meyer MJ, Staveley-Smith L, Webster RL. 2005. *MNRAS* 359:L30–L34

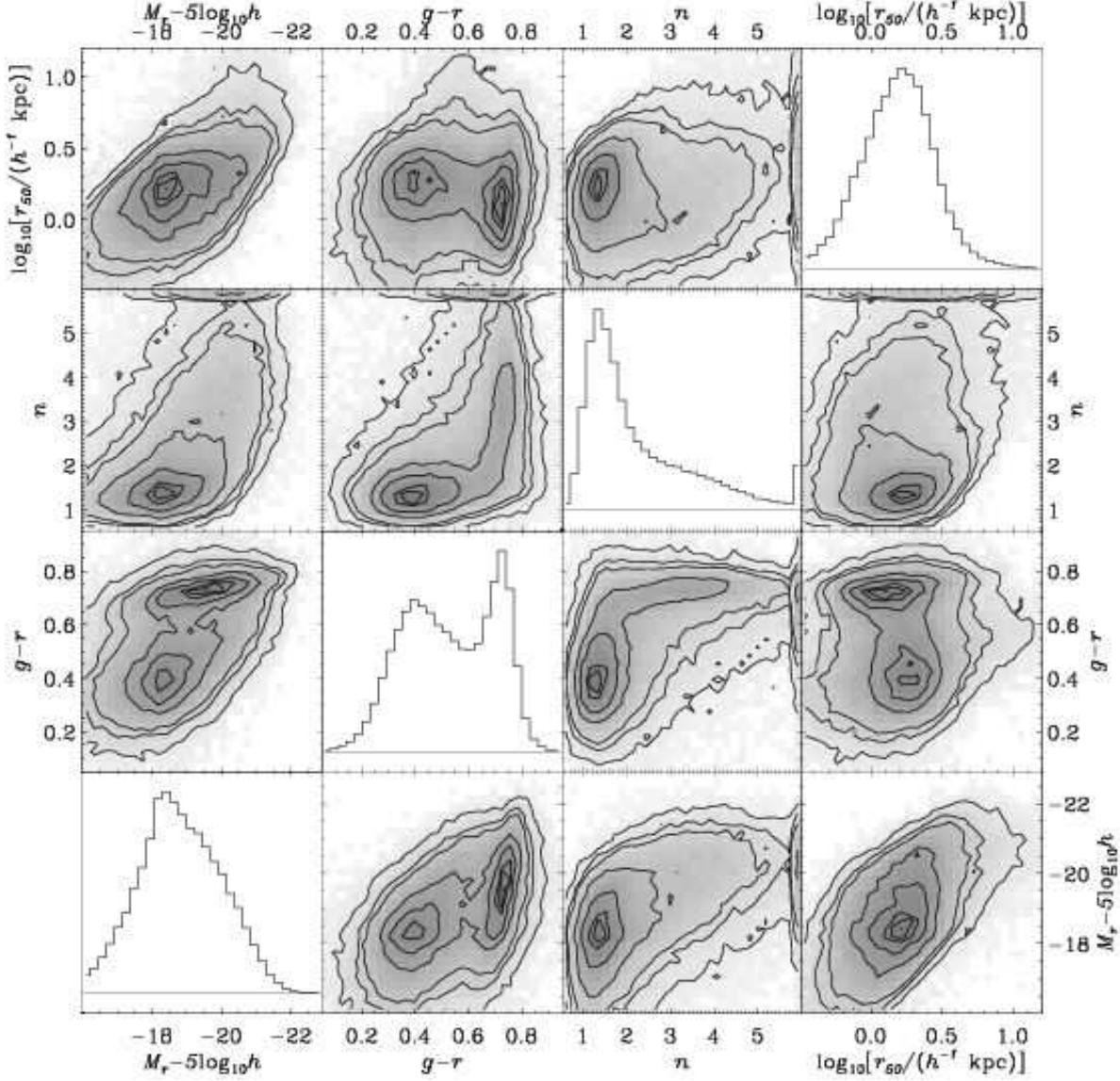


Fig. 1.— Distribution of broad-band galaxy properties in the SDSS. The diagonal panels show the distribution of four properties independently: absolute magnitude M_r , $g-r$ color, Sérsic index n , and half-light radius r_{50} . A bimodal distribution in $g-r$ is apparent. The off-diagonal panels show the bivariate distribution of each pair of properties, revealing the complex relationships among them. The greyscale and contours reflect the number of galaxies in each bin (darker means larger number).

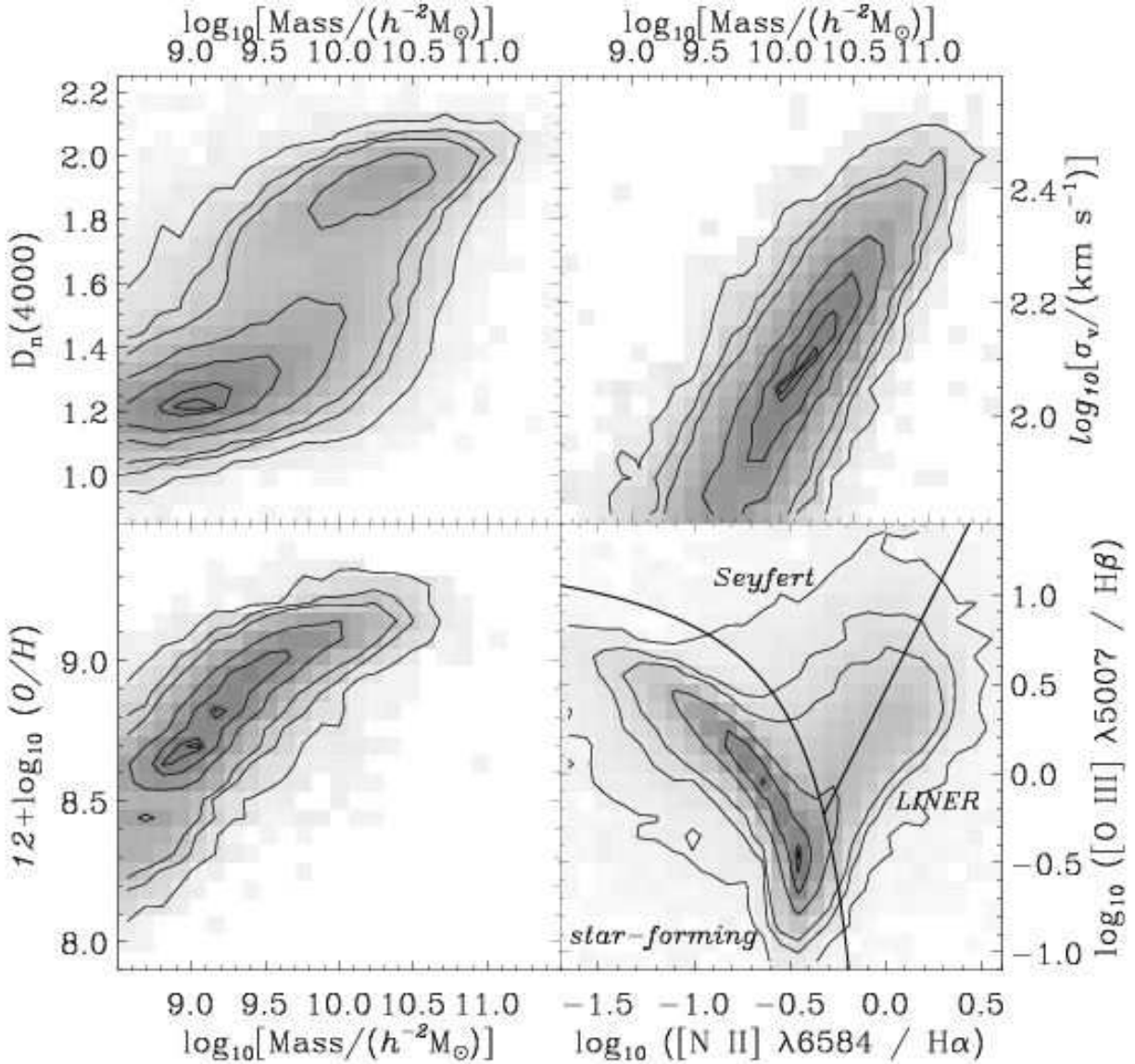


Fig. 2.— Distribution of spectroscopic galaxy properties in the SDSS (data courtesy Brinchmann et al. 2004; Tremonti et al. 2004). Greyscale and contours are similar to those in Figure 1. Upper left panel shows the distribution of stellar mass and $D_n(4000)$, a measure of the stellar population age. As in the color-magnitude diagram, the separation between old and young populations is apparent. Upper right panel shows for red galaxies the distribution of stellar mass and velocity dispersion, revealing the Faber-Jackson relation. Bottom left panel shows for star-forming galaxies the relationship between mass and gas-phase oxygen abundance, the “mass-metallicity” relation. Bottom right panel shows the Baldwin, Phillips & Terlevich (1981) relationship for emission-line galaxies. Shown are the divisions (based on Kauffmann et al. 2003a) among star-forming, Seyfert, and LINER galaxies.

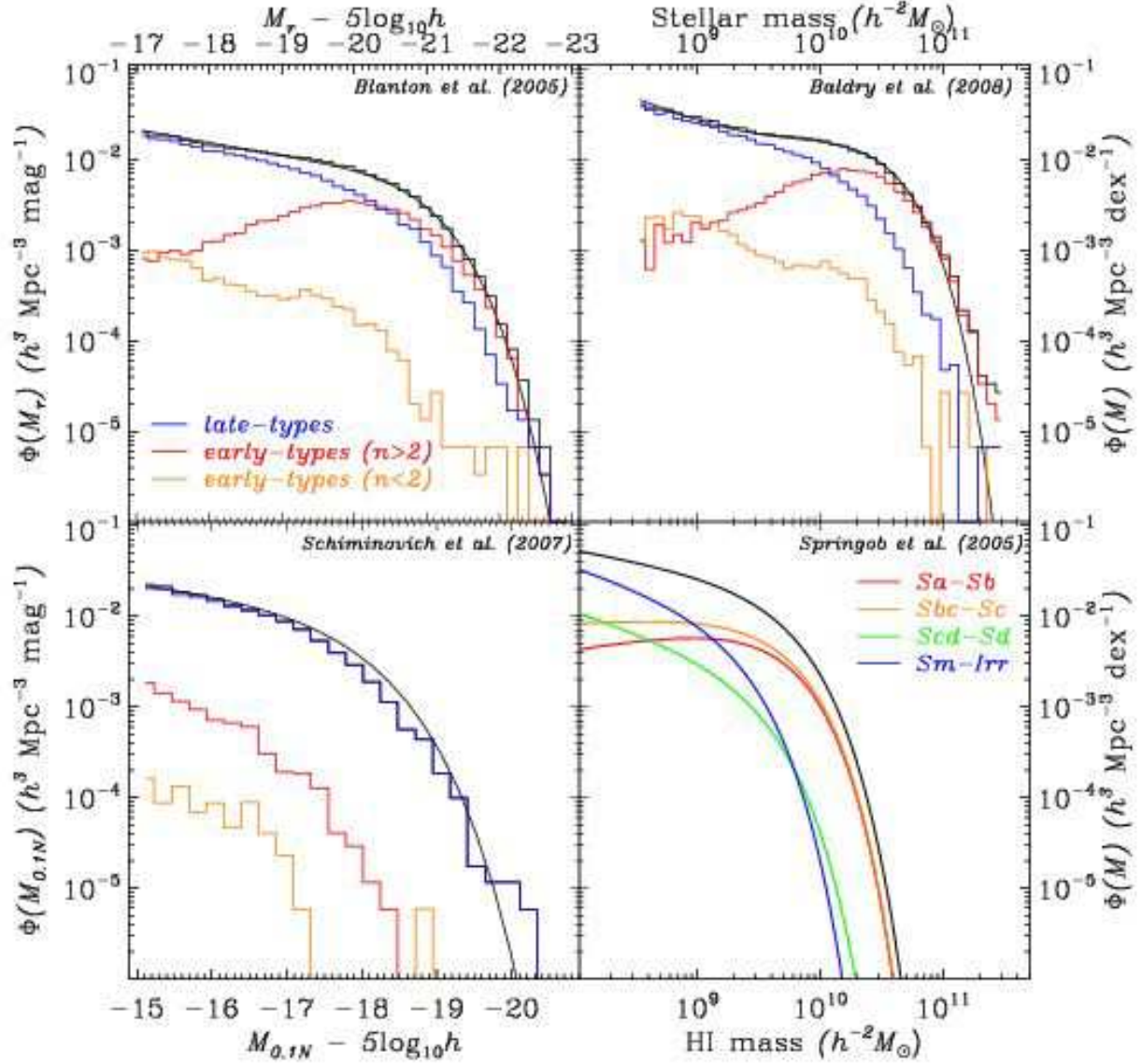


Fig. 3.— Optical and near-UV luminosity function, stellar mass function, and H I mass function of galaxies. The upper left panel shows the local r -band luminosity function of all galaxies (black histogram), as well as the luminosity functions of late-types (blue), concentrated early-types (red) and diffuse early-types (orange), as described in §2.3. Overplotted as the smooth curve is the double Schechter function fit of Blanton et al. (2005b). The upper right panel shows the local stellar mass function for the same galaxies. The bottom left panel shows the $GALEX$ near-UV luminosity function for the various galaxy types and the smooth fit to the full luminosity function from Schiminovich et al. (2007). Finally, the lower right panel shows the H I mass function fits from Springob, Haynes & Giovanelli (2005) for all galaxies and as a function of morphological type.

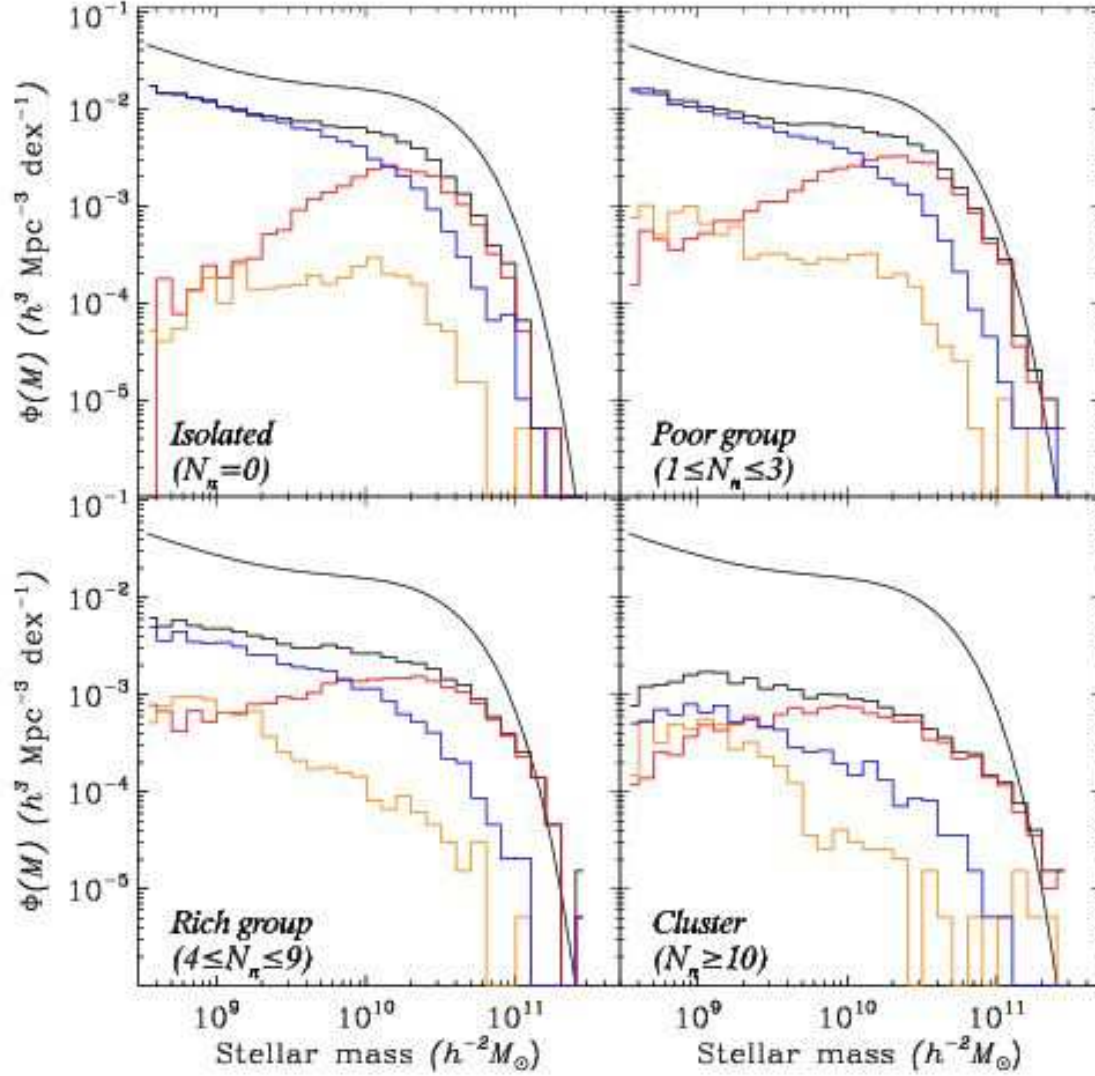


Fig. 4.— Stellar mass function of galaxies as a function of morphological type (see Fig. 3 and §2.3) and local galaxy density. Each panel corresponds to a different environment, ranging from isolated, to poor groups, rich groups, and clusters, based on the number of neighbors N_n with $M_r - 5 \log_{10} h < -18.5$ within $500 h^{-1}$ kpc and 600 km s^{-1} . For reference, this luminosity threshold roughly corresponds to the luminosity of the Large Magellanic Cloud. The double Schechter function fit to all galaxies from Baldry, Glazebrook & Driver (2008) is shown in all panels as a smooth black curve.

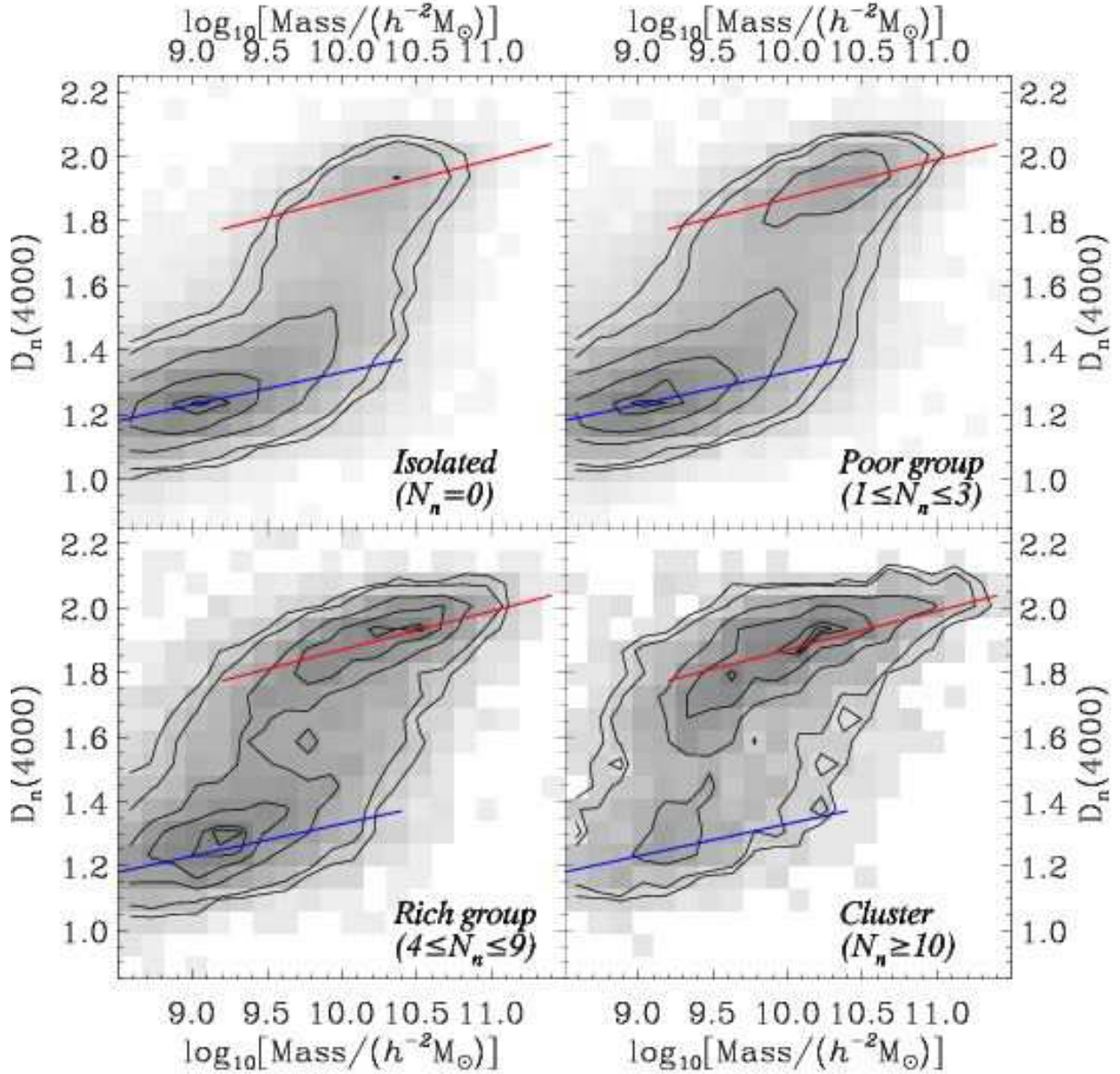


Fig. 5.— Distribution of $D_n(4000)$ and stellar mass as a function of environment as defined in §4. In each panel we show references for the young and old galaxy sequences as the blue and red lines, respectively.

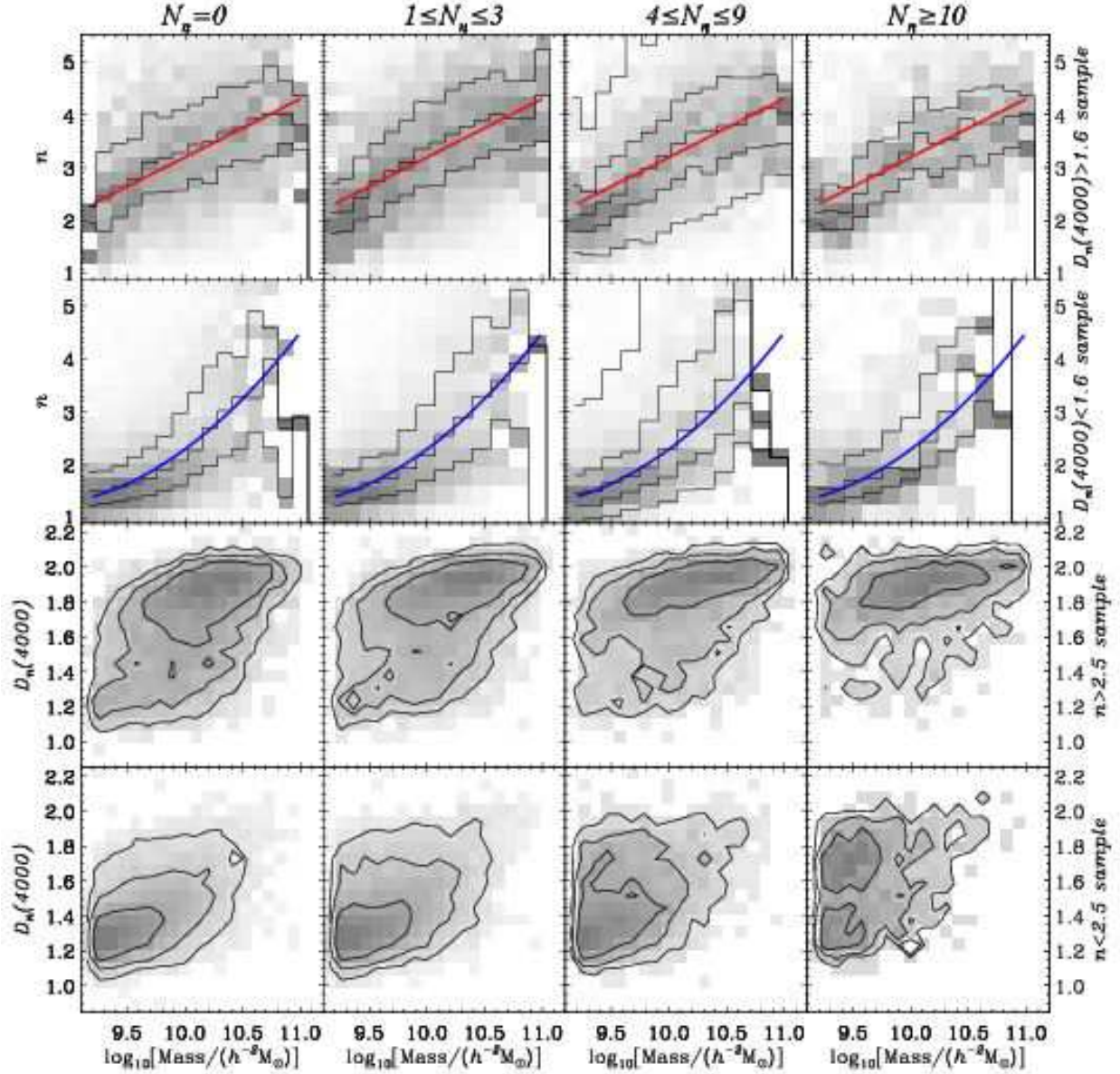


Fig. 6.— Demonstration of the asymmetric relations between structure and star-formation history. Each column isolates a range of densities using the number of neighbors N_n , as defined in §2.5. The top two rows show the relationship between Sérsic index and stellar mass in an “old” sample and a “young” sample. For the old sample plots, the red line remains the same in all plots. For the young sample plots, the blue line remains the same. The bottom two rows show the relationship between $D_n(4000)$ and stellar mass in a “concentrated” sample and a “diffuse” sample. At fixed Sérsic index the stellar population ages clearly depend strongly on density (even at fixed mass). However, at fixed stellar population age, the Sérsic index does not vary significantly with density.

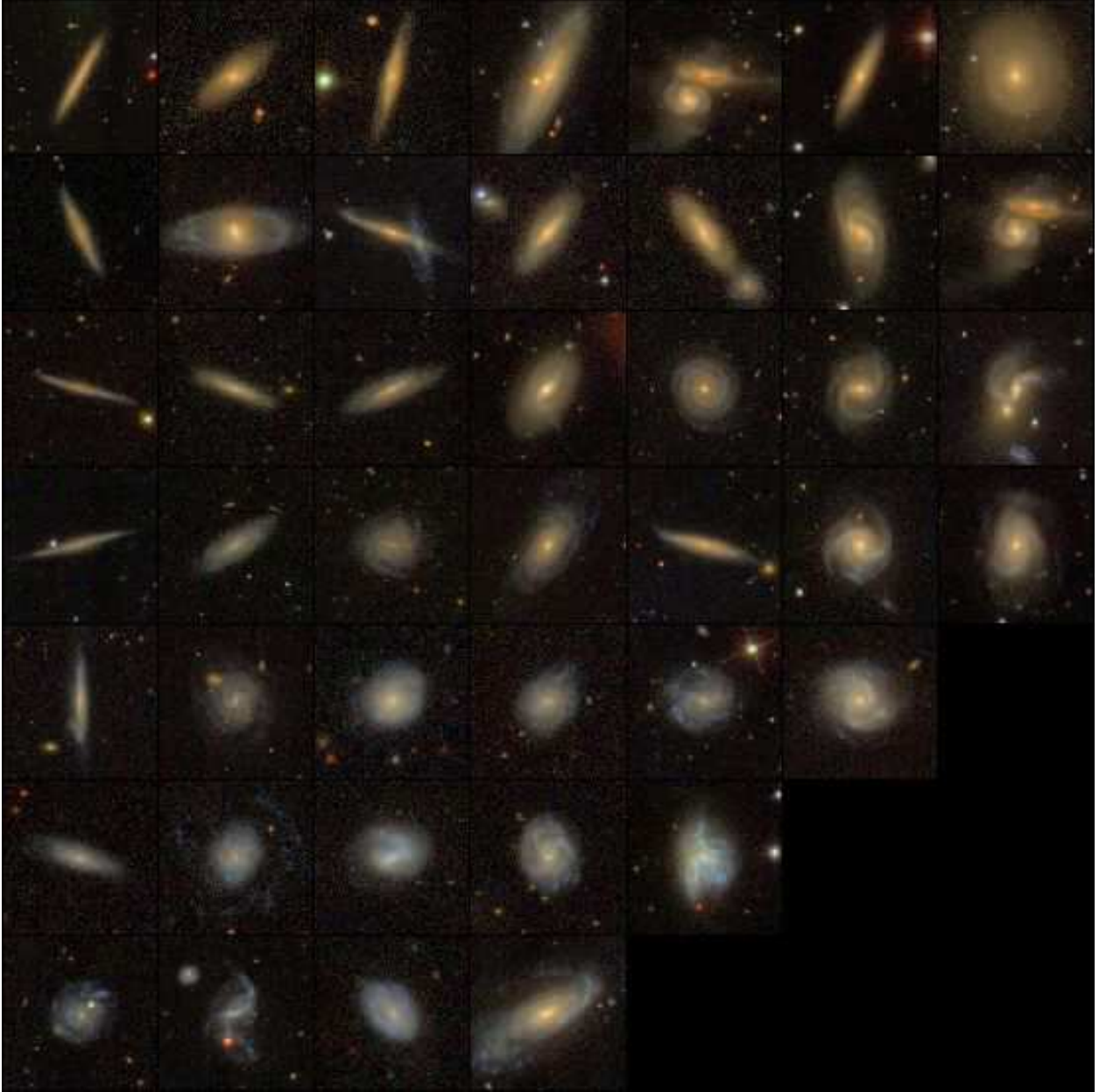


Fig. 7.— SDSS images of spiral galaxies, selected according to classifications in NED to be Sa–Sd (including barred types). The images are sorted by absolute magnitude in the horizontal direction, ranging between $M_r - 5 \log_{10} h \sim -18.5$ and -22 from left to right, and $g - r$ color in the vertical direction, ranging between 0.2 and 0.9 mag from the bottom to the top. Thus, the brightest, reddest spirals are in the upper-right. The galaxies shown were selected randomly, except we excluded two cases from the original set due to image defects.

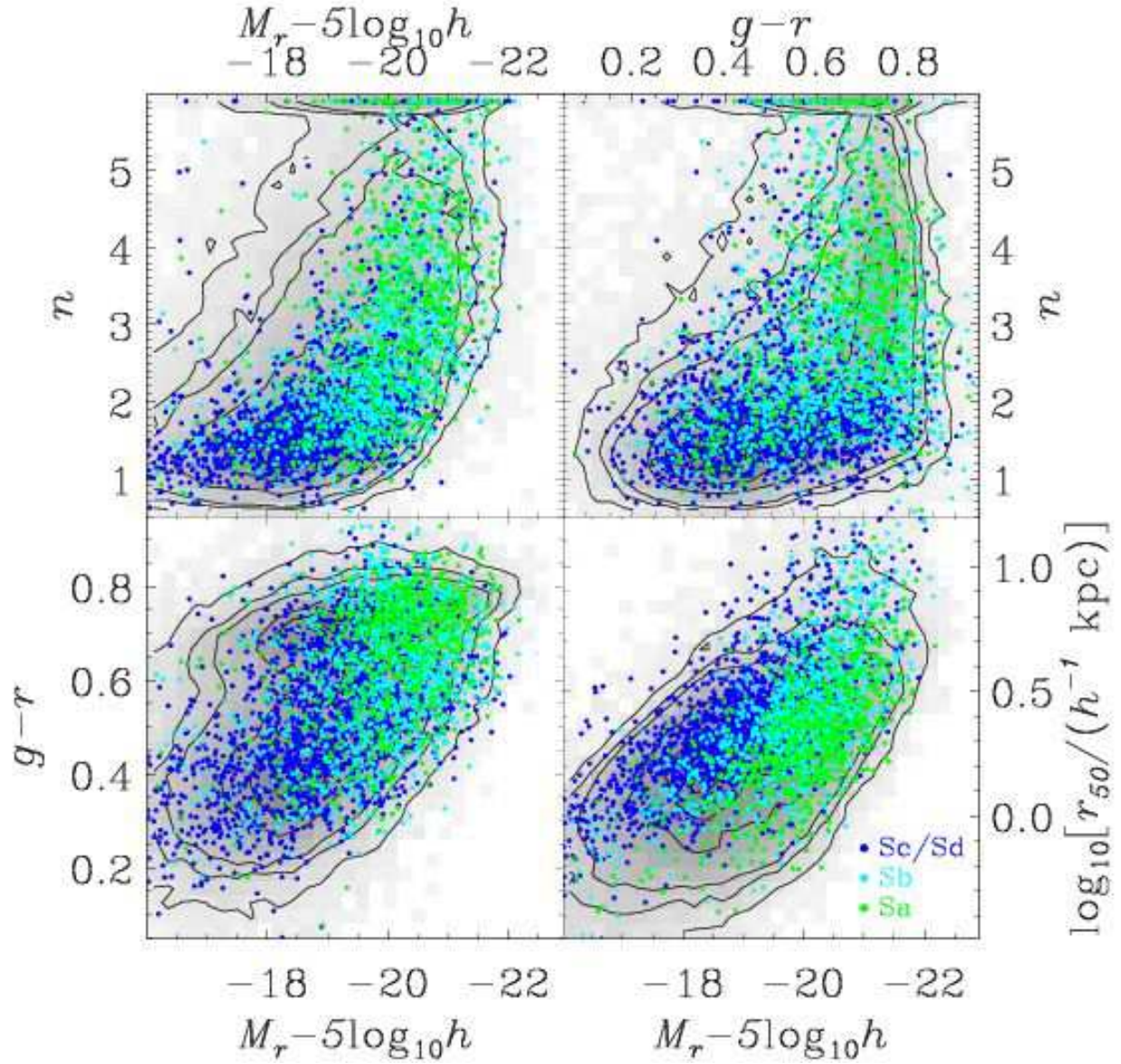


Fig. 8.— Distribution of various spiral galaxy types in optical broadband properties. The underlying greyscale and contours are from the full data of Figure 1. Using classifications stored in NED, we overplot the positions of Sa (green), Sb (cyan), and Sc or Sd (blue) galaxies. We include the barred varieties.

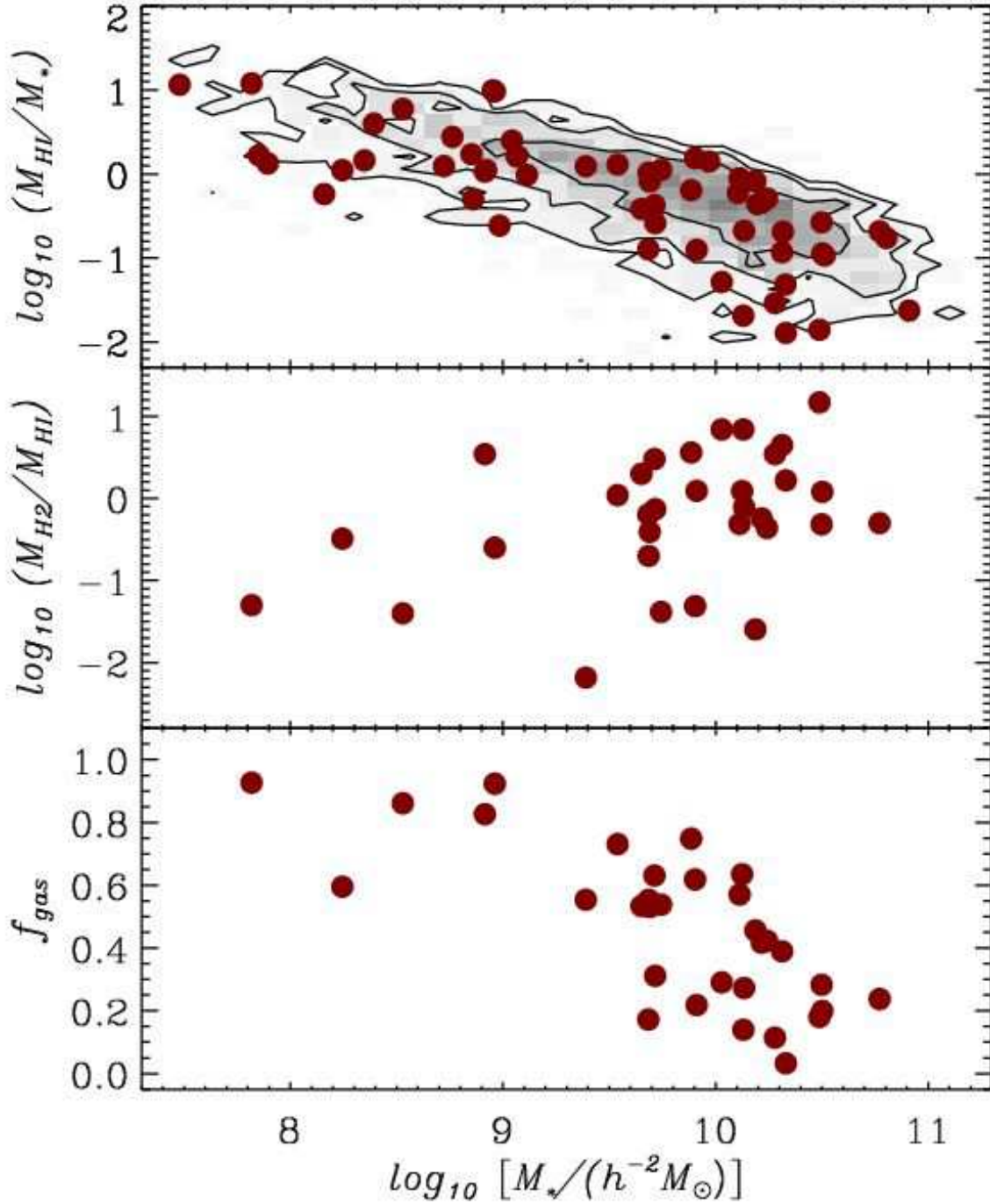


Fig. 9.— Neutral and molecular gas content of spiral galaxies. The top panel shows the fraction of neutral gas relative to the stellar mass, as a function of stellar mass. The greyscale is from a combination of data in the Springob et al. (2005) compilation of HI data, matched to the SDSS sample (using the formulae of Bell et al. 2003 to determine stellar mass). The points are from SINGS. The middle panel shows the ratio of molecular hydrogen gas mass (inferred from the CO (1→0) transition) to neutral gas mass for the SINGS sample. The bottom panel shows the total neutral plus molecular gas fraction as a function of stellar mass.

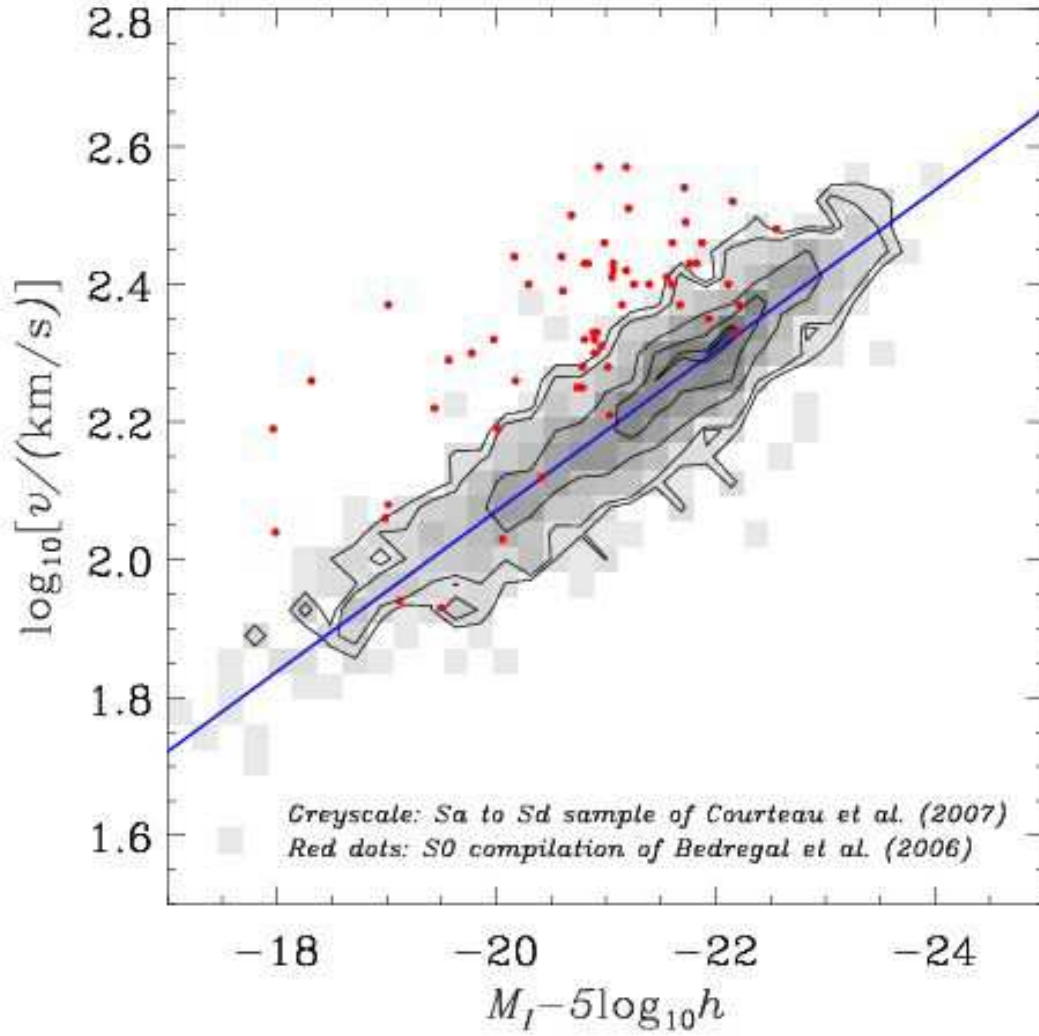


Fig. 10.— Tully-Fisher relation in the I -band (Vega-relative). The greyscale and contours show the data from Courteau et al. (2007), along with the fit to all morphological types given in their Table 2. The red points are the S0 data from the compilation of Bedregal, Aragón-Salamanca & Merrifield (2006), converted to I band using the approximate relation $I = K + 1.99$.

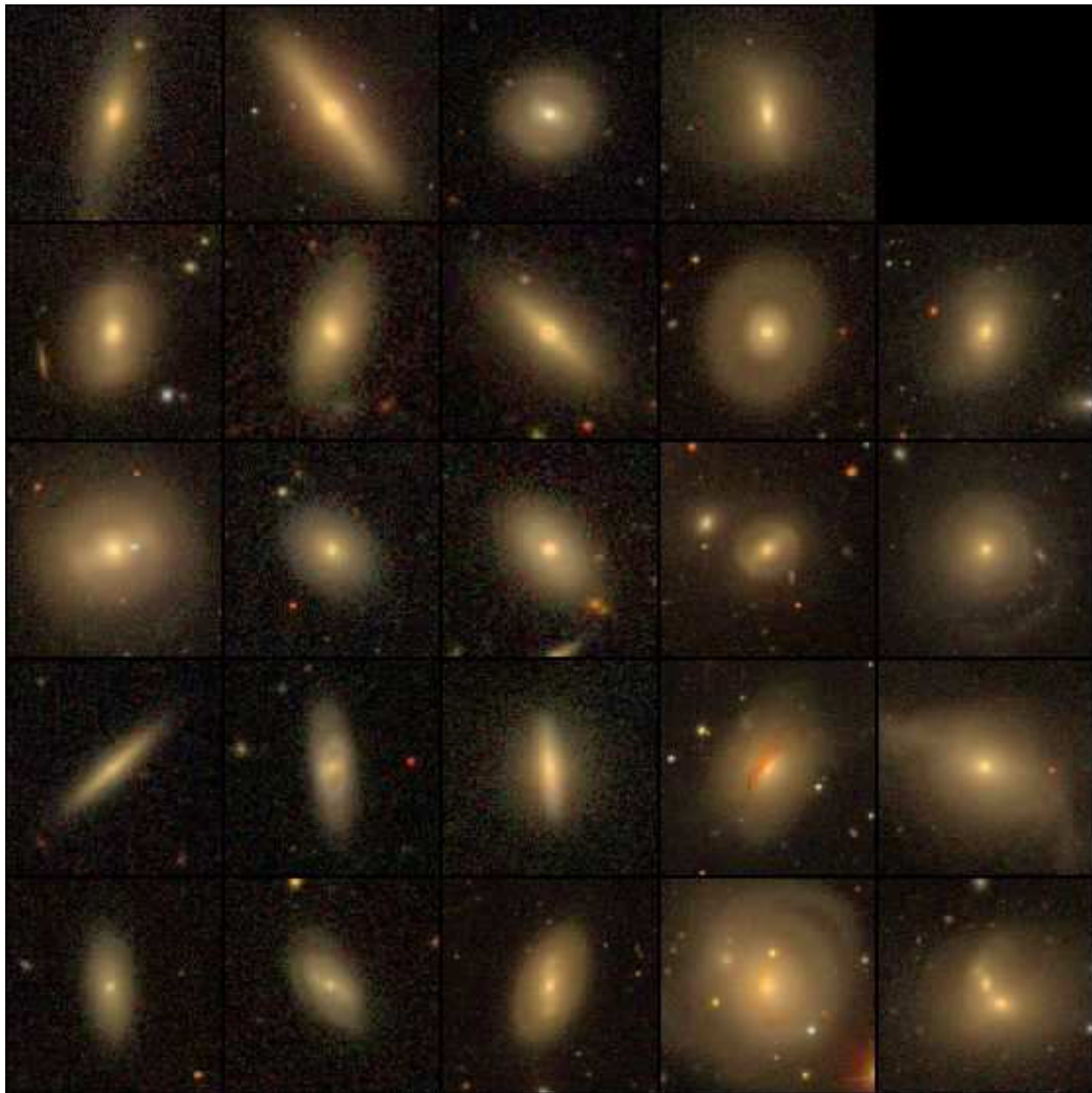


Fig. 11.— SDSS images of lenticular (S0) galaxies, selected according to classifications in NED. The images are sorted by absolute magnitude in the horizontal direction, ranging between $M_r - 5 \log_{10} h \sim -18.5$ and -22 from left to right, and concentration (r_{90}/r_{50}) in the vertical direction, ranging between 2.2 and 3.8 from the bottom to the top. Thus, the brightest, most concentrated S0s are in the upper right. The galaxies shown were selected randomly, but roughly one-quarter were replaced because their NED classifications were clearly incorrect. We left cases that could be considered ambiguous in the figure.

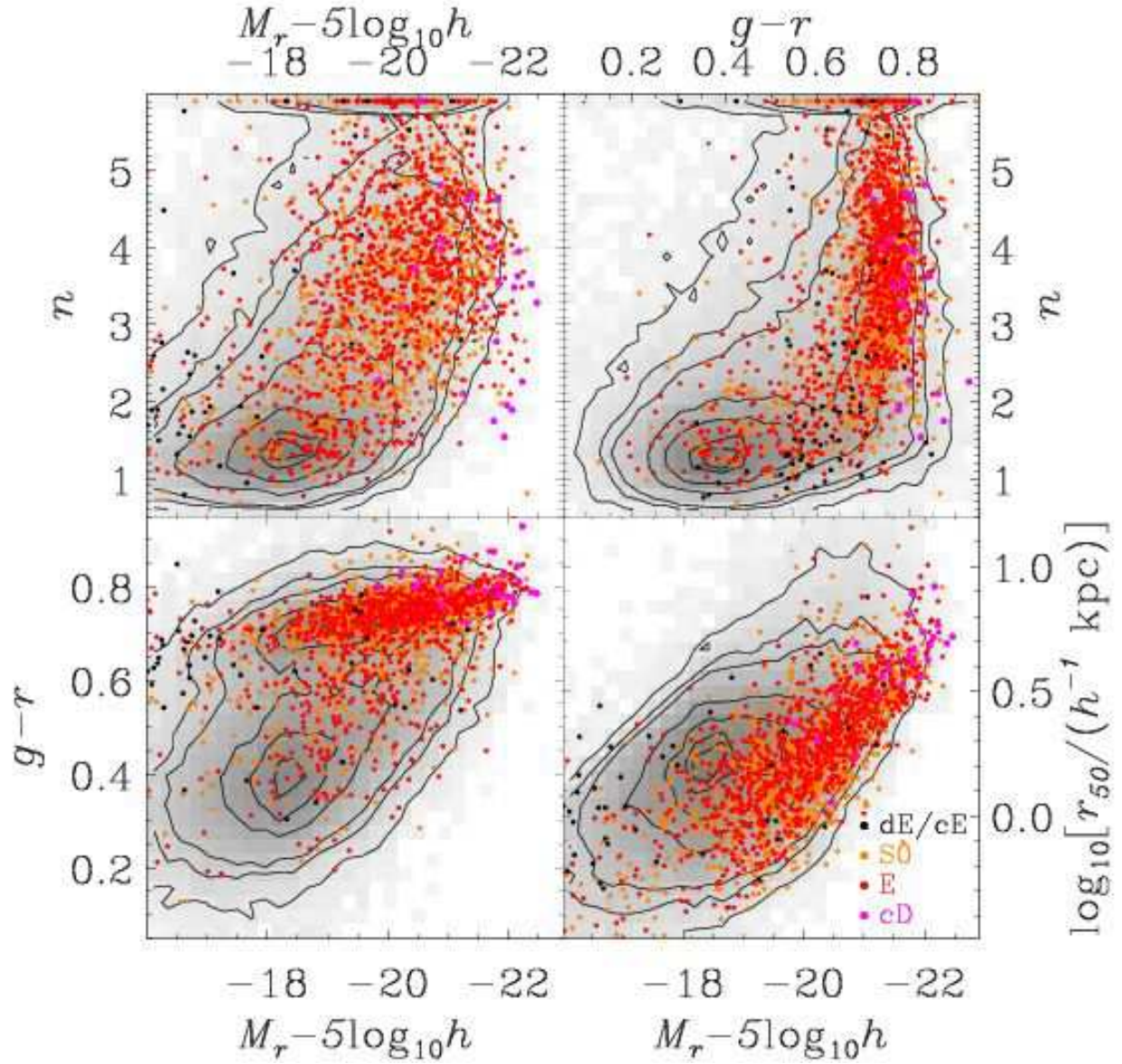


Fig. 12.— Distribution of elliptical and lenticular galaxy types in optical broadband properties. Similar to Figure 8, but now showing S0 galaxies (orange), E galaxies (red), dE galaxies (black) and cD galaxies (magenta).

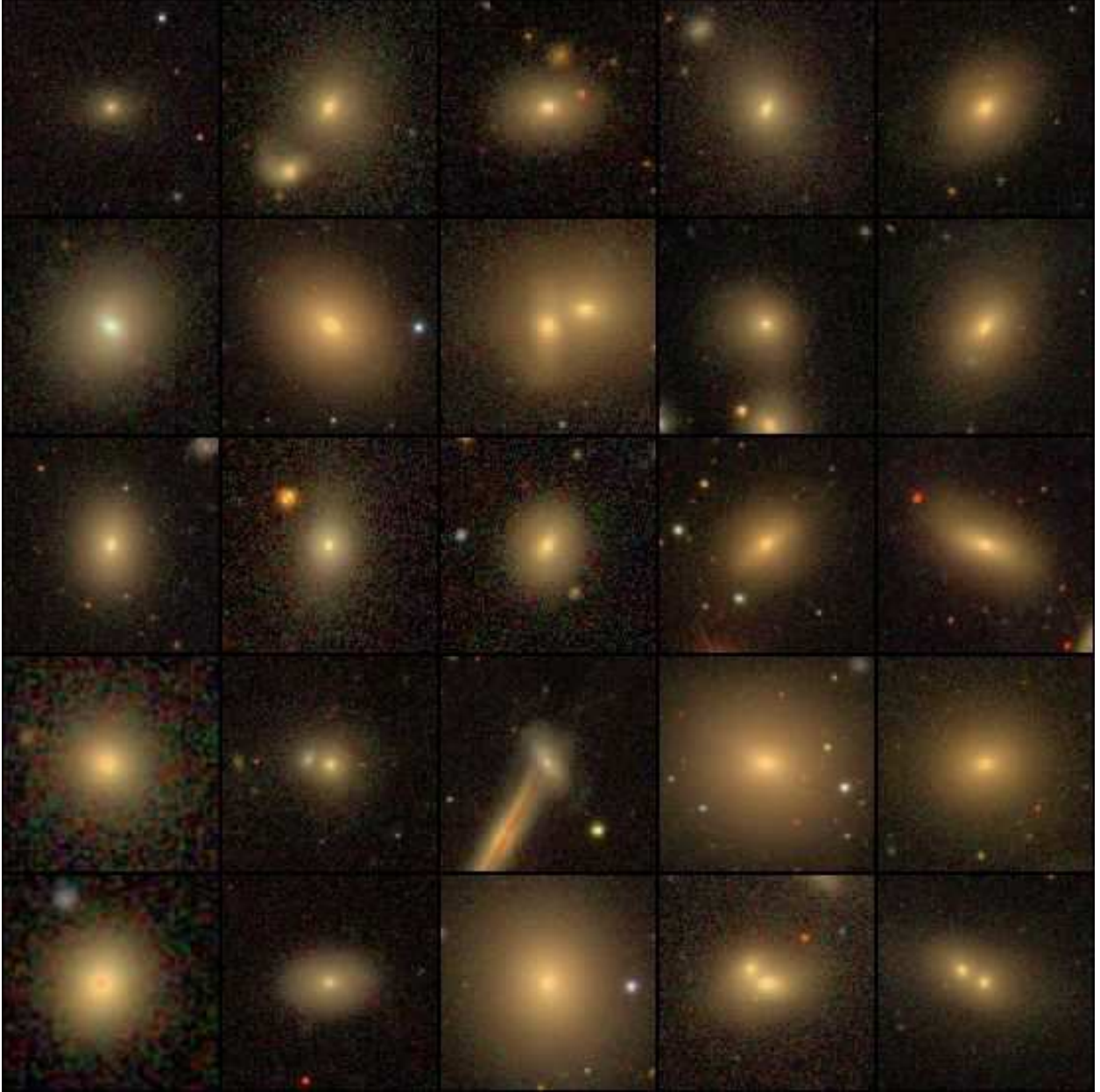


Fig. 13.— SDSS images of elliptical galaxies, selected according to classifications in NED. The images are sorted by absolute magnitude in the horizontal direction, ranging between $M_r - 5 \log_{10} h \sim -18.5$ and -22 from left to right, and concentration (r_{90}/r_{50}) in the vertical direction, ranging between 2.2 and 3.8 from the bottom to the top. Thus, the brightest, most concentrated ellipticals are in the upper right. The galaxies shown were selected randomly, but roughly one-third were replaced because their NED classifications were clearly incorrect. We left cases that could be considered ambiguous in the figure.

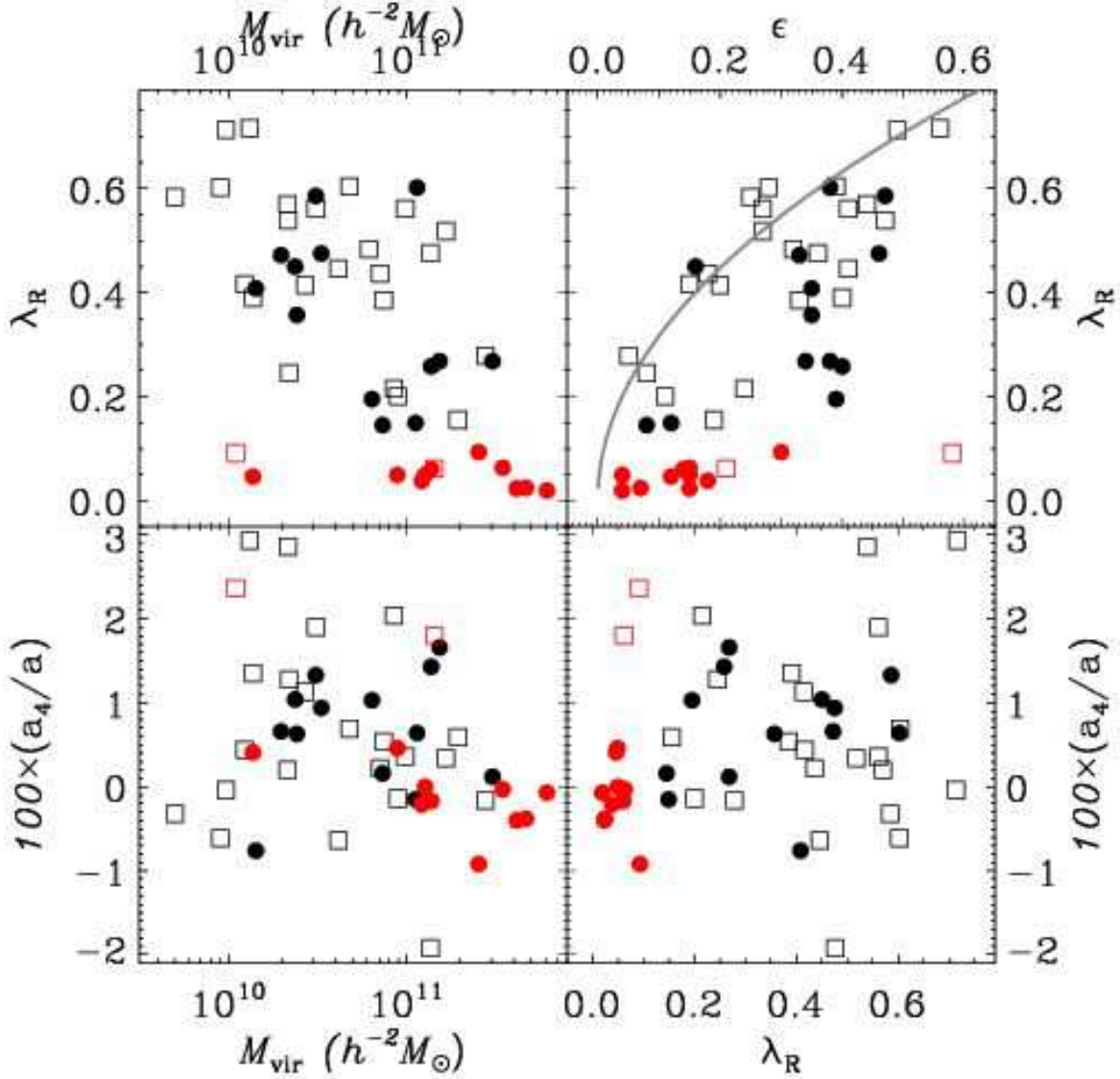


Fig. 14.— Distribution of E/S0 galaxy properties from the SAURON sample of Emsellem et al. (2007). Black symbols indicate “fast rotators,” while red points indicate “slow rotators”. Filled points indicate optically classified elliptical galaxies, while open square symbols indicate S0s. M_{vir} indicates the virial mass; λ_R indicates the angular momentum content as defined by Emsellem et al. (2007) and described in §5.4; ϵ is the ellipticity within r_{50} ; and a_4/a is the boxy/disky parameter (positive is disk, negative is boxy). The solid grey curve corresponds to an oblate rotator with an isotropic velocity dispersion observed edge-on.

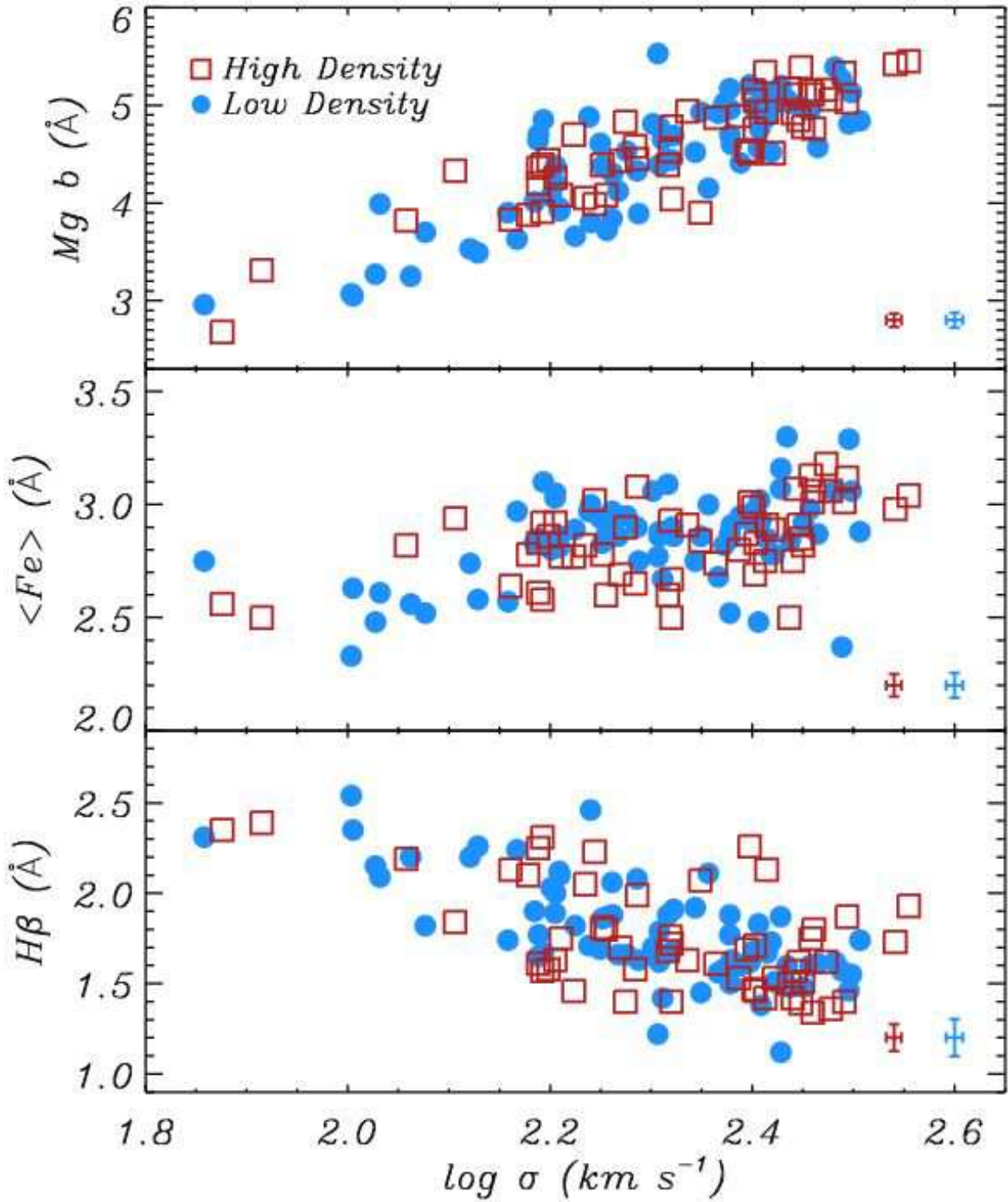


Fig. 15.— Dependence of E/S0 spectral indices on σ and environment from Thomas et al. (2005). Filled blue circles are low density points; open red squares are high density points. Top panel is the Mg b indicator (α abundance), middle panel is the $\langle Fe \rangle$ indicator (iron abundance), and bottom panel is $H\beta$ (an age indicator). Typical uncertainties in the measurements are shown in the lower right corners.

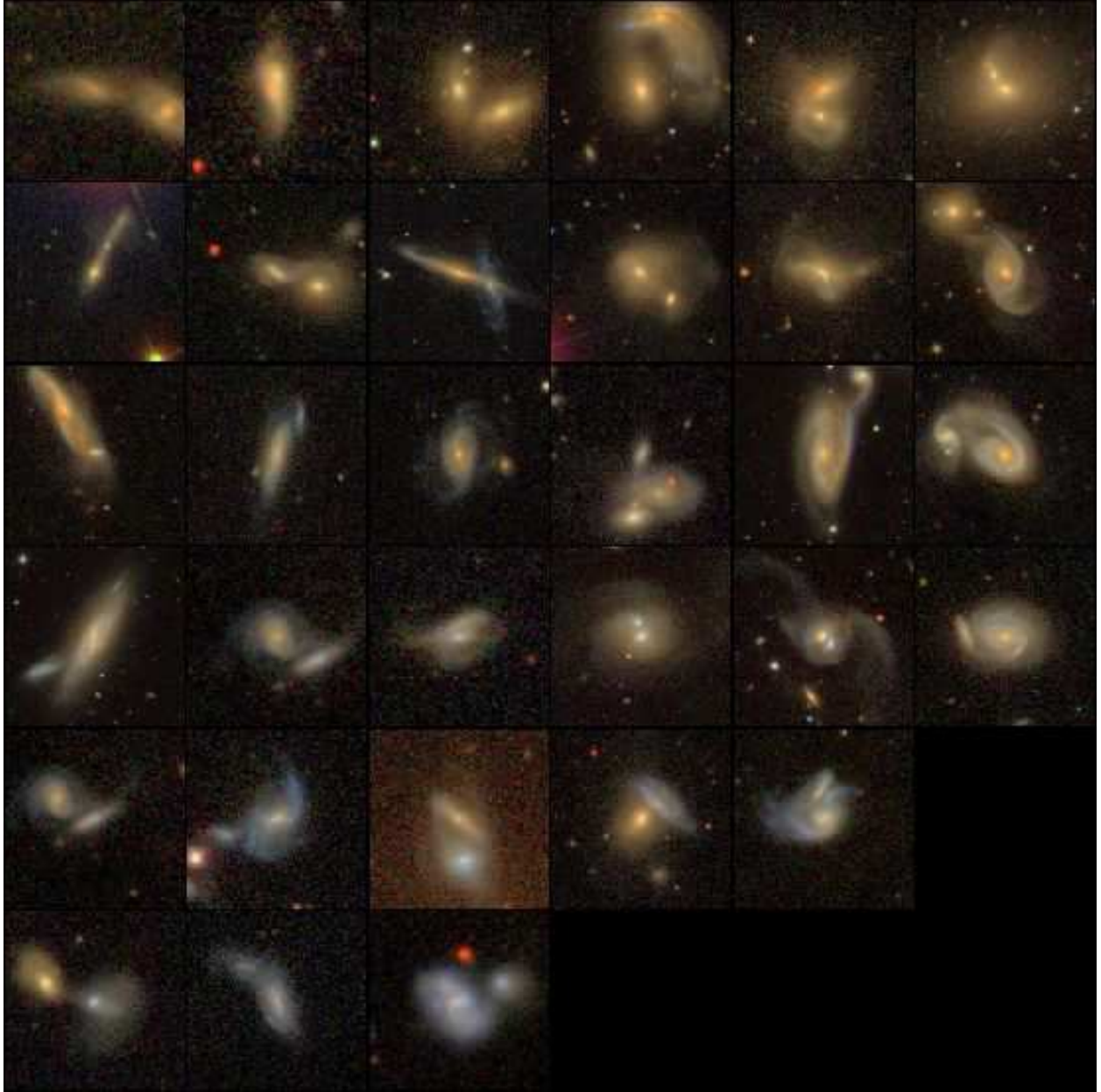


Fig. 16.— SDSS images of merging galaxies, selected by eye from the SDSS DR6 (Christina Ignarra 2008, private communication). The images are sorted by absolute magnitude in the horizontal direction, ranging between $M_r - 5 \log_{10} h \sim -18.5$ and -22 from left to right, and $g - r$ color in the vertical direction, ranging between 0.2 and 0.9 mag from the bottom to the top. Thus, the brightest, reddest mergers are in the upper-right.

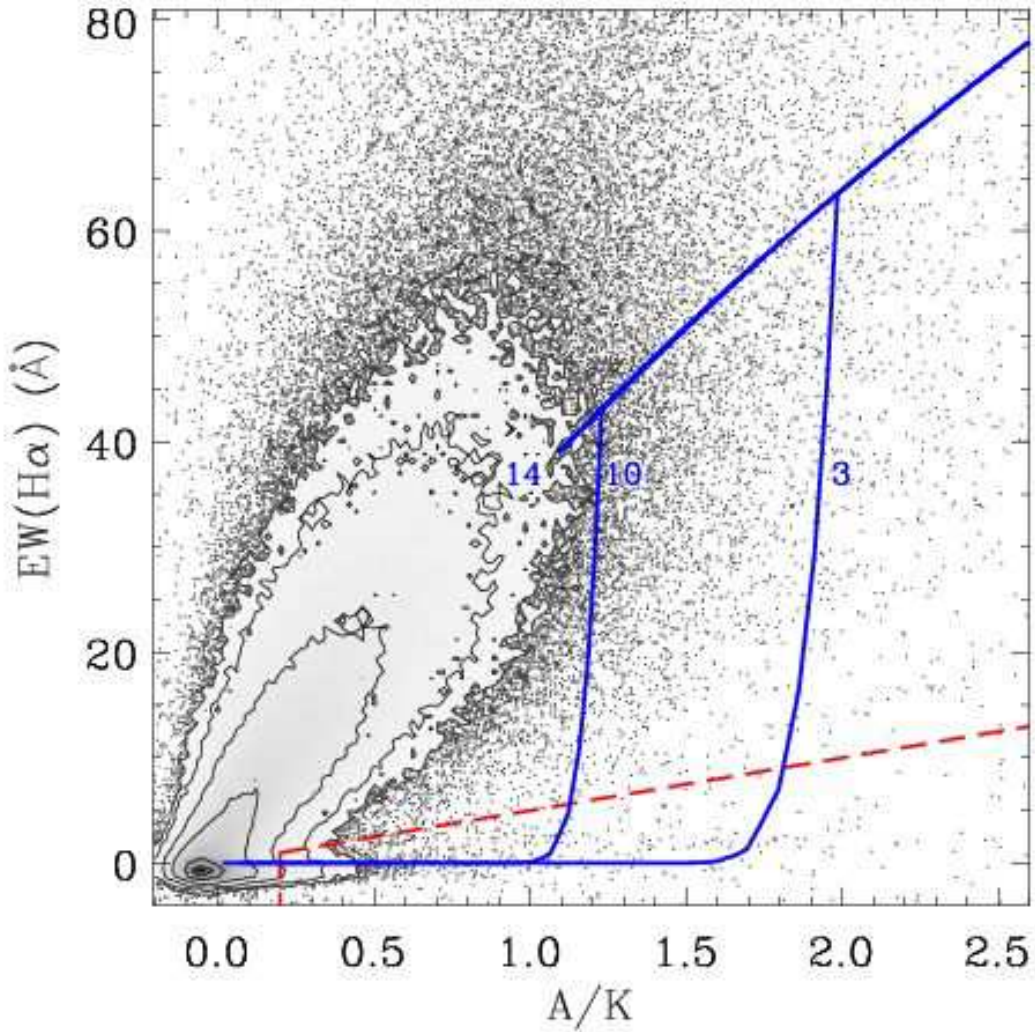


Fig. 17.— Distribution of A/K and $H\alpha$ equivalent width for SDSS galaxies, as determined by Quintero et al. (2004). The greyscale and contours indicate the density of points in this plane. Outliers are shown individually. In blue are shown several toy models: the line labeled “14” corresponds to a constant star-formation rate model over 14 Gyrs; the line labeled “10” corresponds to cutting off that star-formation abruptly at 10 Gyrs; the line labeled “3” corresponds to a cutoff at 3 Gyrs. In each of the latter two cases, the abrupt cutoff results in a post-starburst spectrum. The dashed red lines indicate the criteria for selection that Quintero et al. (2004) use.